

Ductile Fracture

2022 Fall Semester

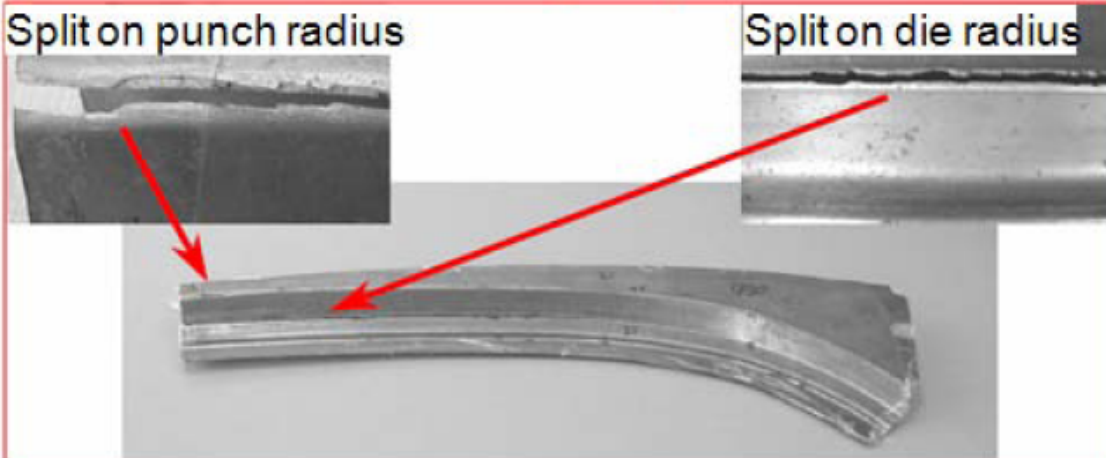
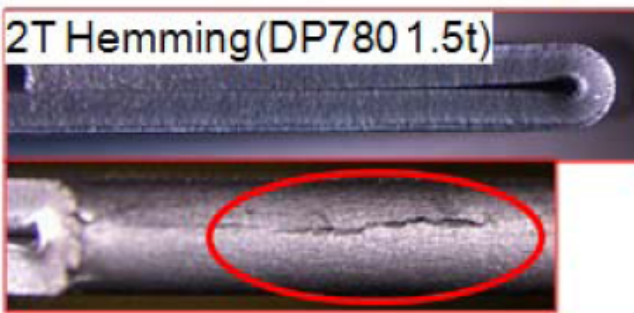
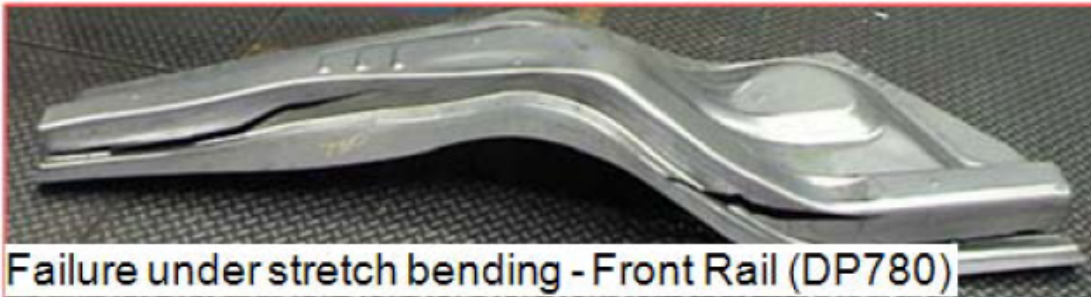
Jeong Whan Yoon

**Professor of Mechanical Engineering
KAIST**

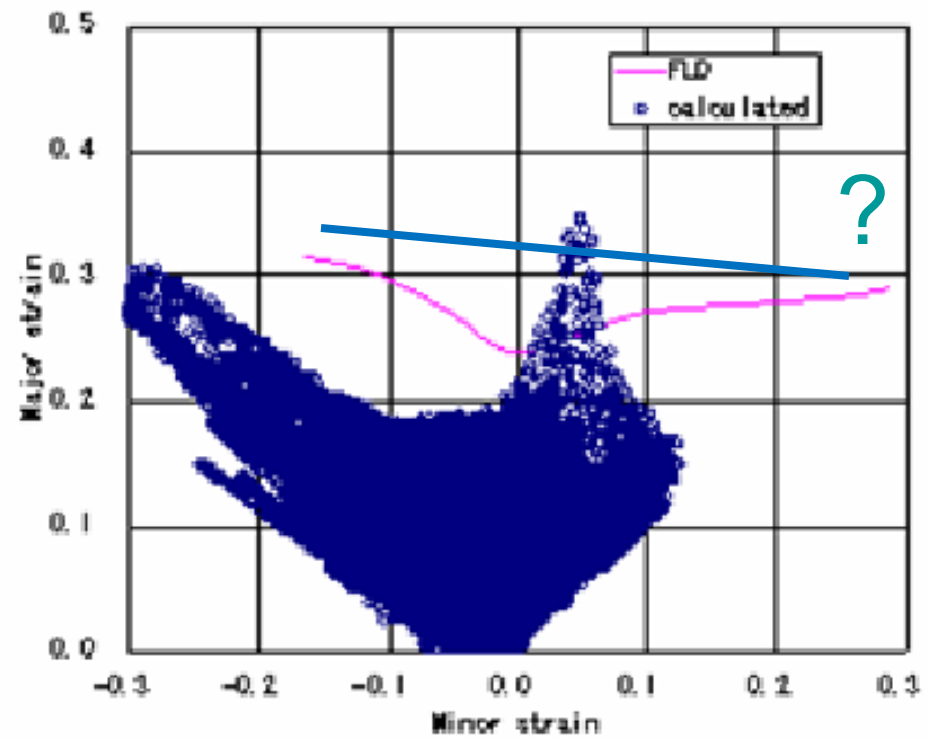
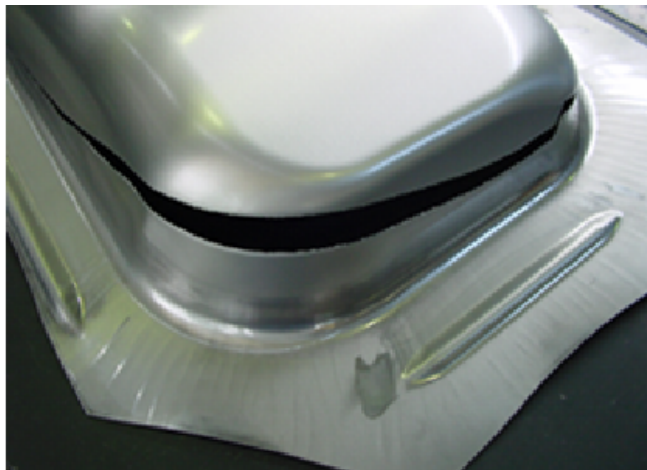
References

- Wierzbicki, T., Bao, Y., Lee, Y.-W., Bai, Y., 2005. Calibration and evaluation of seven fracture models. International Journal of Mechanical Sciences 47 (4–5), 719–743.
- Wierzbicki, T., Bai., 2008. A new model of metal plasticity and fracture with pressure and Lode dependence. Int. J. Plasticity 24, 1071-1096
- Wierzbicki, T., Bai. Y., 2010. Application of extended Mohr–Coulomb criterion to ductile fracture. Int. J. Fracture 161, 1-20.
- Stoughton, T.B., Yoon, J.W., 2011. A new approach for failure criterion for sheet metals. International Journal of Plasticity 27: 440–459.
- Lou, Y., Huh, H., 2013. Prediction of ductile fracture for advanced high strength steel with a new criterion: Experiments and simulation. Journal of Materials Processing Technology 213 (8), 1284-1302.
- Lou, Y., Yoon, J.W., Huh, H., 2014. Modeling of shear ductile fracture considering a changeable cut-off value for stress triaxiality. Int. J. Plasticity 54, 56-80.
- Lou. Y., Yoon, J.W., 2017, “Anisotropic ductile fracture criterion based on linear transformation”, International Journal of Plasticity, Volume 93, June 2017, Pages 3-25.
- Lou, Y., Yoon, J.W., 2018, “Alternative approach to model ductile fracture by incorporating anisotropic yield function, Int. J. Solids and Structures, Volume 164, pp.12-24.
- Chung, K., Lee, Myoung-Gyu, 2018, “Basics of Continuum Plasticity, Springer.

Ductile Failure During Forming

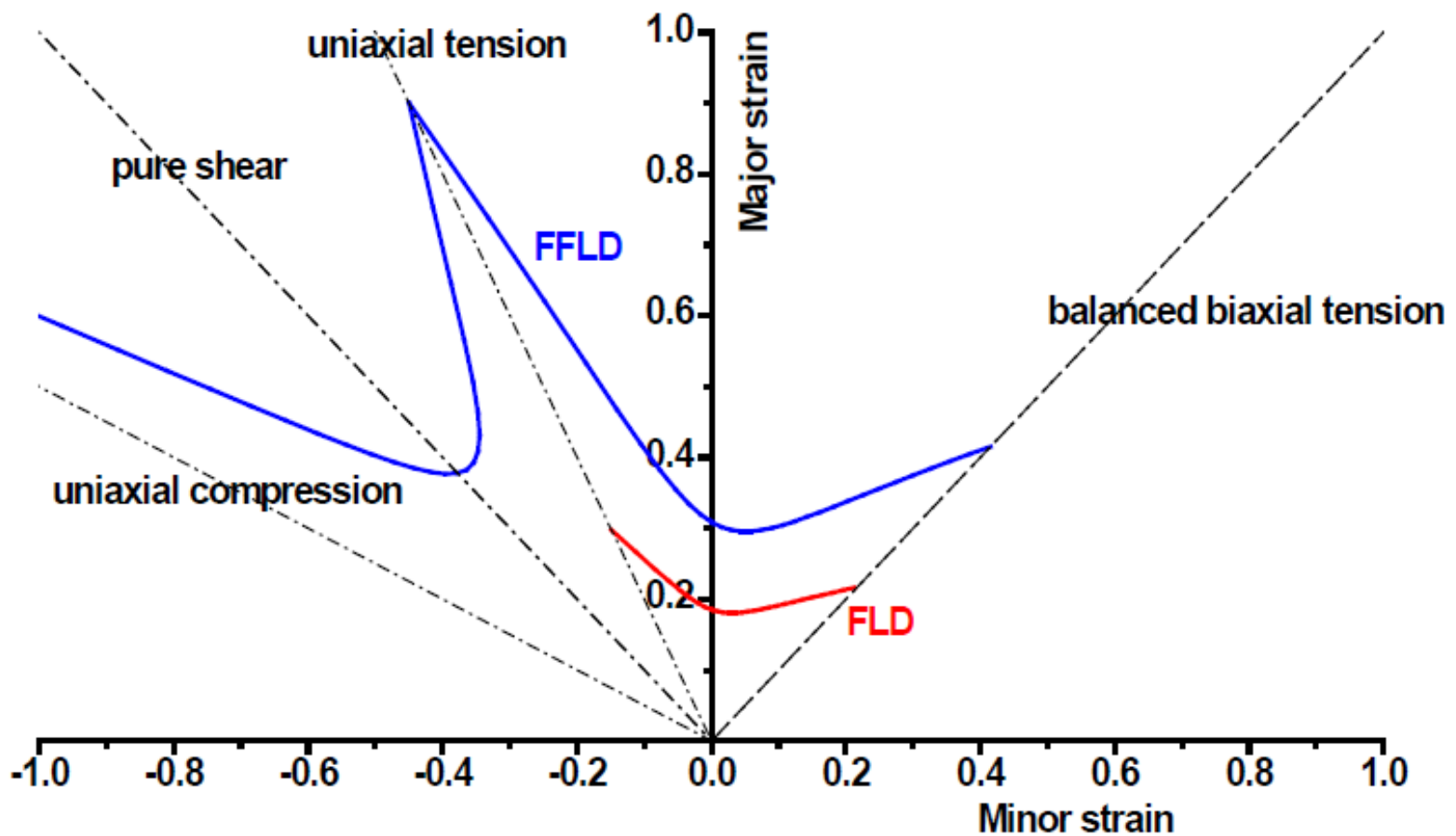


Necking Limit vs. Fracture Limit



Necking Limit \neq Fracture Limit

Representation of Fracture Surface in Strain Space



Definition of Triaxiality for Various Stress :

$$\eta = \frac{\sigma_m}{\bar{\sigma}} = \frac{\sigma_1 + \sigma_2 + \sigma_3}{3\bar{\sigma}}$$

(Uniaxial Compression)

$$\eta = \frac{\sigma_m}{\bar{\sigma}} = \frac{\sigma_2}{3\bar{\sigma}} = \frac{-\sigma_f}{3\sigma_f} = -\frac{1}{3}$$

(Pure Shear)

$$\eta = \frac{\sigma_m}{\bar{\sigma}} = \frac{\sigma_f - \sigma_f}{3\bar{\sigma}} = \frac{0}{3\bar{\sigma}} = 0$$

(Uniaxial Tension)

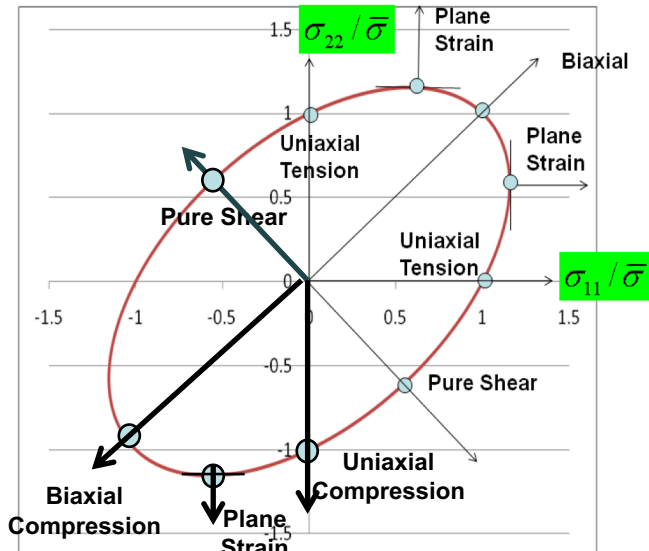
$$\eta = \frac{\sigma_m}{\bar{\sigma}} = \frac{\sigma_1}{3\bar{\sigma}} = \frac{\sigma_f}{3\sigma_f} = \frac{1}{3}$$

(Plane Strain)

$$\eta = \frac{\sigma_m}{\bar{\sigma}} = \frac{3\sigma_f}{3\sqrt{3}\sigma_f} = \frac{1}{\sqrt{3}}$$

(Biaxial Tension)

$$\eta = \frac{\sigma_m}{\bar{\sigma}} = \frac{\sigma_f + \sigma_f}{3\bar{\sigma}} = \frac{2\sigma_f}{3\sigma_f} = \frac{2}{3}$$



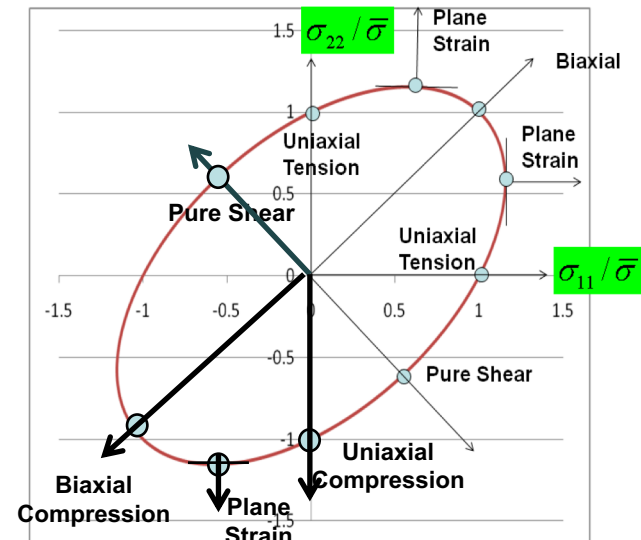
$$\bar{\sigma}(\underline{\sigma}) = \sqrt{(\sigma_{11})^2 + (\sigma_{22})^2 - \sigma_{11}\sigma_{22}}$$

$$\frac{\partial \bar{\sigma}}{\partial \sigma_{22}} = \frac{2\sigma_{22} - \sigma_{11}}{2\bar{\sigma}} = 0 \longrightarrow \sigma_{11} = 2\sigma_{22}$$

$$if \sigma_{22} = \sigma_f, \sigma_{11} = 2\sigma_f$$

$$\bar{\sigma}(\underline{\sigma}) = \sqrt{3}\sigma_f$$

Differentiation between Necking and Fracture



$$\text{Triaxiality : } \eta = \frac{\sigma_m}{\bar{\sigma}} = \frac{\sigma_1 + \sigma_2 + \sigma_3}{3\bar{\sigma}}$$

(Major and Minor Strain Space)
- Path Dependence ! (Not Useful)

$$\eta = 1/3$$

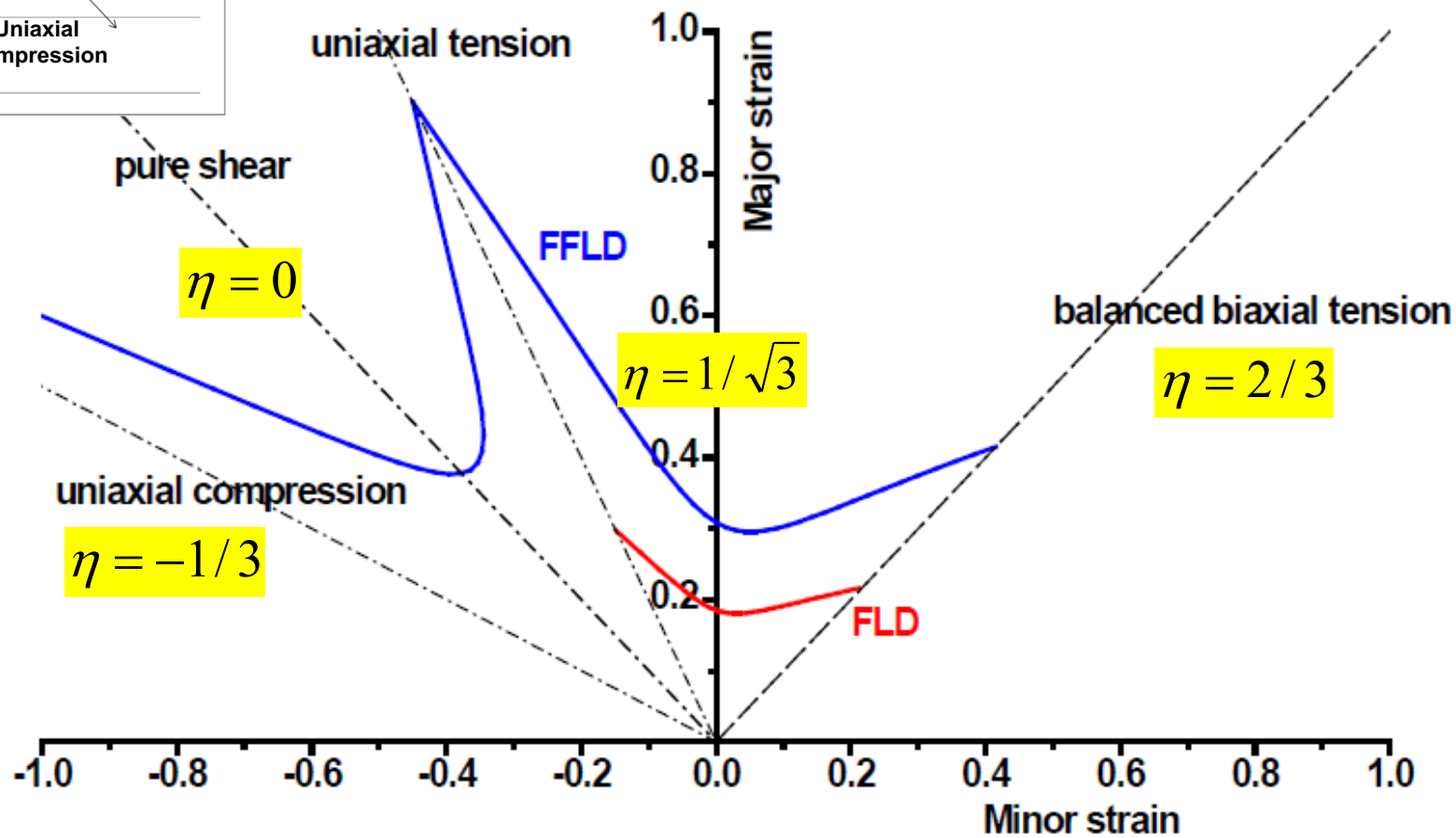
uniaxial tension

pure shear

$$\eta = 0$$

uniaxial compression

$$\eta = -1/3$$



Invariants (Deviatoric Stress)

$$S_p^3 - J_1 S_p^2 - J_2 S_p - J_3 = 0$$

$$\begin{cases} J_1 = \text{tr}(\mathbf{S}) = S_{ii} = S_I + S_{II} + S_{III} = 0 \\ J_2 = \frac{1}{2}(S_{ij}S_{ji} - S_{ii}S_{jj}) = \frac{1}{2}S_{ij}S_{ij} = \frac{1}{2}(S_I^2 + S_{II}^2 + S_{III}^2) \\ J_3 = \det(\mathbf{S}) = \frac{1}{3}(S_{ij}S_{jk}S_{ki}) = S_IS_{II}S_{III} \end{cases} \longrightarrow$$

$$|\mathbf{S}^*| = \sqrt{2J_2}$$

where $J_2 = \frac{1}{2}S_{ij}S_{ij} = \frac{1}{2}(S_{11}^2 + S_{22}^2 + S_{33}^2) + S_{12}^2 + S_{23}^2 + S_{31}^2$

$$= -(S_{11}S_{22} + S_{22}S_{33} + S_{33}S_{11}) + S_{12}^2 + S_{23}^2 + S_{31}^2$$

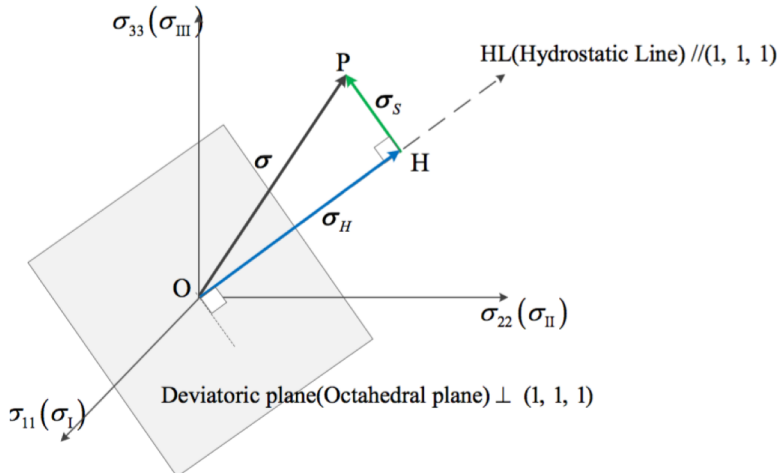
$$= \frac{1}{6}((S_{11} - S_{22})^2 + (S_{22} - S_{33})^2 + (S_{33} - S_{11})^2) + S_{12}^2 + S_{23}^2 + S_{31}^2$$

$$= \frac{1}{6}((\sigma_{11} - \sigma_{22})^2 + (\sigma_{22} - \sigma_{33})^2 + (\sigma_{33} - \sigma_{11})^2) + \sigma_{12}^2 + \sigma_{23}^2 + \sigma_{31}^2$$

$\downarrow \longleftrightarrow \bar{\sigma}_M(\underline{\underline{\sigma}}) = \sqrt{\frac{1}{2}[(\sigma_{11} - \sigma_{22})^2 + (\sigma_{22} - \sigma_{33})^2 + (\sigma_{33} - \sigma_{11})^2 + 6(\sigma_{12}^2 + \sigma_{23}^2 + \sigma_{31}^2)]}$

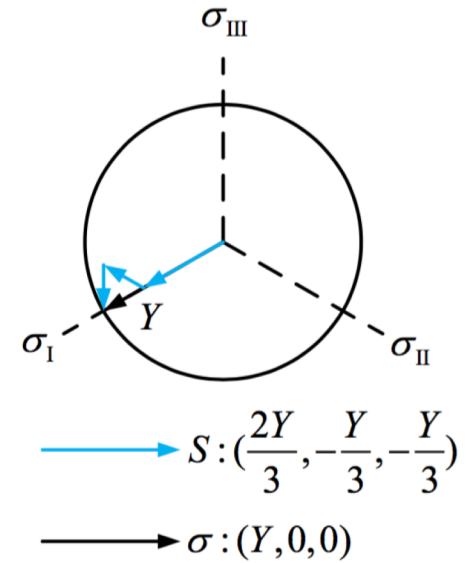
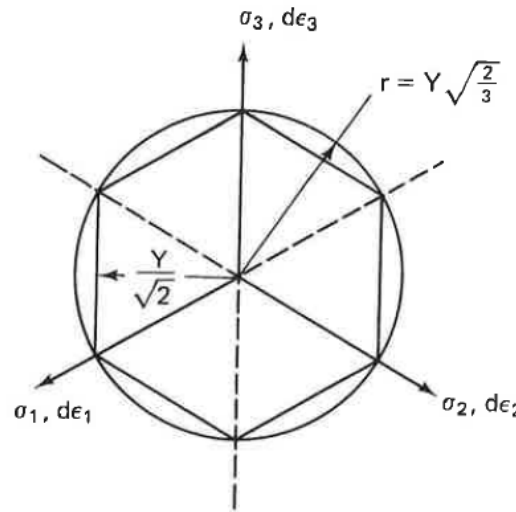
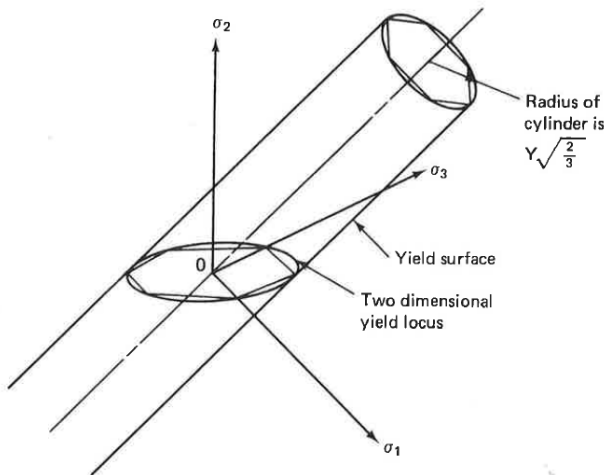
$$\bar{\sigma}_M(\underline{\underline{\sigma}}) = \sqrt{3J_2}$$

Hydrostatic and Deviatoric Planes

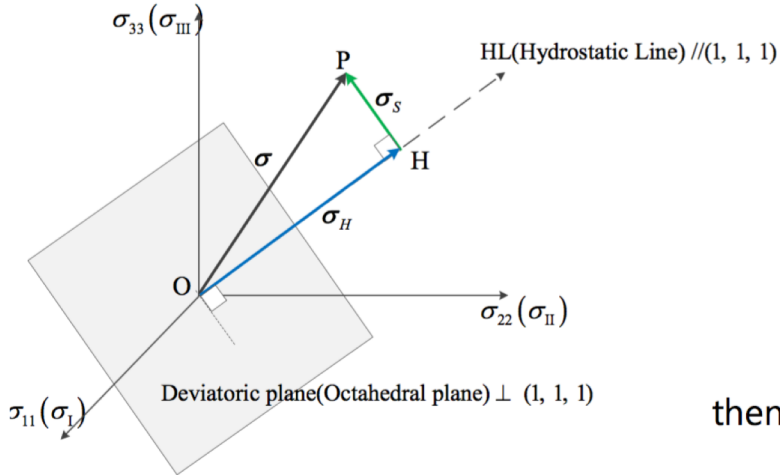


$$\tilde{\mathbf{e}}_1 = \tilde{\mathbf{e}}_{1S} + \tilde{\mathbf{e}}_{1H} = \begin{pmatrix} 1 \\ 0 \\ 0 \end{pmatrix} = \begin{pmatrix} \frac{1}{3} \\ -\frac{1}{3} \\ -\frac{1}{3} \end{pmatrix} + \begin{pmatrix} \frac{1}{3} \\ \frac{1}{3} \\ \frac{1}{3} \end{pmatrix}$$

$$|\tilde{\mathbf{e}}_{1S}| = \sqrt{\left(\frac{2}{3}\right)^2 + \left(-\frac{1}{3}\right)^2 + \left(-\frac{1}{3}\right)^2} = \sqrt{\frac{6}{9}} = \sqrt{\frac{2}{3}}$$



Lode Angle Definition



$$\tilde{\mathbf{e}}_1 = \tilde{\mathbf{e}}_{1S} + \tilde{\mathbf{e}}_{1H} = \begin{pmatrix} 1 \\ 0 \\ 0 \end{pmatrix} = \begin{pmatrix} \frac{2}{3} \\ \frac{-1}{3} \\ \frac{-1}{3} \end{pmatrix} + \begin{pmatrix} \frac{1}{3} \\ \frac{1}{3} \\ \frac{1}{3} \end{pmatrix}$$

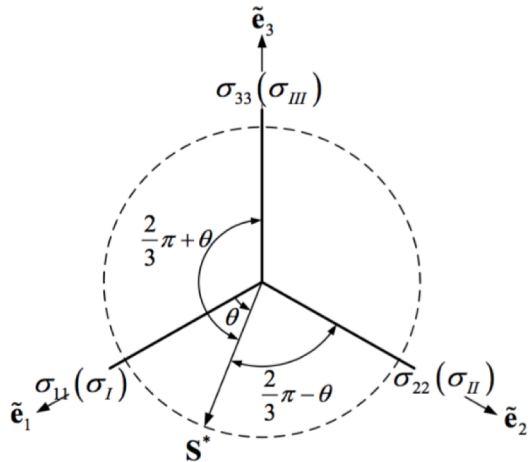
then, with $\mathbf{S}^* \cdot \tilde{\mathbf{e}}_{1H} = 0$,

$$S_I = \mathbf{S}^* \cdot \tilde{\mathbf{e}}_1 = \mathbf{S}^* \cdot \tilde{\mathbf{e}}_{1S} = |\mathbf{S}^*| |\tilde{\mathbf{e}}_{1S}| \cos \theta = \sqrt{\frac{2}{3}} |\mathbf{S}^*| \cos \theta = 2 \sqrt{\frac{J_2}{3}} \cos \theta$$

where θ , known as the **Lode angle**, is the angle between $\tilde{\mathbf{e}}_{1S}$ and \mathbf{S}^* on the deviatoric plane. Similarly,

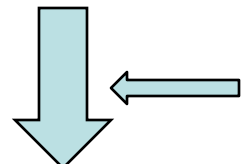
$$S_{II} = \mathbf{S}^* \cdot \tilde{\mathbf{e}}_2 = \mathbf{S}^* \cdot \tilde{\mathbf{e}}_{2S} = \sqrt{\frac{2}{3}} |\mathbf{S}^*| \cos\left(\frac{2\pi}{3} - \theta\right) = 2 \sqrt{\frac{J_2}{3}} \cos\left(\frac{2\pi}{3} - \theta\right)$$

$$S_{III} = \mathbf{S}^* \cdot \tilde{\mathbf{e}}_3 = \mathbf{S}^* \cdot \tilde{\mathbf{e}}_{3S} = \sqrt{\frac{2}{3}} |\mathbf{S}^*| \cos\left(\frac{2\pi}{3} + \theta\right) = 2 \sqrt{\frac{J_2}{3}} \cos\left(\frac{2\pi}{3} + \theta\right)$$



Lode Angle Form

$$S_p^3 - J_2 S_p - J_3 = 0$$


 $\Longleftarrow S_I = 2\sqrt{\frac{J_2}{3}} \cos \theta$

The Lode angle θ is

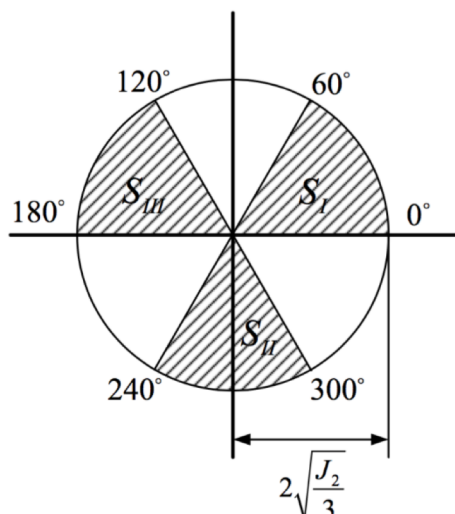
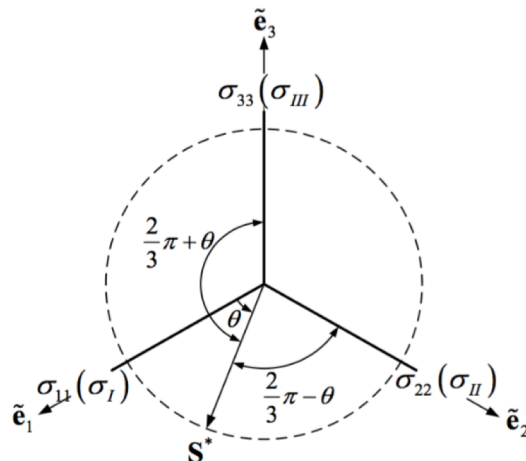
$$8\left(\frac{J_2}{3}\right)^{\frac{3}{2}} \cos^3 \theta - 2\sqrt{\frac{J_2}{3}} J_2 \cos \theta - J_3 = 0$$

which becomes

$$2\left(\frac{J_2}{3}\right)^{\frac{3}{2}} (4\cos^3 \theta - 3\cos \theta) = J_3$$

Since $(4\cos^3 \theta - 3\cos \theta) = \cos(3\theta)$,

$$\cos(3\theta) = \frac{J_3}{2} \left(\frac{3}{J_2}\right)^{\frac{3}{2}}$$



$$\left(0 \leq \theta \leq \frac{\pi}{3}\right)$$

three solutions are $\cos \theta$, $\cos(\frac{2\pi}{3} - \theta)$ and $\cos(\frac{2\pi}{3} + \theta)$

Lode Angle Summary

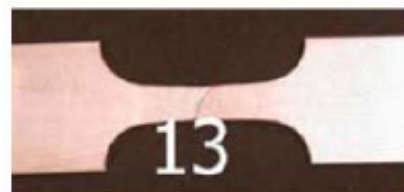
$$\cos(3\theta) = \frac{J_3}{2} \left(\frac{3}{J_2} \right)^{\frac{3}{2}}$$

$$J_2 = \frac{(\bar{\sigma}_M)^2}{3}$$

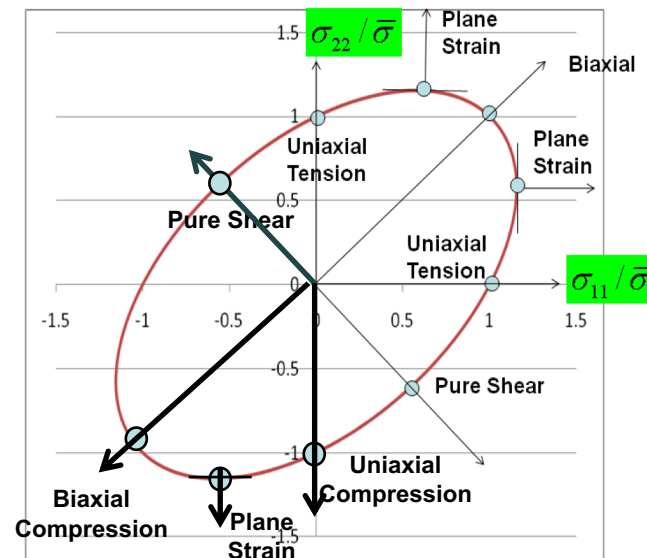
$$\xi = \cos(3\theta) = \frac{J_3}{2} \left(\frac{3}{J_2} \right)^{\frac{3}{2}} = \frac{J_3}{2} \left(\frac{3^2}{(\bar{\sigma}_M)^2} \right)^{\frac{3}{2}} = \frac{27}{2} \frac{J_3}{(\bar{\sigma}_M)^3} = \left(\frac{r}{\bar{\sigma}_M} \right)^3$$

$$r = \left(\frac{27}{2} J_3 \right)^{1/3}$$

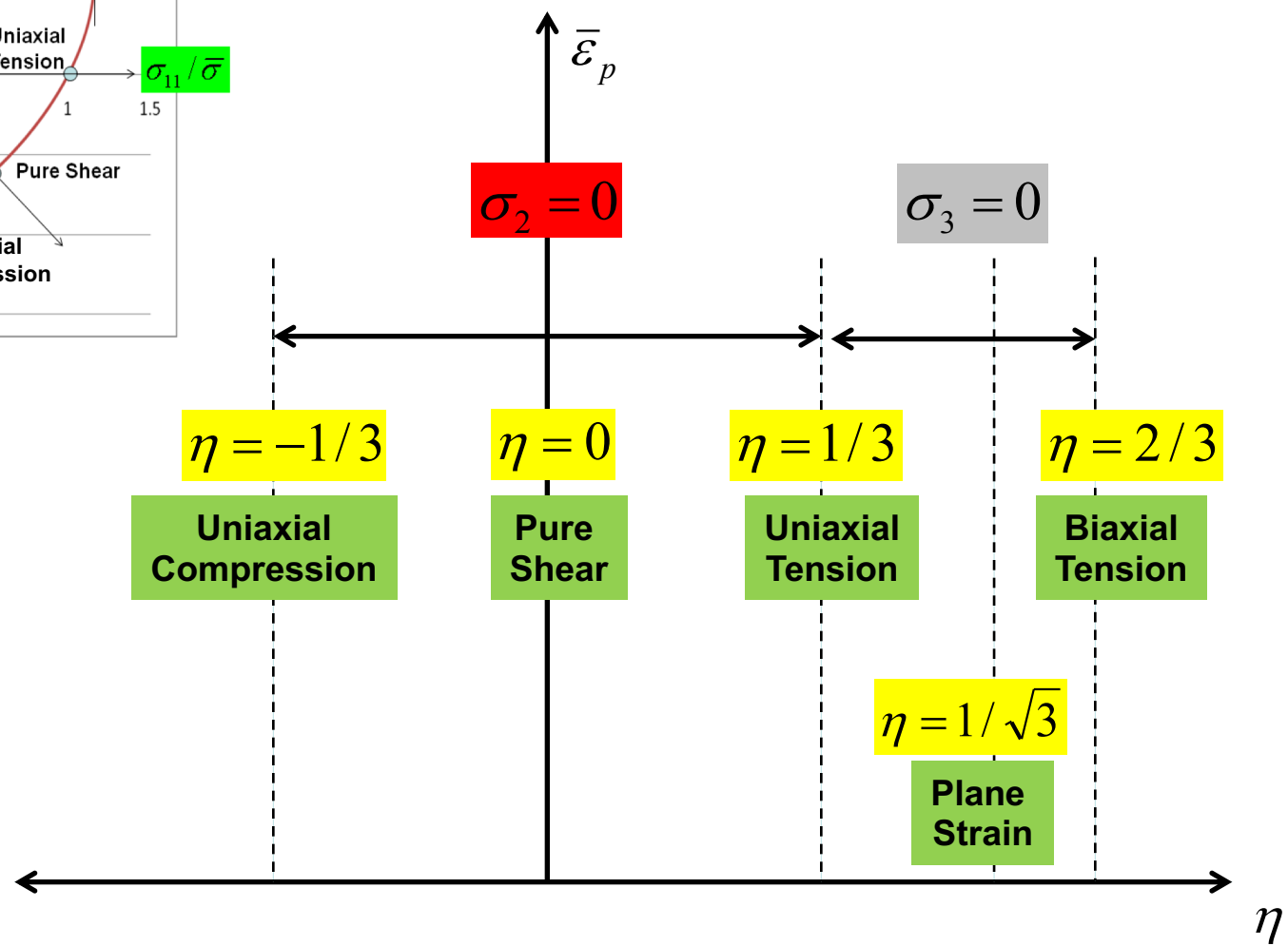
Wierzbicki's Experiment (IJMS, 2005)



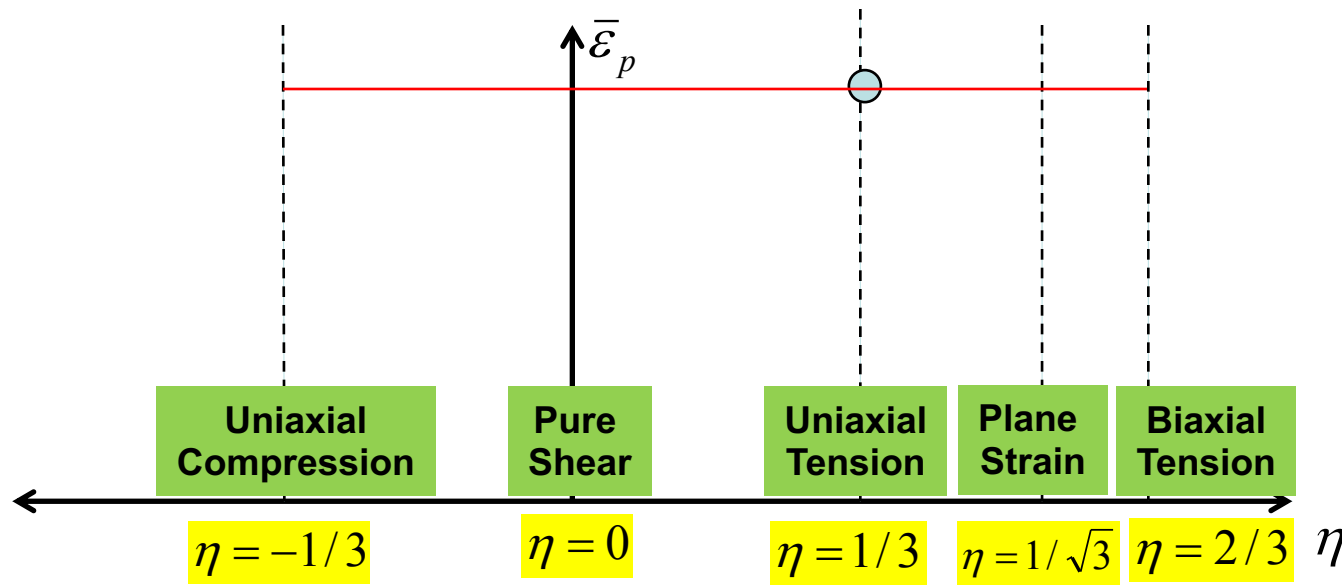
$$\text{Triaxiality : } \eta = \frac{\sigma_m}{\bar{\sigma}} = \frac{\sigma_1 + \sigma_2 + \sigma_3}{3\bar{\sigma}}$$



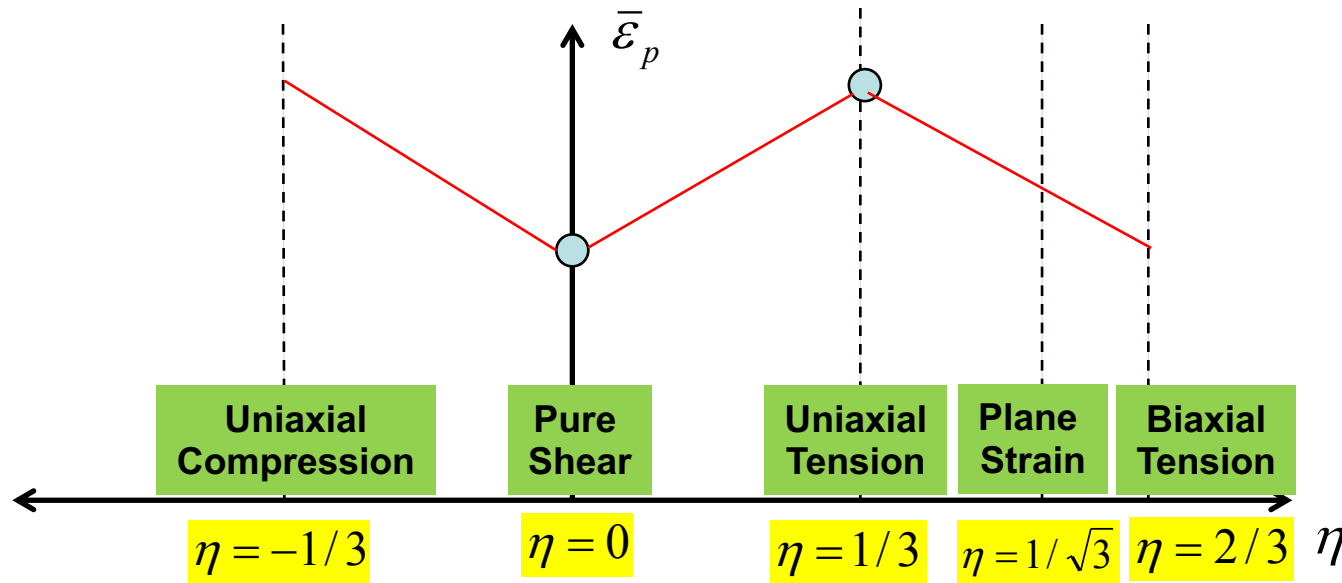
(Fracture Strain vs. Triaxiality Space)



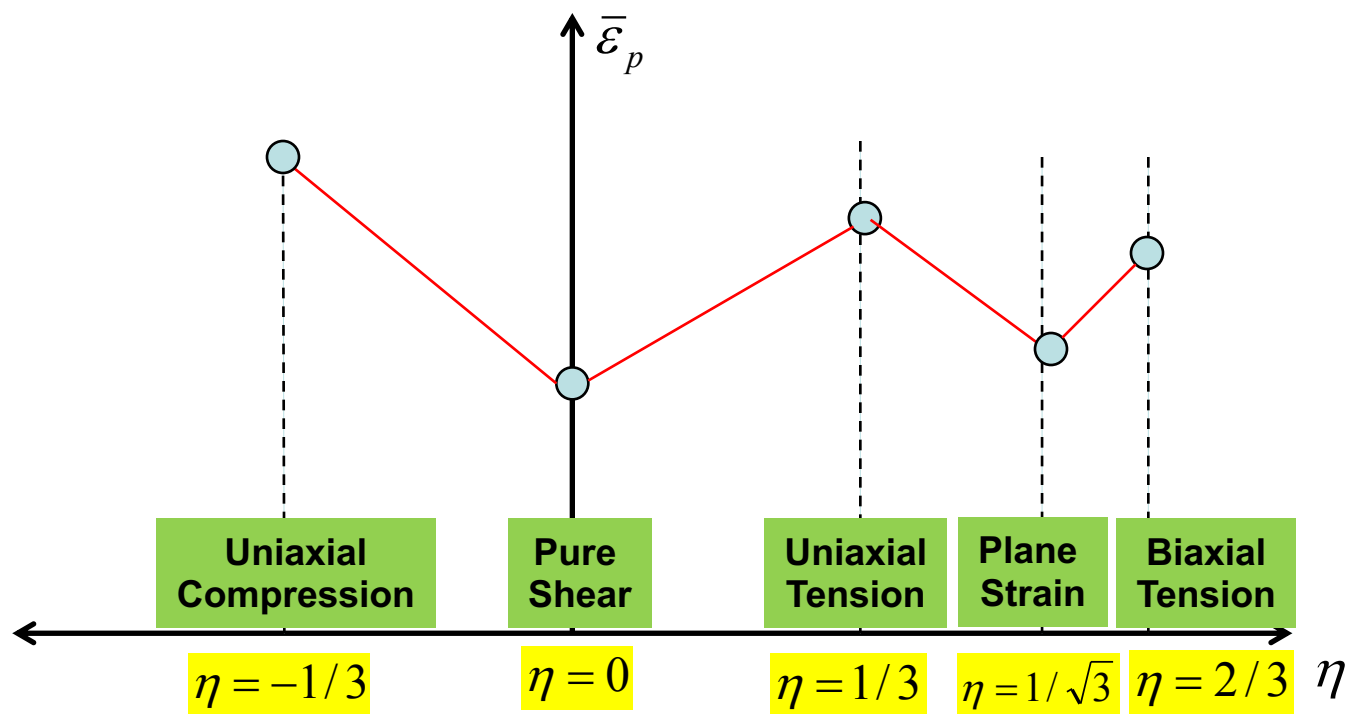
One Parameter Linear Model



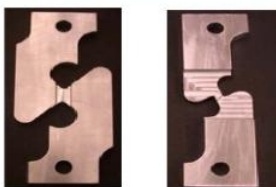
Two Parameters Linear Model



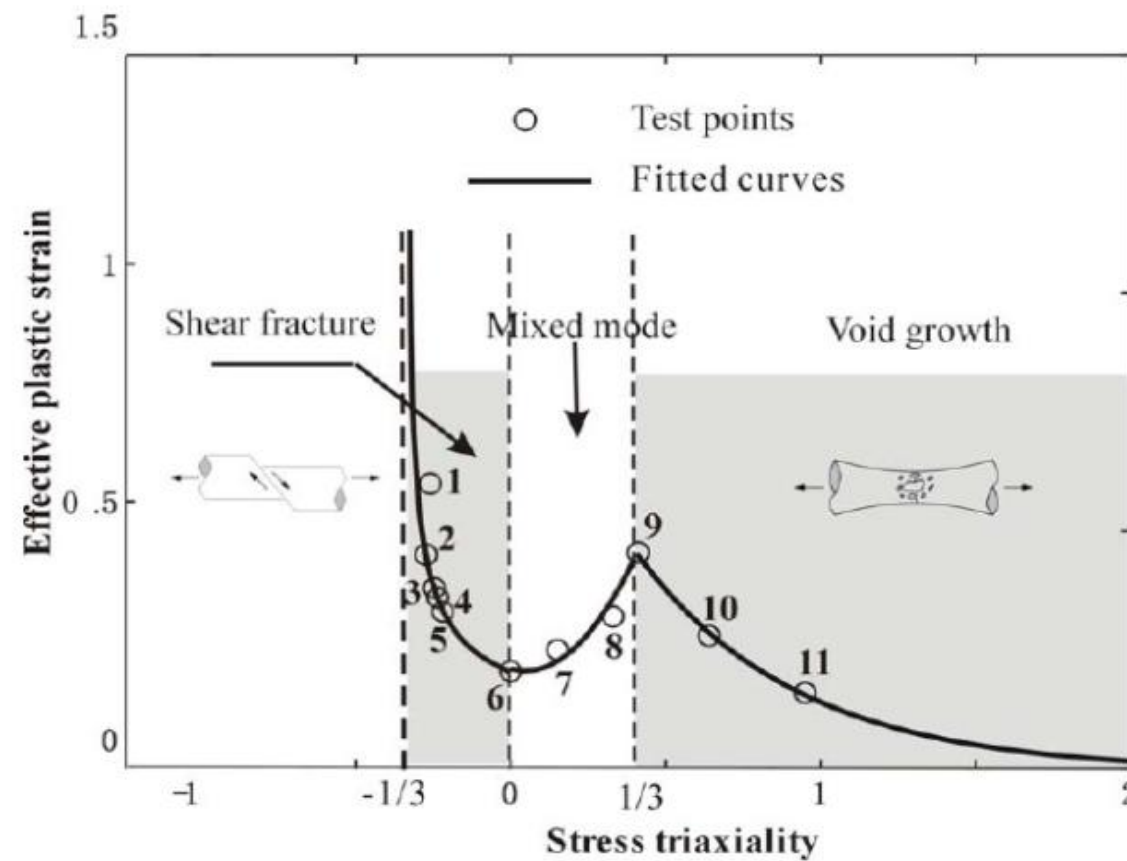
Multiple Parameters Linear Model



Multiple Parameters Non-Linear Model (Representation of Wierzbicki's data)

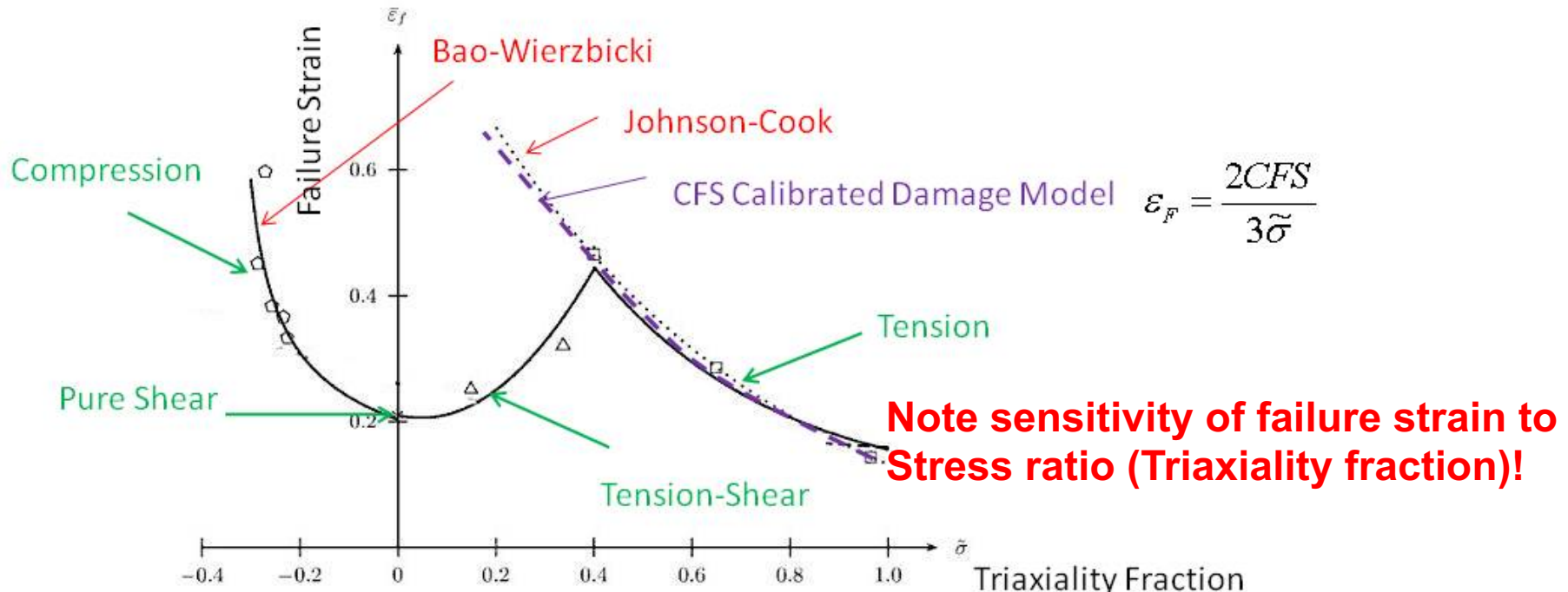


(9-11)



Three Distinct Regimes of Failure Mode

(Data points are for 2024-T351)



Bao-Wierzbicki

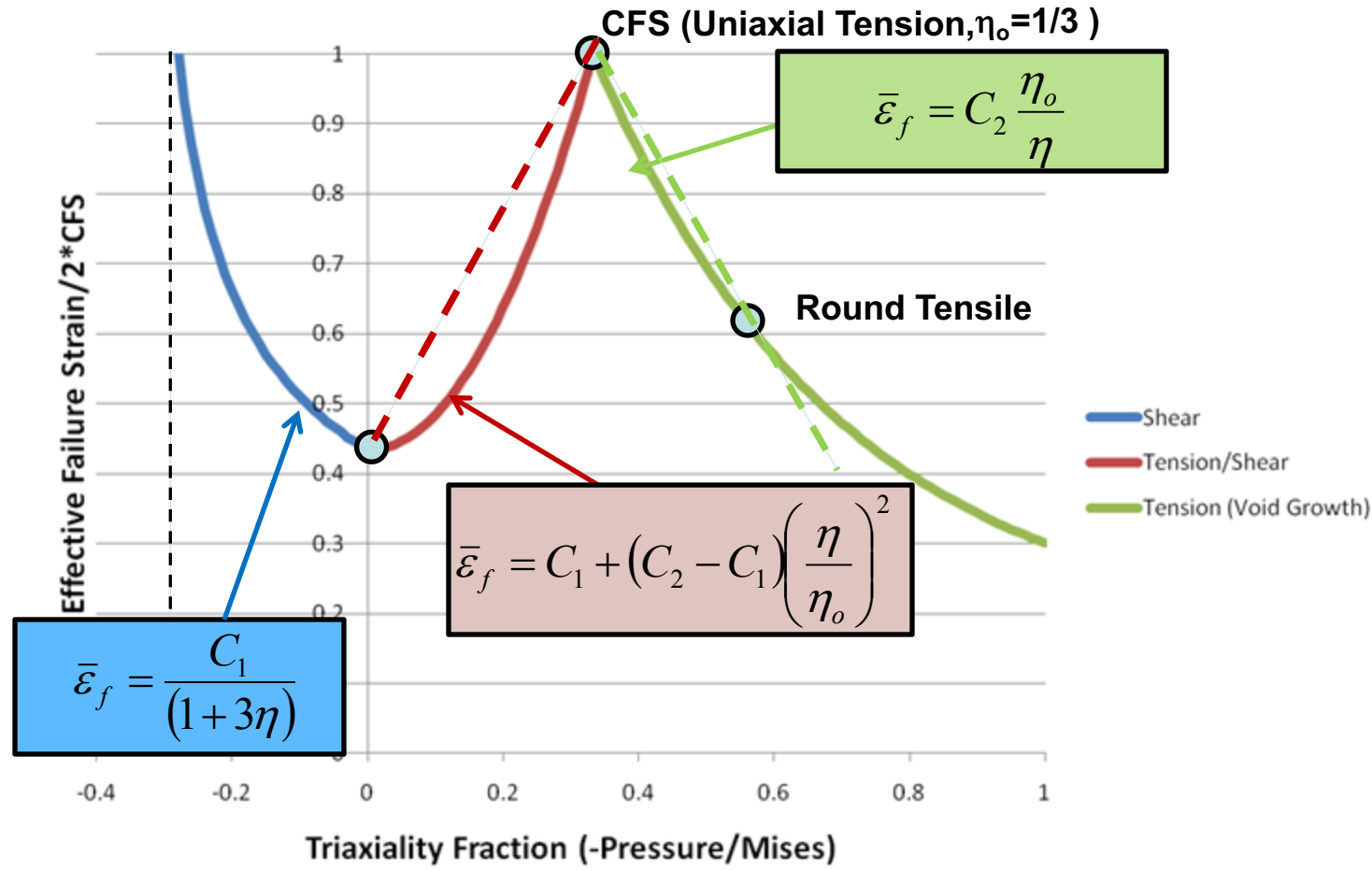
$$\bar{\varepsilon}^f(\tilde{\sigma}) = \begin{cases} \infty & \tilde{\sigma} \leq \frac{1}{3} \\ 0.1225 \left(\tilde{\sigma} + \frac{1}{3} \right)^{-0.46} & -\frac{1}{3} < \tilde{\sigma} \leq 0 \\ 1.9 \tilde{\sigma}^2 - 0.18 \tilde{\sigma} + 0.21 & 0 < \tilde{\sigma} \leq 0.4 \\ 0.0846 + 1.0694 \exp(-2.7149 \tilde{\sigma}) & 0.4 < \tilde{\sigma} \end{cases}$$

Johnson-Cook

$$\bar{\varepsilon}^f = [D_1 + D_2 \exp D_3 \sigma^*] [1 + D_4 \ln \dot{\varepsilon}^*]$$

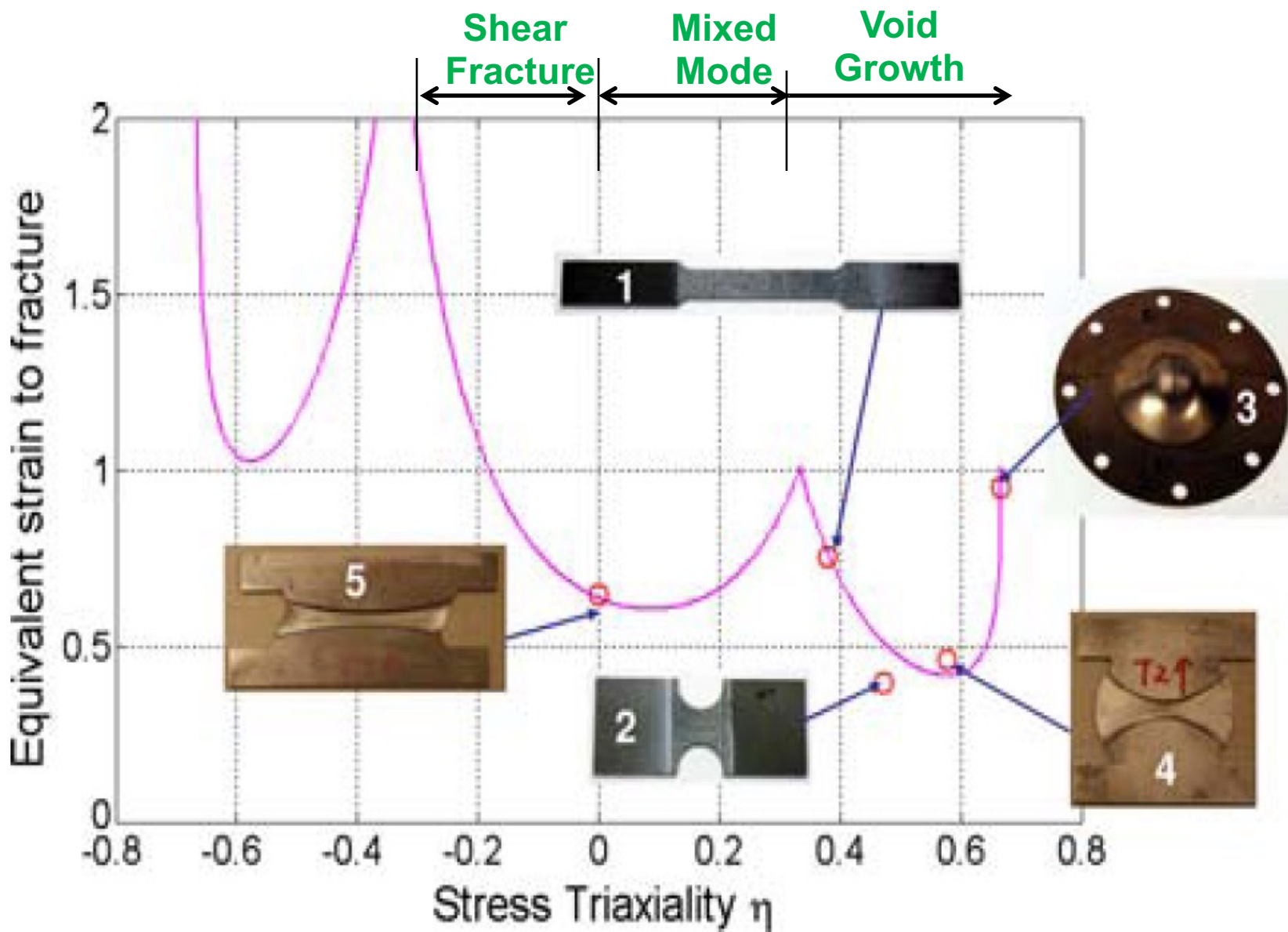
Procedure to Calibrate Failure Strain

Failure Branches Based on CFS and Axial Round Tensile Specimens



Multiple Parameters Non-Linear Model

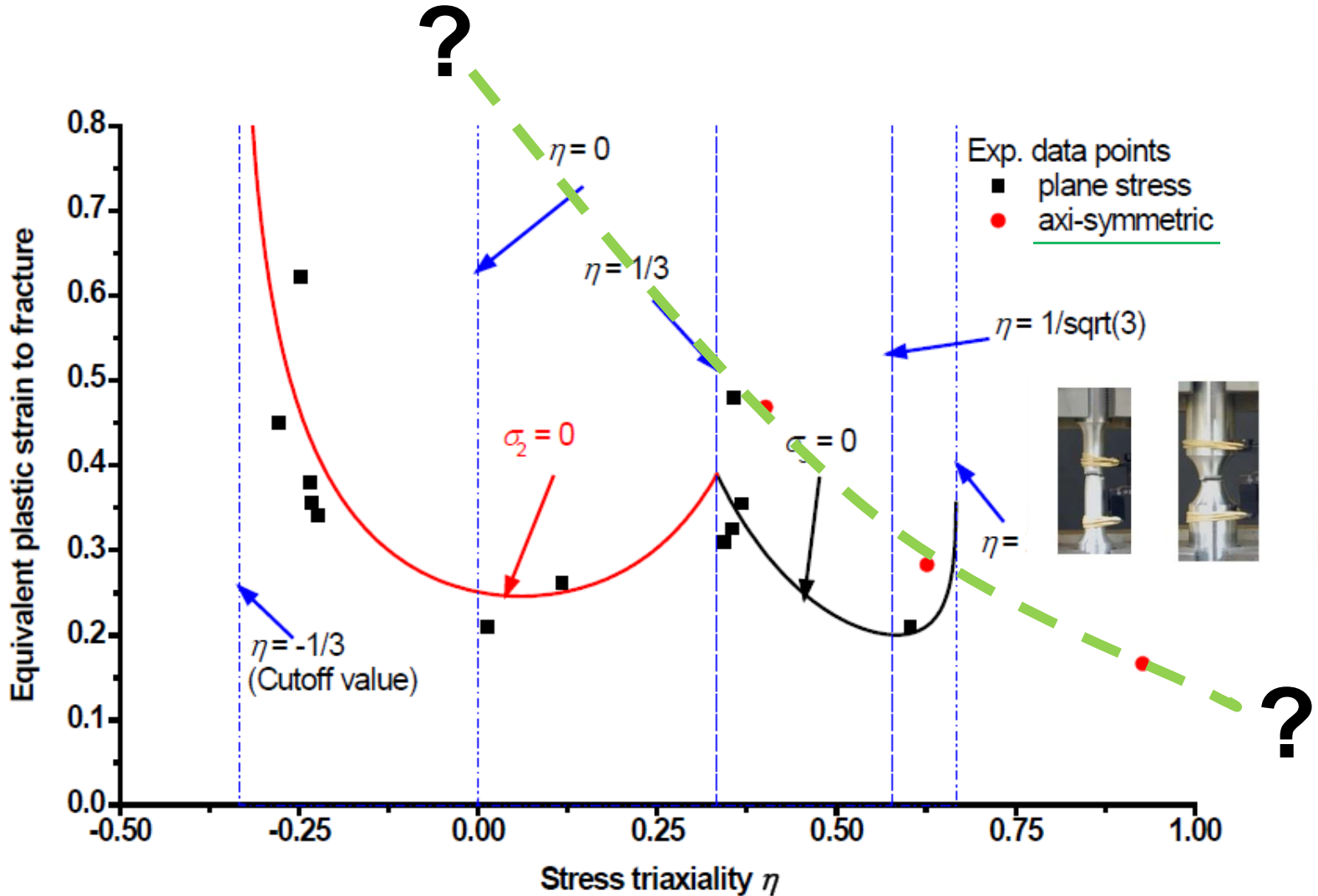
(Wierzbicki et. al, 2005; Bai and Wierzbicki, 2010)



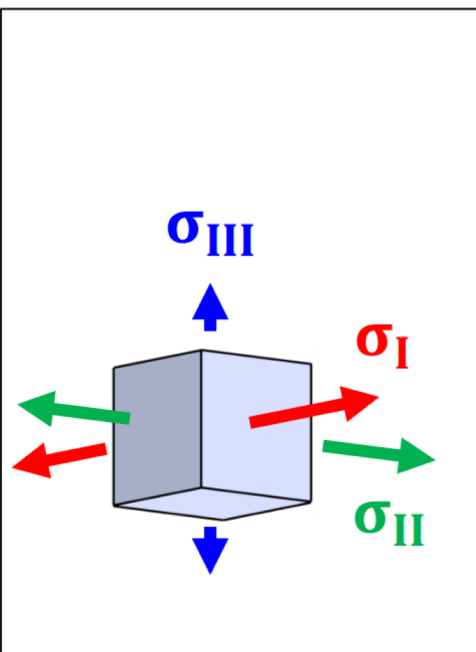
Axi-symmetric data is not matching !



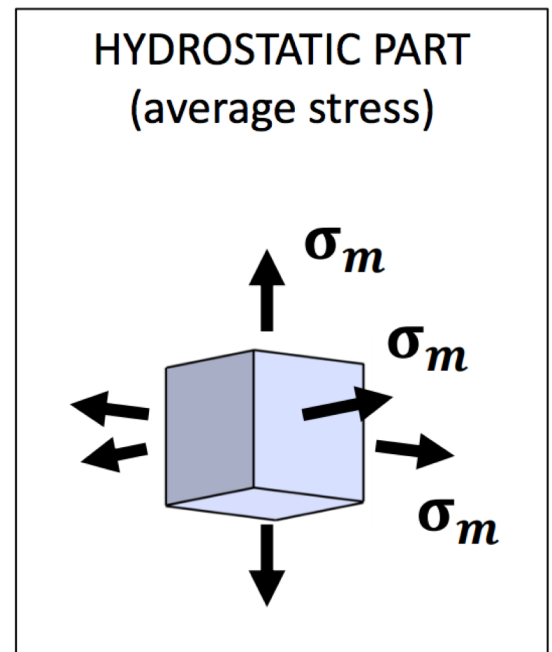
Introduce Lode Parameter



Decomposition of the Stress Tensor

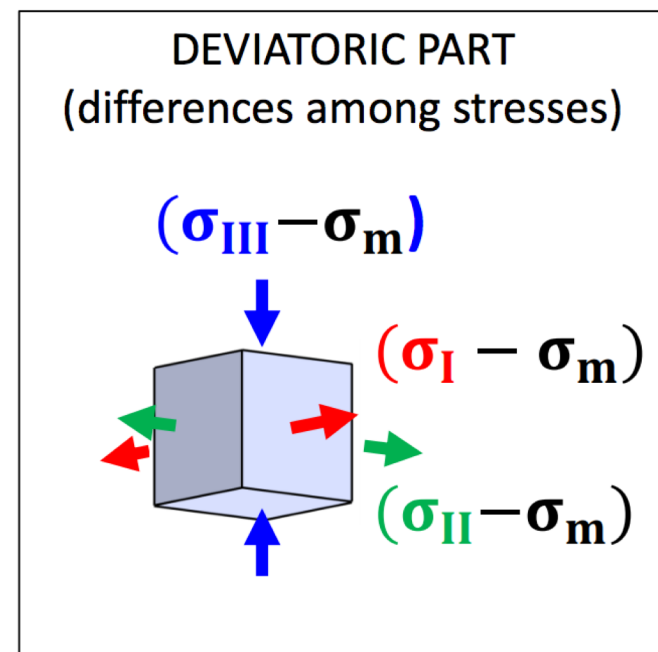


=



HYDROSTATIC PART
(average stress)

+

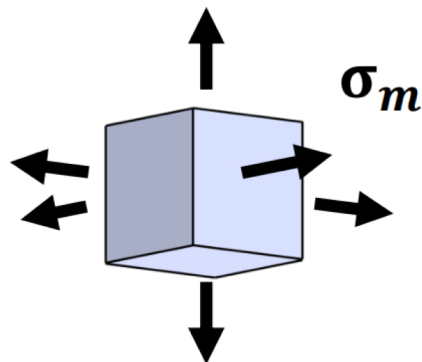


DEVIATORIC PART
(differences among stresses)

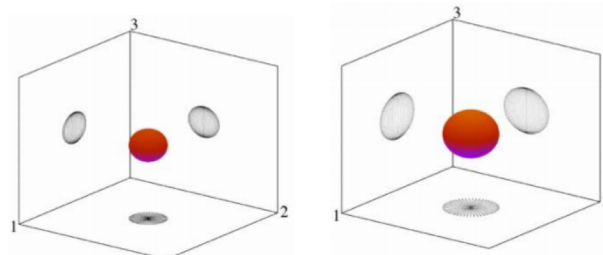
$$\sigma_m = \frac{\sigma_I + \sigma_{II} + \sigma_{III}}{3}$$

Effect of Stress State on Void Evolution

HYDROSTATIC PART



... controls void growth

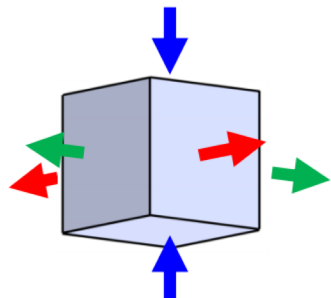


... is characterized by:

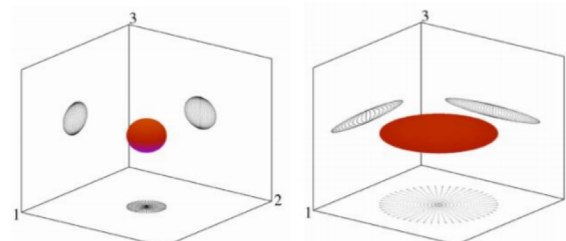
STRESS TRIAXIALITY

$$\eta = \frac{\sigma_m}{\bar{\sigma}}$$

DEVIATORIC PART



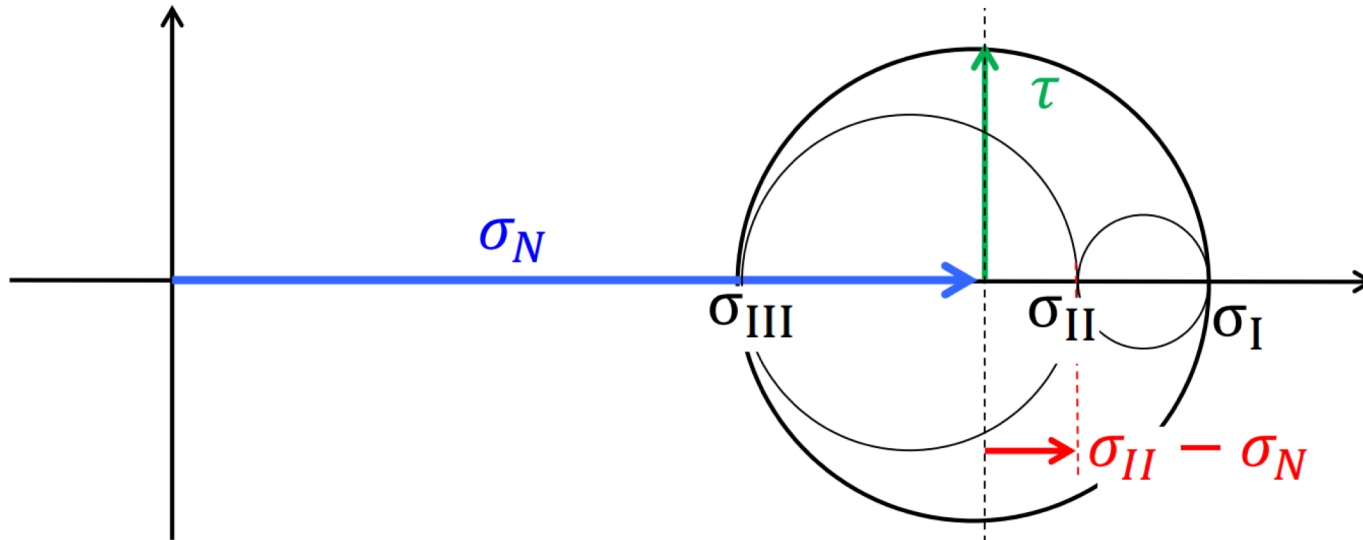
... controls shape change



... is characterized by:

LODE PARAMETER

Definition of Lode Parameter



- Maximum shear stress (radius of biggest circle):
- Normal stress on plane of max. shear (center of biggest circle)
- Position of the intermediate principal stress:

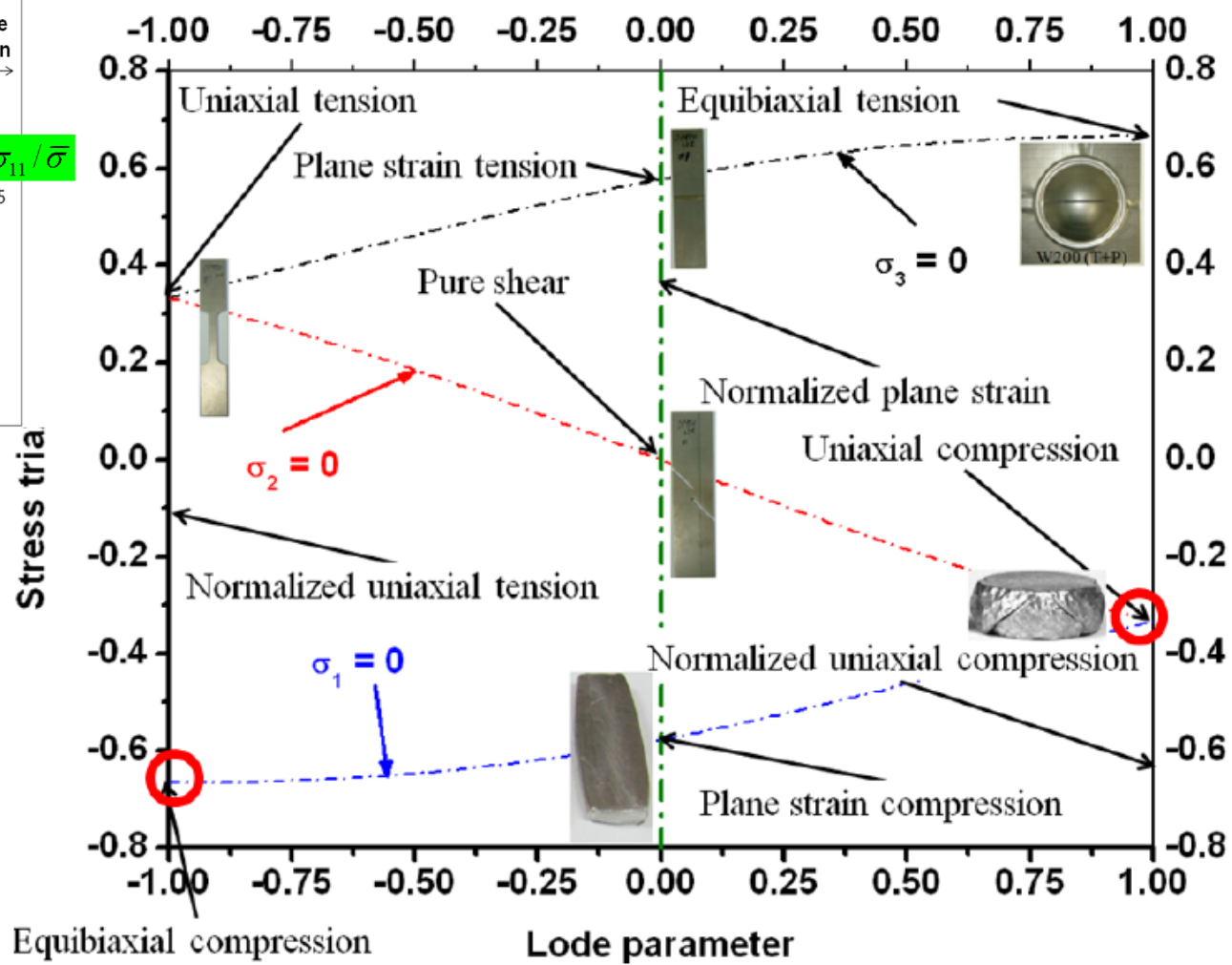
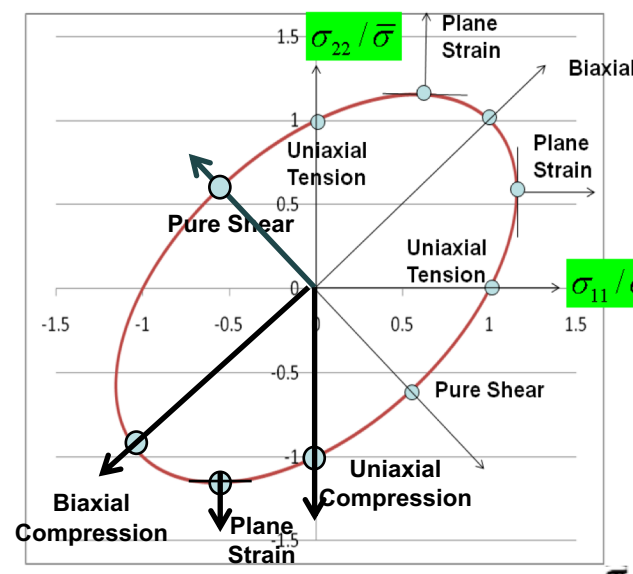
$$\tau = \frac{\sigma_I - \sigma_{III}}{2}$$

$$\sigma_N = \frac{\sigma_I + \sigma_{III}}{2}$$

$$L = \frac{\sigma_{II} - \sigma_N}{\tau} \quad \text{LODE PARAMETER}$$

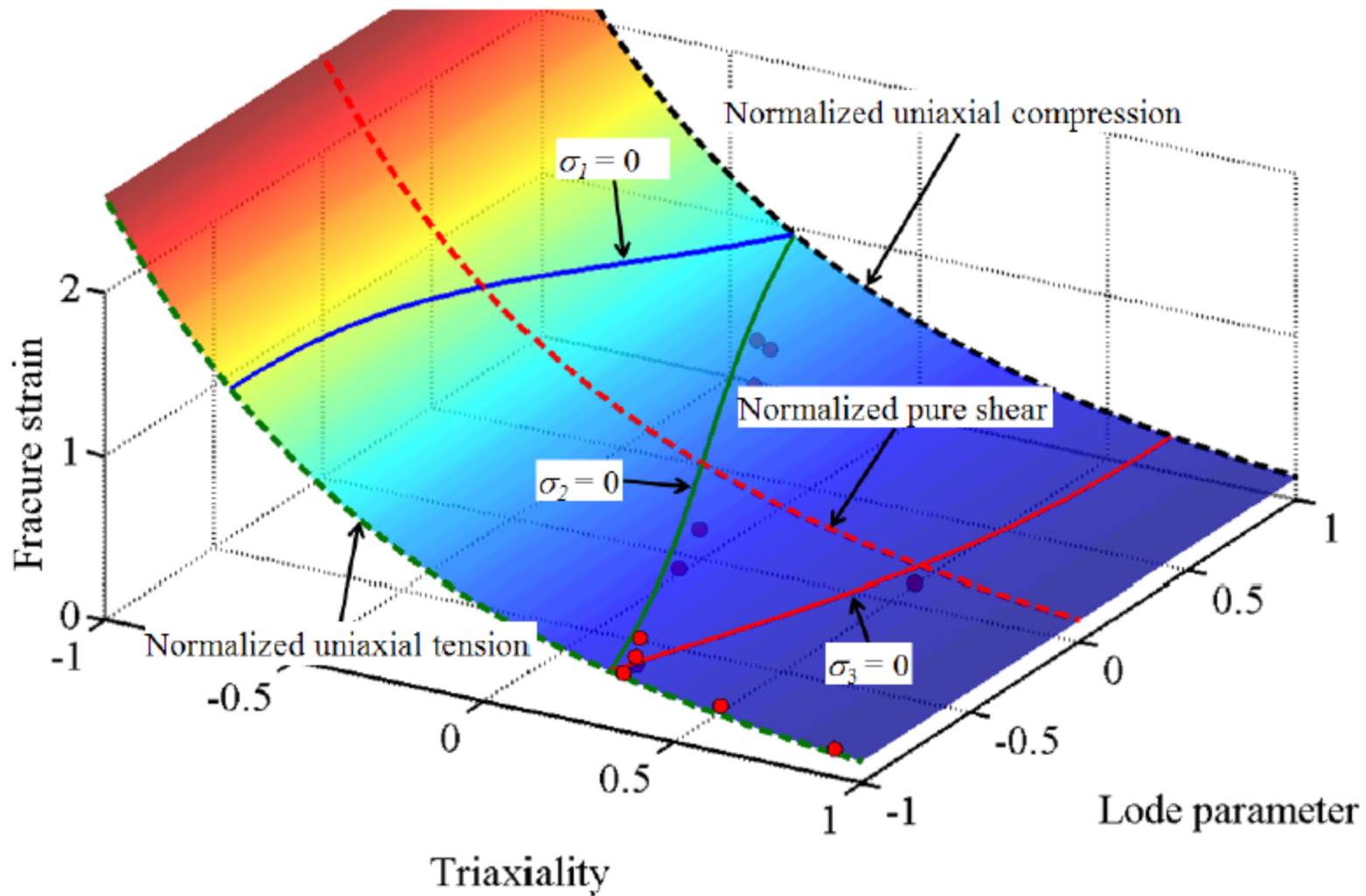
Triaxiality : $\eta = \frac{\sigma_m}{\bar{\sigma}} = \frac{\sigma_1 + \sigma_2 + \sigma_3}{3\bar{\sigma}}$

Lode parameter: $L = \frac{2\sigma_2 - \sigma_1 - \sigma_3}{\sigma_1 - \sigma_3}$



Rice Tracy Model

$$\bar{\varepsilon}_p = f(\eta) = Ce^{-\lambda\eta}$$



Lode angle parameter

- Stress triaxiality:

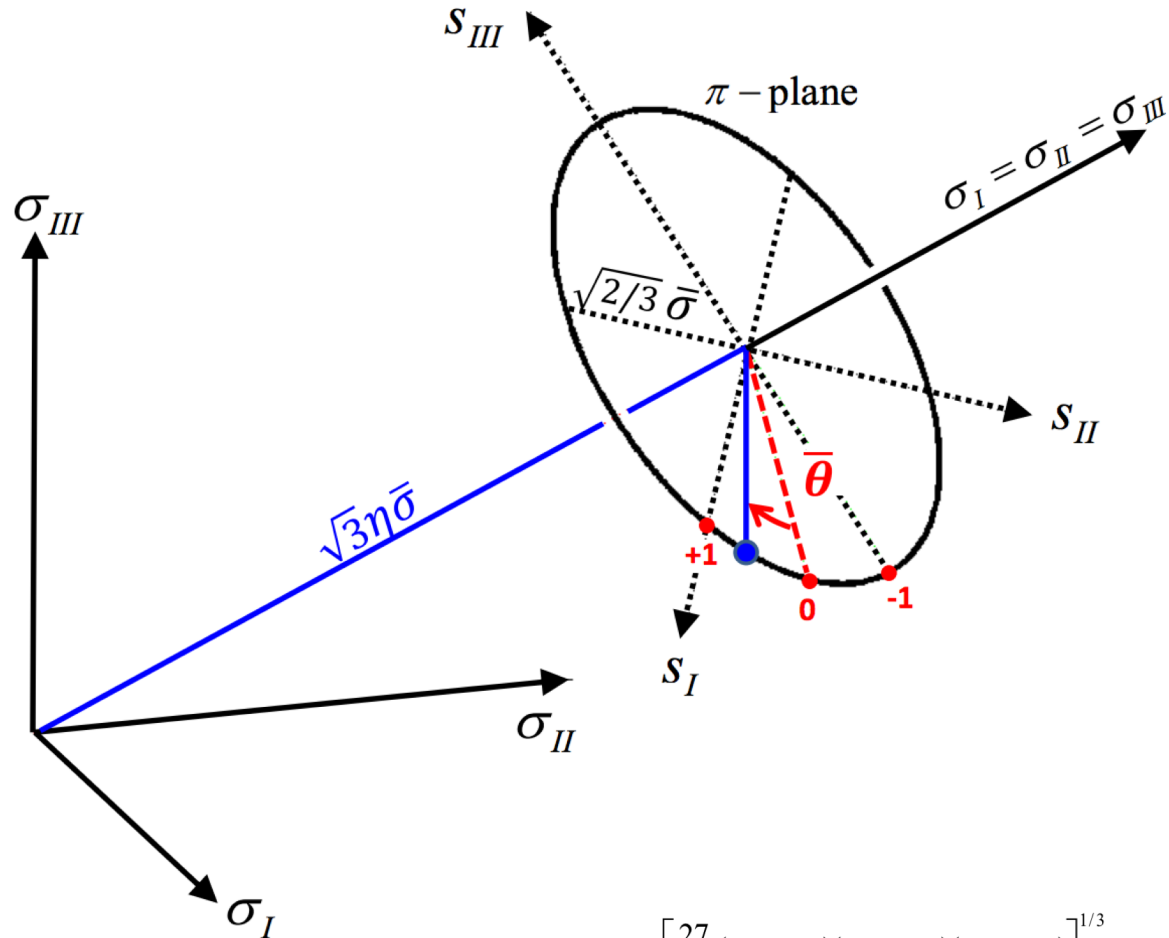
$$\eta = \frac{\sigma_m}{\bar{\sigma}}$$

- Normalized third stress invariant

$$\xi = \frac{27}{2} \frac{J_3}{\bar{\sigma}^3}$$

- Lode angle parameter

$$\bar{\theta} = 1 - \frac{2}{\pi} \arccos(\xi)$$



$$r = \left[\frac{27}{2} (\sigma_1 - \sigma_m)(\sigma_2 - \sigma_m)(\sigma_3 - \sigma_m) \right]^{1/3}$$

$$\xi = \cos(3\theta) = \left(\frac{r}{\bar{\sigma}} \right)^3 \quad (\text{Lode angle : } \theta)$$

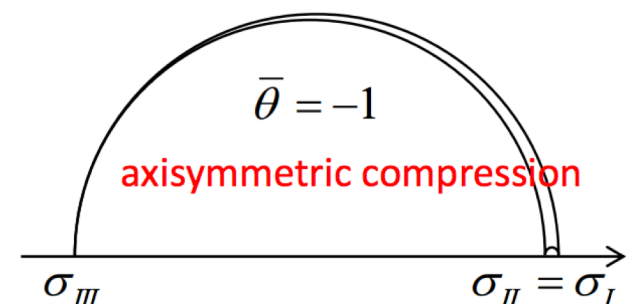
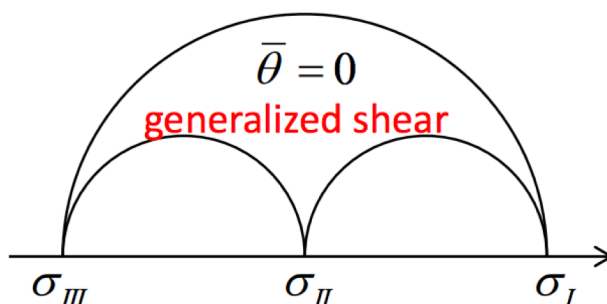
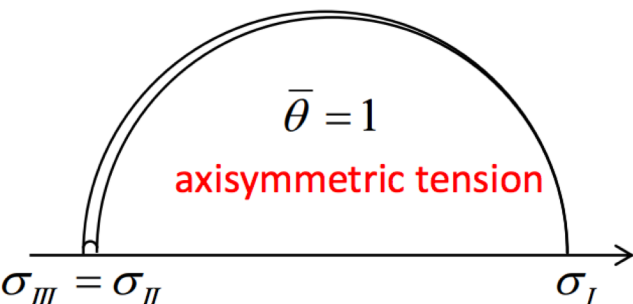
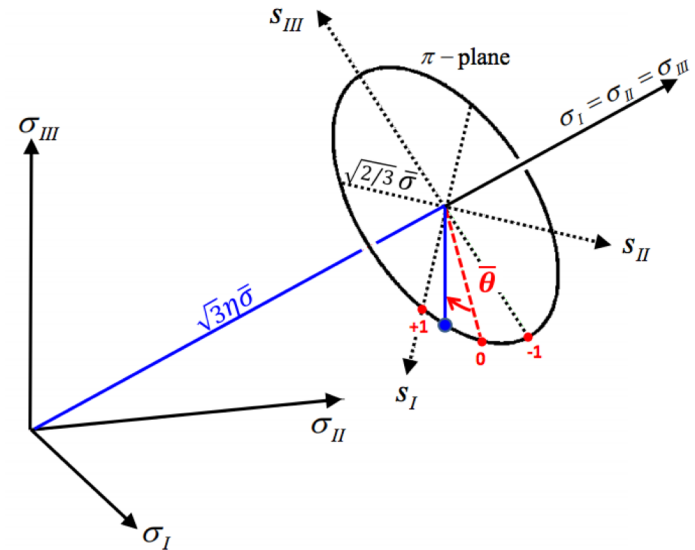
Lode angle parameter

- Lode parameter (Lode, 1926)

$$L = \frac{2\sigma_{II} - \sigma_I - \sigma_{III}}{\sigma_I - \sigma_{III}}$$

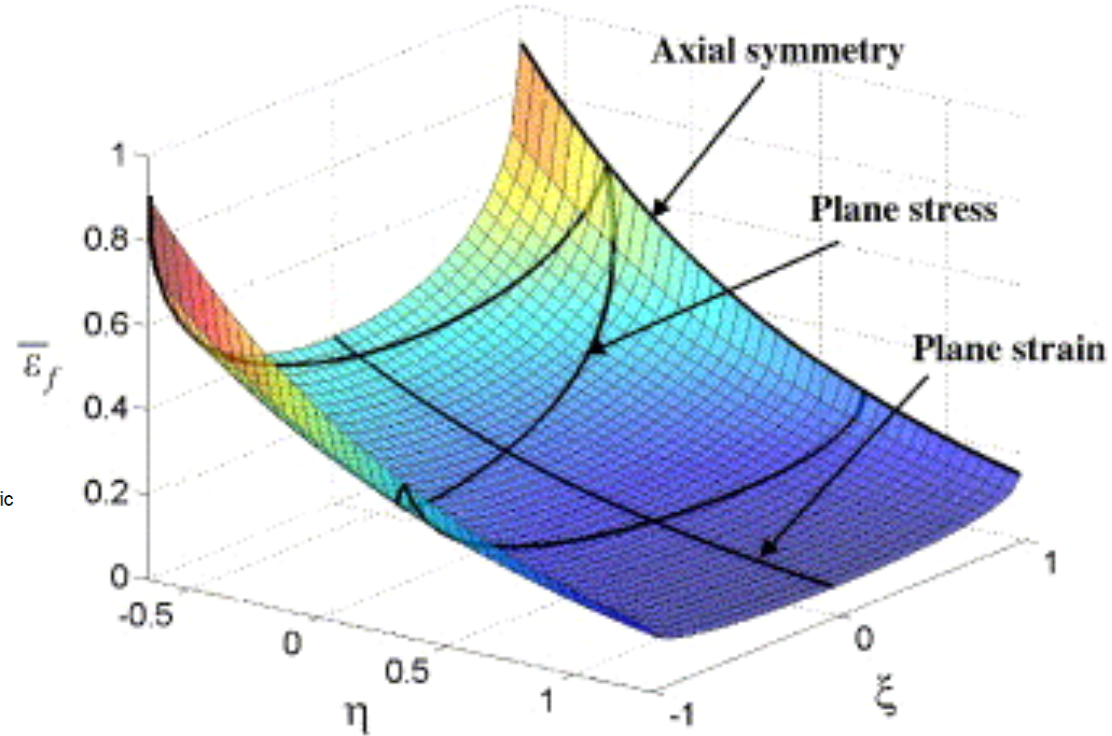
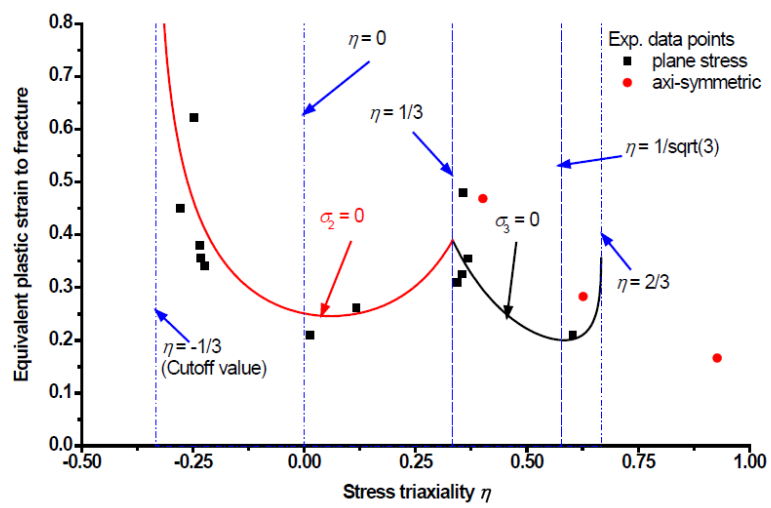
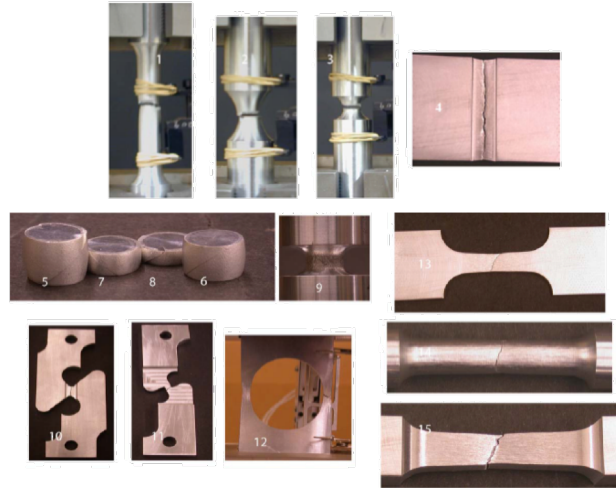
- Lode angle parameter

$$\bar{\theta} = 1 - \frac{2}{\pi} \arccos(\xi) \cong -L$$

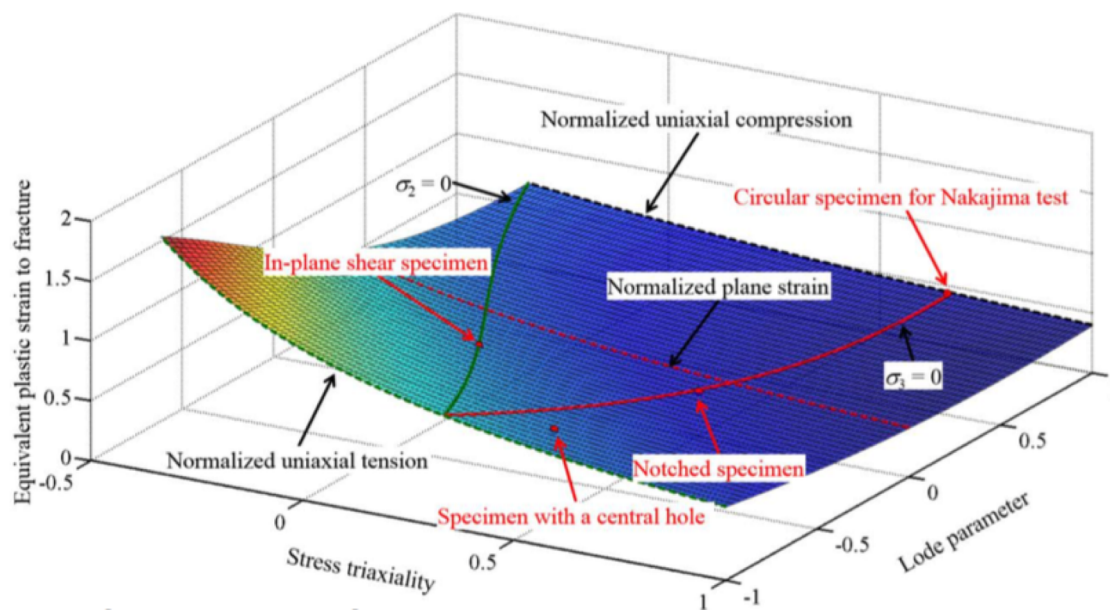
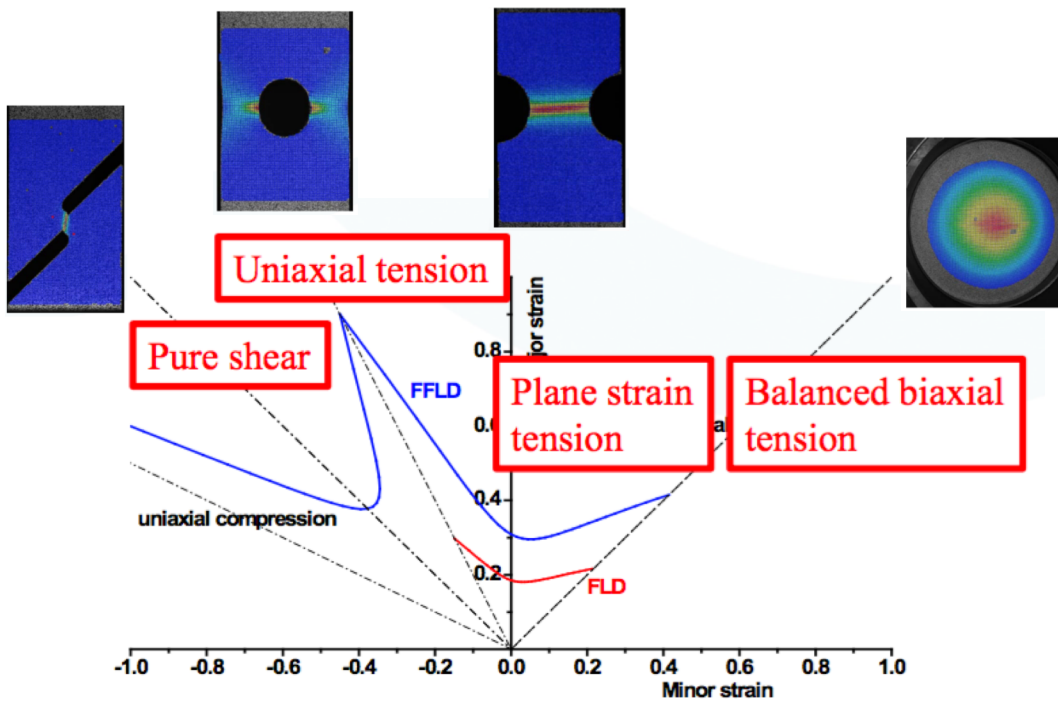


Wierzbicki et al. (2005) Model

$$\bar{\varepsilon}_p = f_o(\eta)(1 - \bar{\theta}^2) + f_1(\eta)\bar{\theta}^2$$



Fracture Experiment and Calibration



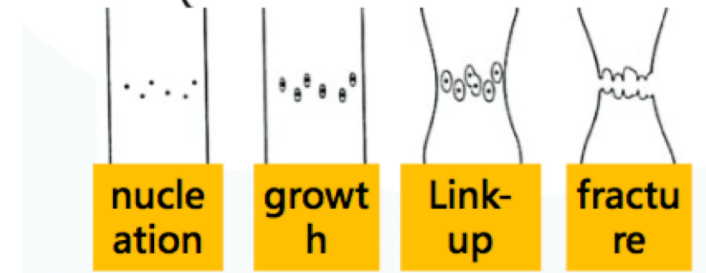
Recent Fracture Models

Lou-Huh (2012)

$$\left(\frac{2\tau_{\max}}{\bar{\sigma}}\right)^{C_1} \left(\frac{\langle 1 + 3\eta \rangle}{2}\right)^{C_2} \bar{\varepsilon}_f = C_3$$

Shear coalescence Void growth nucleation

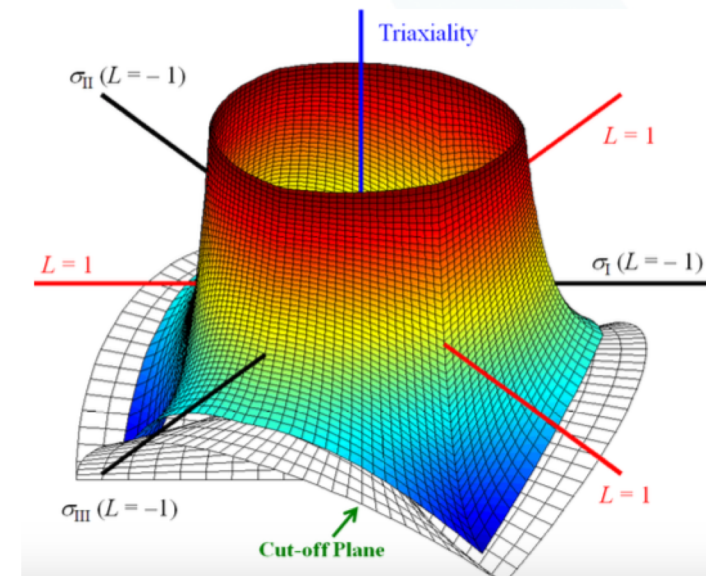
$$\langle x \rangle = \begin{cases} x & \text{when } x \geq 0 \\ 0 & \text{when } x < 0 \end{cases}$$



Lou et al. (2014, Int. J. Plasticity)

$$\left(\frac{2\tau_{\max}}{\bar{\sigma}}\right)^{C_1} \left(\frac{f(\eta, L)}{f(1/3, -1)}\right)^{C_2} \bar{\varepsilon}_f = C_3$$

with $f(\eta, L) = \frac{\sigma_1}{\bar{\sigma}} + C = \eta + \frac{(3+L)}{3\sqrt{L^2+3}} + C$



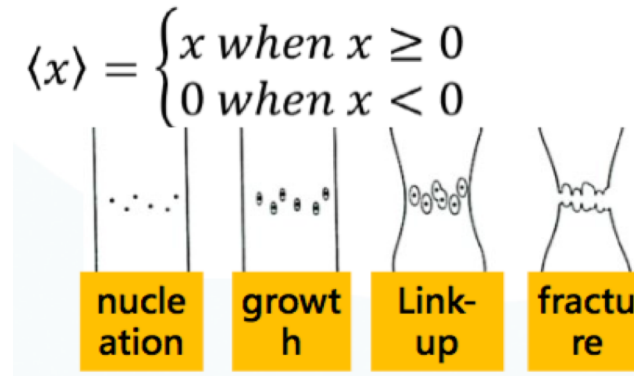
Approach-1 (Anisotropic Fracture Model):

Incorporating Linear Transformation in Strain Space (Lou and Yoon (2017), Int. J. Plasticity)

$$\left(\frac{2\tau_{\max}}{\bar{\sigma}}\right)^{C_1} \left(\frac{\langle 1 + 3\eta \rangle}{2}\right)^{C_2} \bar{\varepsilon}_f = C_3$$

Shear coalescence
 Void growth
 nucleation

(Lou and Huh, 2012)



Fracture strain from Strain-rate potential (Barlat et al., 1993)

$$\psi = |d\boldsymbol{\epsilon}_1^d|^b + |d\boldsymbol{\epsilon}_2^d|^b + |d\boldsymbol{\epsilon}_3^d|^b = 2(d\bar{\boldsymbol{\epsilon}}^p)^b$$

$$d\boldsymbol{\epsilon}^d = \mathbf{D} d\boldsymbol{\epsilon}^p$$

$$\mathbf{D} = \begin{bmatrix} 0 & -d_{12} & -d_{13} & 0 & 0 & 0 \\ -d_{21} & 0 & -d_{23} & 0 & 0 & 0 \\ -d_{31} & -d_{32} & 0 & 0 & 0 & 0 \\ 0 & 0 & 0 & d_{44} & 0 & 0 \\ 0 & 0 & 0 & 0 & d_{55} & 0 \\ 0 & 0 & 0 & 0 & 0 & d_{66} \end{bmatrix}, \quad d\boldsymbol{\epsilon}^p = \begin{bmatrix} d\boldsymbol{\epsilon}_{xx}^p \\ d\boldsymbol{\epsilon}_{yy}^p \\ d\boldsymbol{\epsilon}_{zz}^p \\ d\boldsymbol{\epsilon}_{yz}^p \\ d\boldsymbol{\epsilon}_{xz}^p \\ d\boldsymbol{\epsilon}_{xy}^p \end{bmatrix}$$

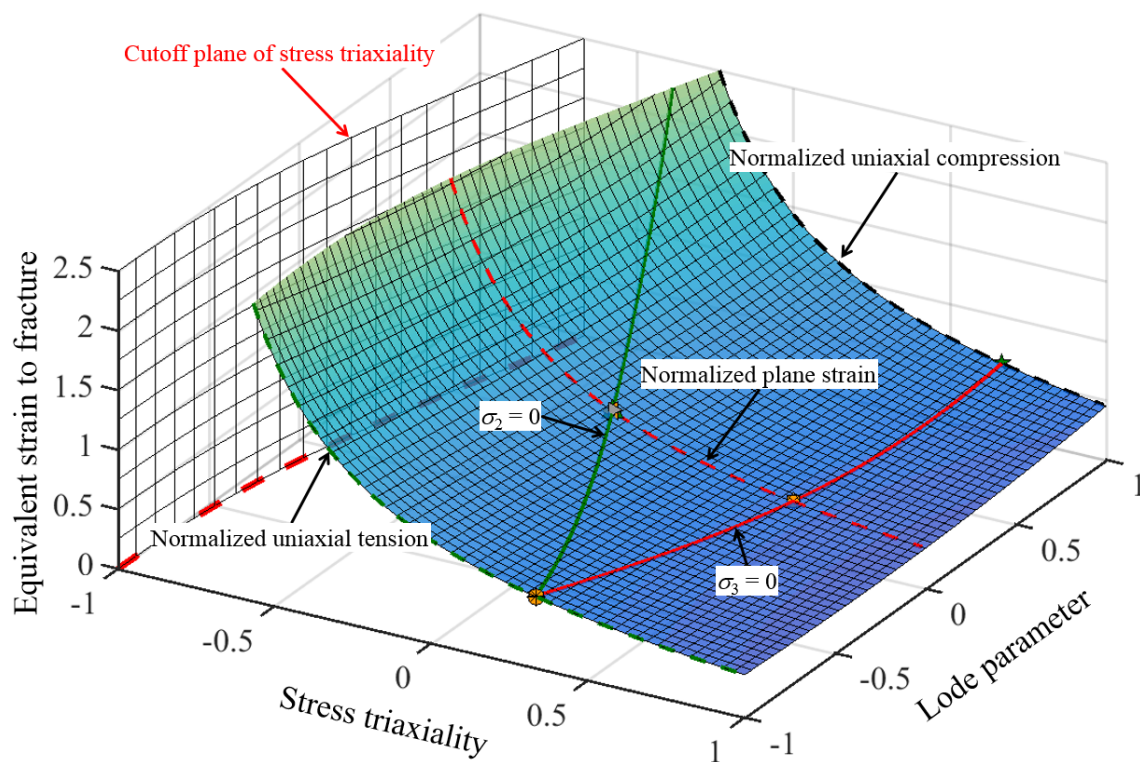
Isotropic equivalent damage strain of 10 experiments

Data Calibration (AA 6k21-IH T4)

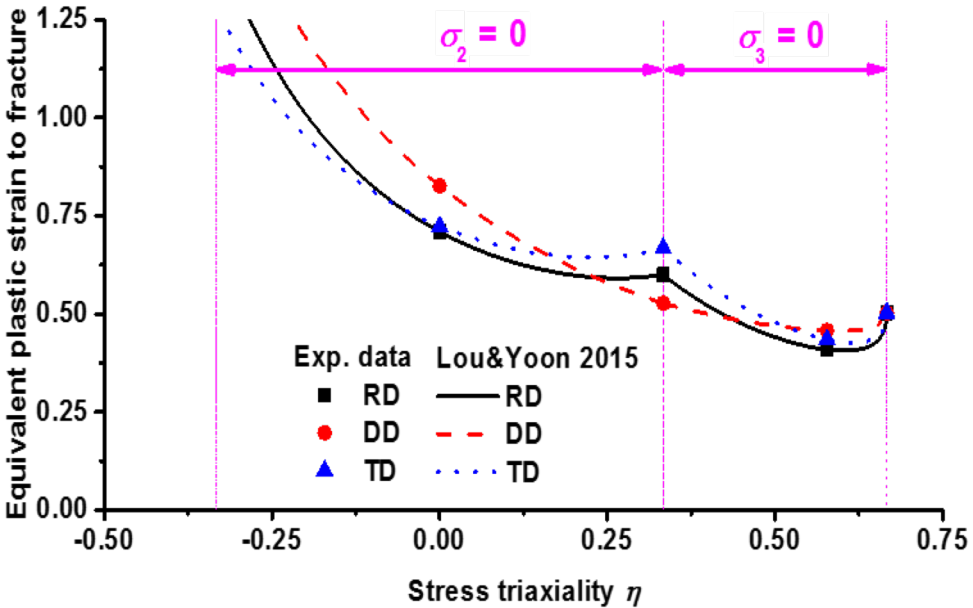
Test type	Pure shear			Uniaxial tension			Plane strain tension			Nakajima test
Loading direction	RD	DD	TD	RD	DD	TD	RD	DD	TD	
$\bar{\varepsilon}^d$	0.8581	0.8665	0.8751	0.6004	0.5996	0.6006	0.4656	0.4672	0.4655	0.6014

Fracture coefficients calibrated by experiments in Table 2 ($C_3 = 0.6005, C = 1/3, d_{44} = d_{55} = d_{66}$)

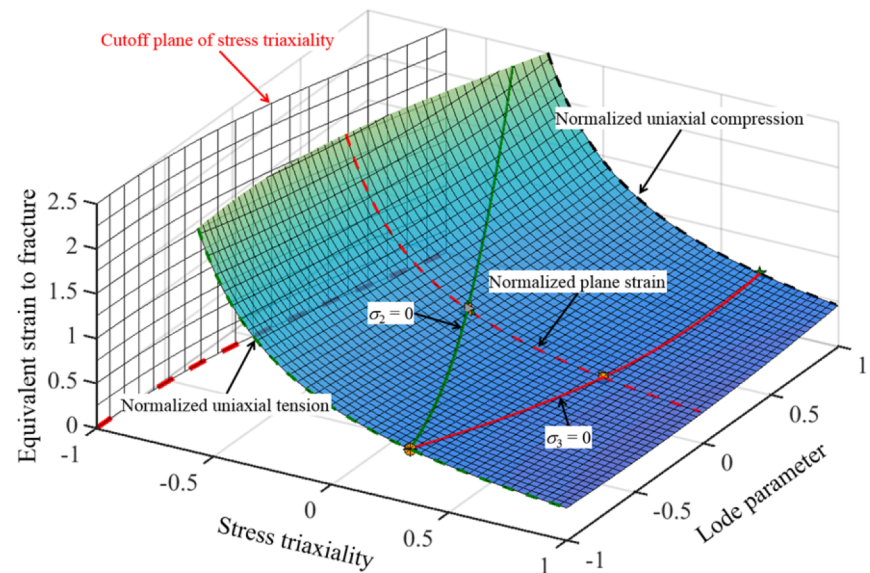
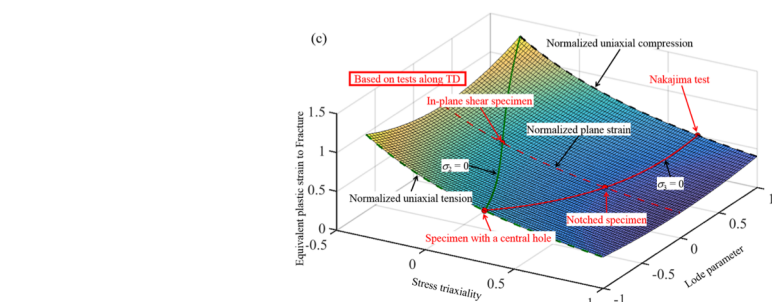
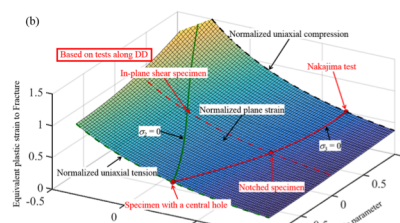
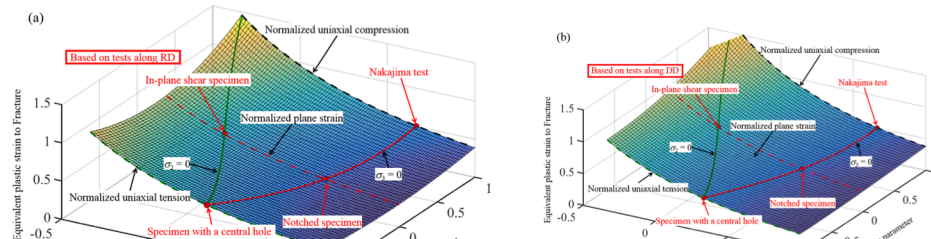
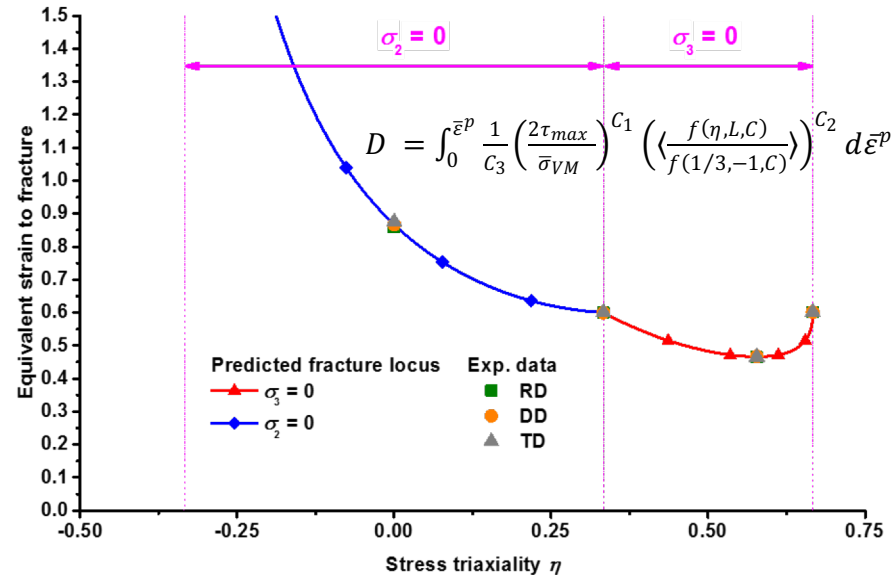
C_1	C_2	d_{12}	d_{13}	d_{23}	d_{21}	d_{31}	d_{32}	d_{66}
0.7966	1.2625	1.1408	1.7796	1.6986	1.1592	0.3140	0.0402	1.3966



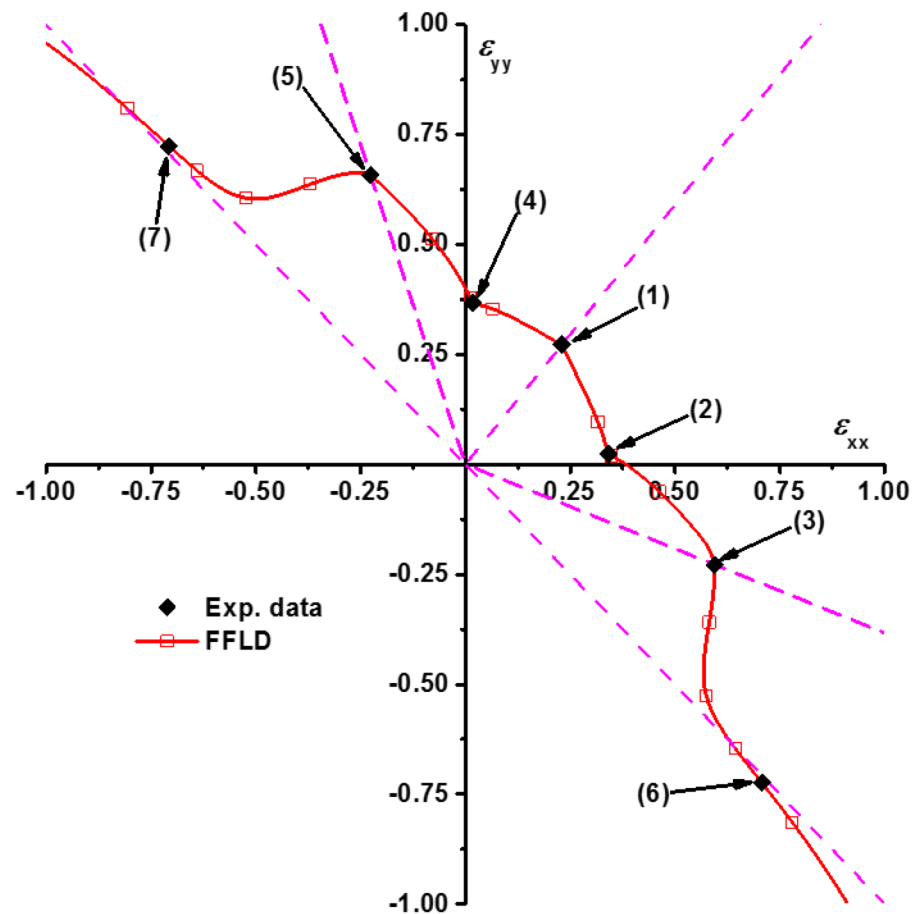
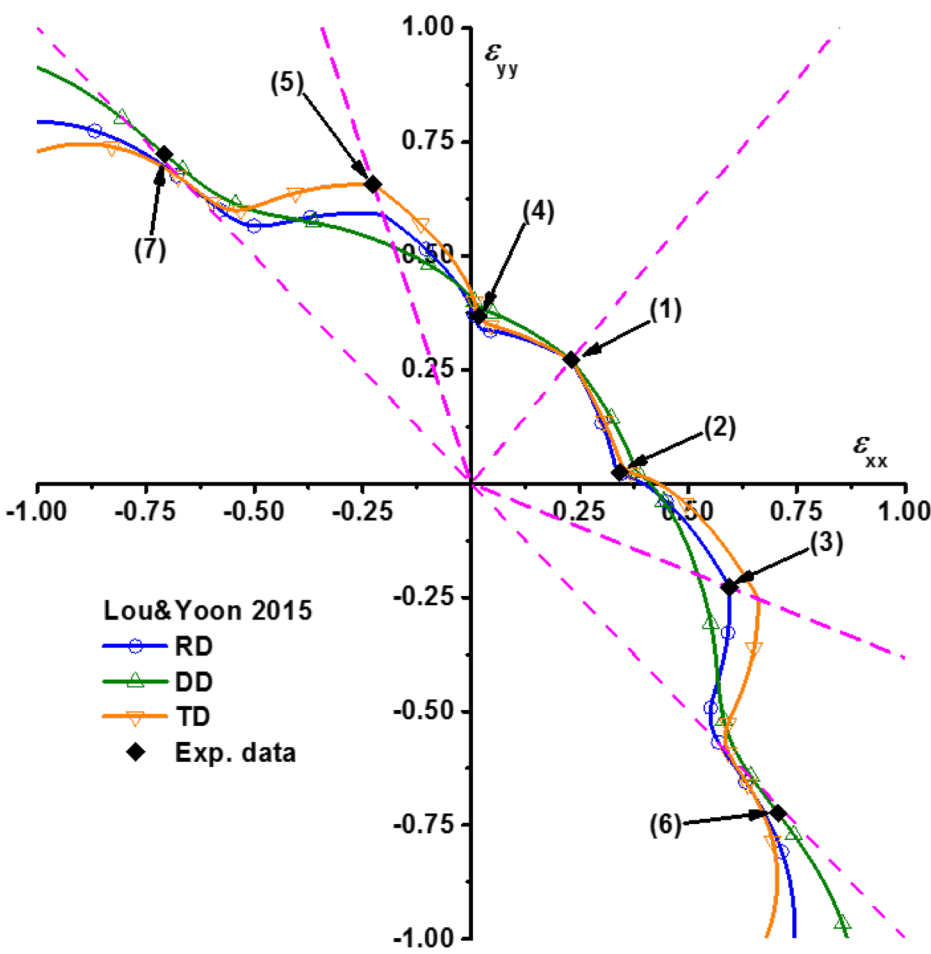
Isotropic fracture model



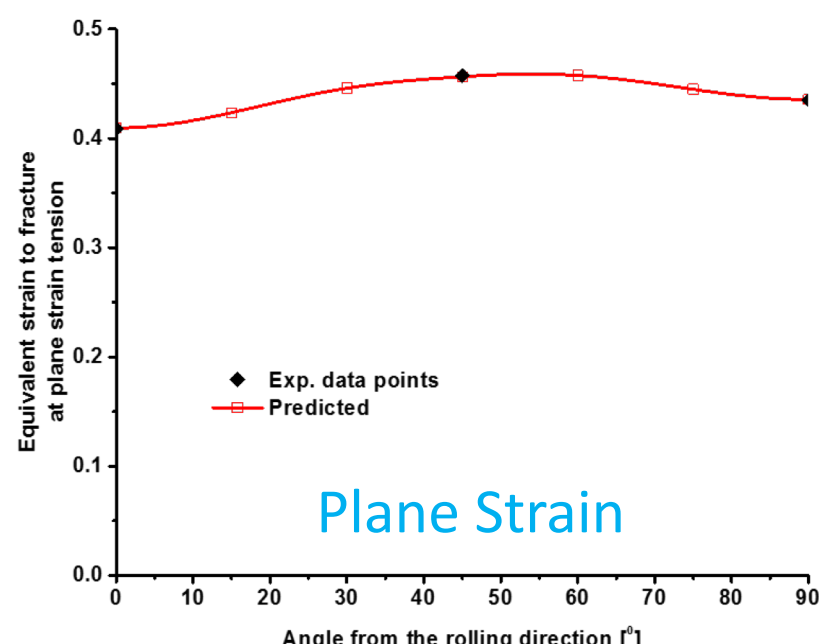
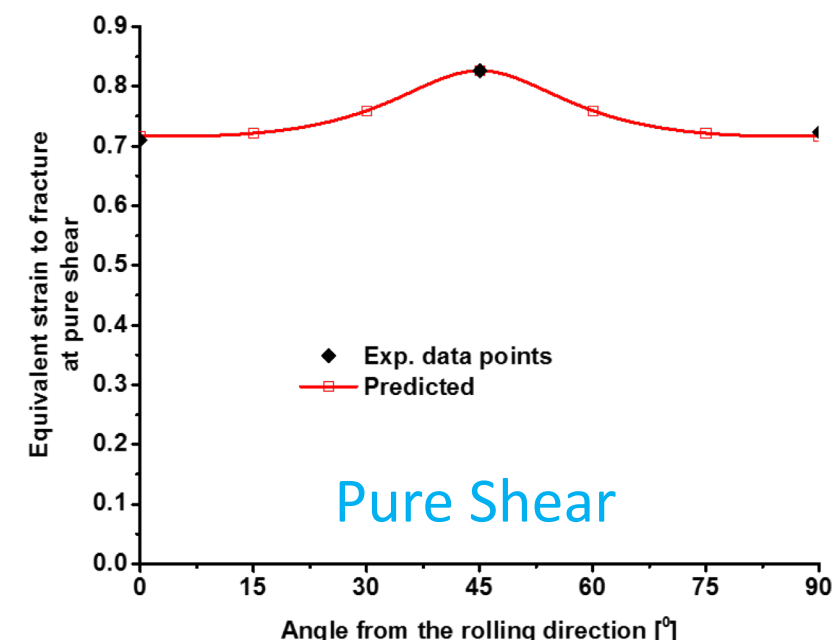
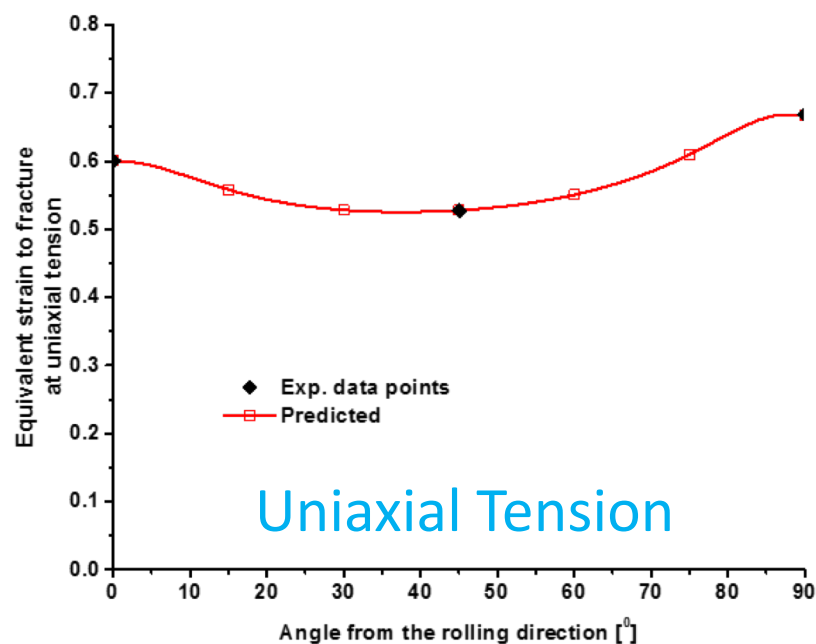
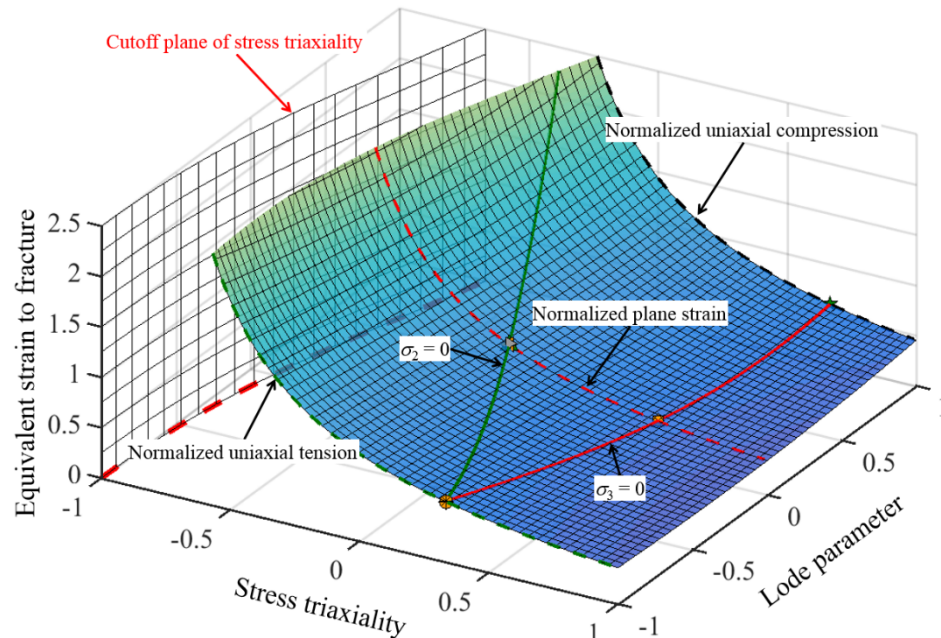
Anisotropic fracture model



Comparison between isotropic and anisotropic fracture models in the principal space



Linear Transformation-Based Anisotropic Fracture Model



Approach-2 (Anisotropic Fracture Model): Incorporating anisotropic yield function

Lou, Y., Yoon, J.W., 2018, “Alternative approach to model ductile fracture by incorporating anisotropic yield function, Int. J. Solids and Structures, Volume 164, pp.12-24.

$$\left(\frac{2\tau_{max}}{\bar{\sigma}}\right)^{C_1} \left(\frac{f(\eta, L)}{f(1/3, -1)}\right)^{C_2} \bar{\varepsilon}_f = C_3$$

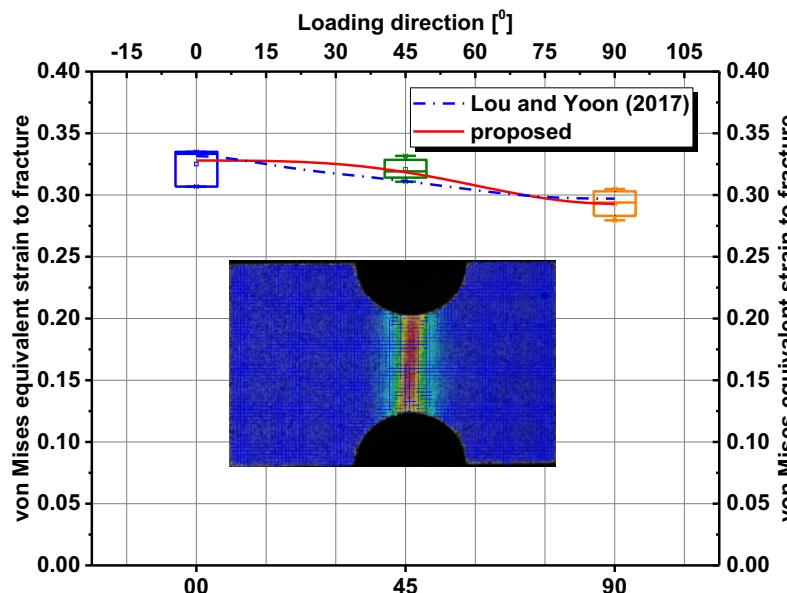
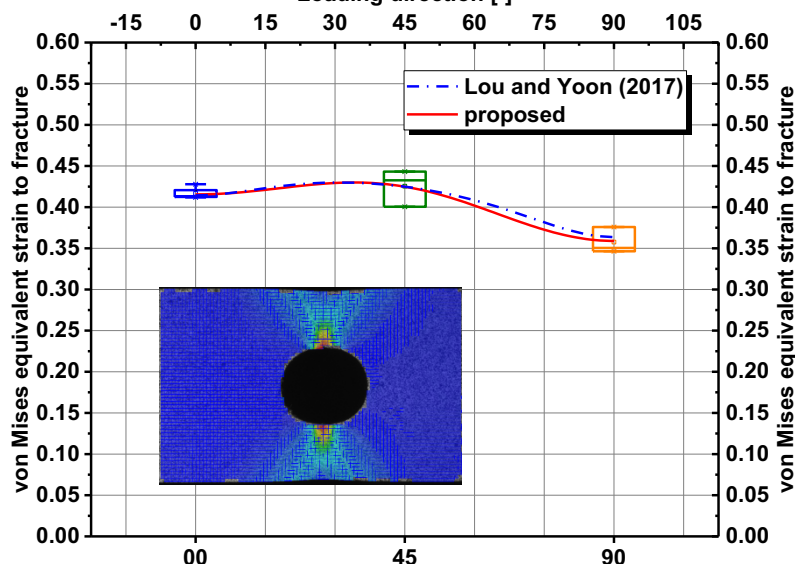
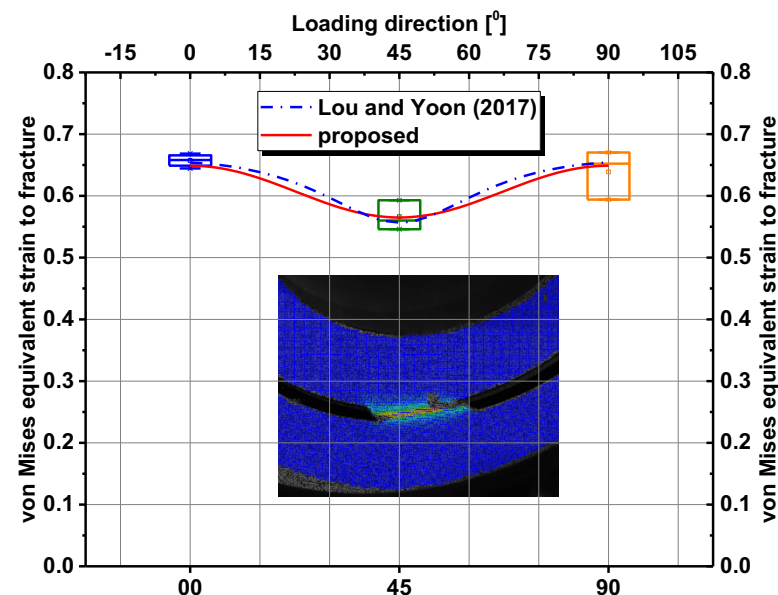
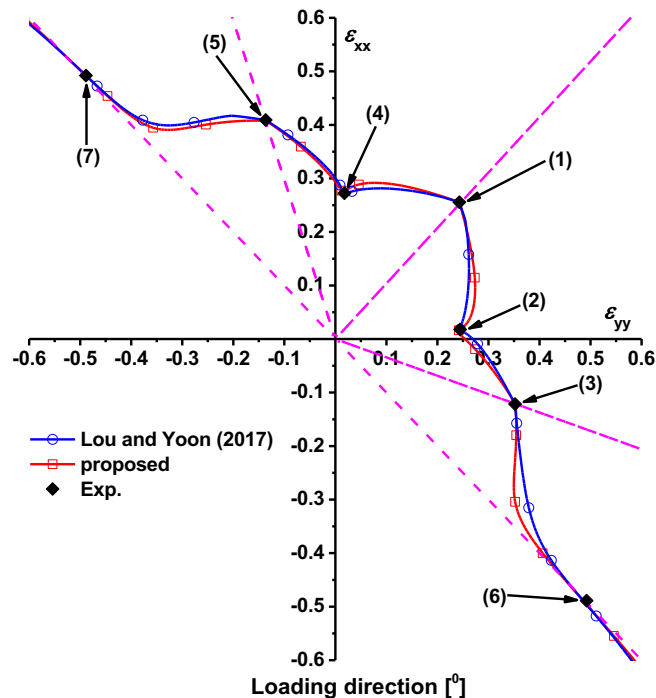
with $f(\eta, L, C) = \eta + C_4 \frac{(3 - L)}{3\sqrt{L^2 + 3}} + C$

and

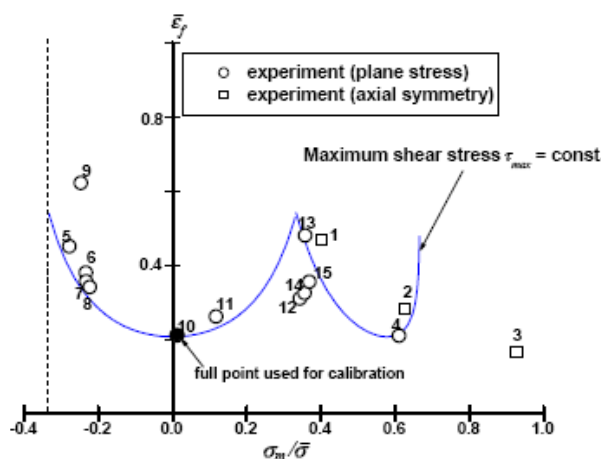
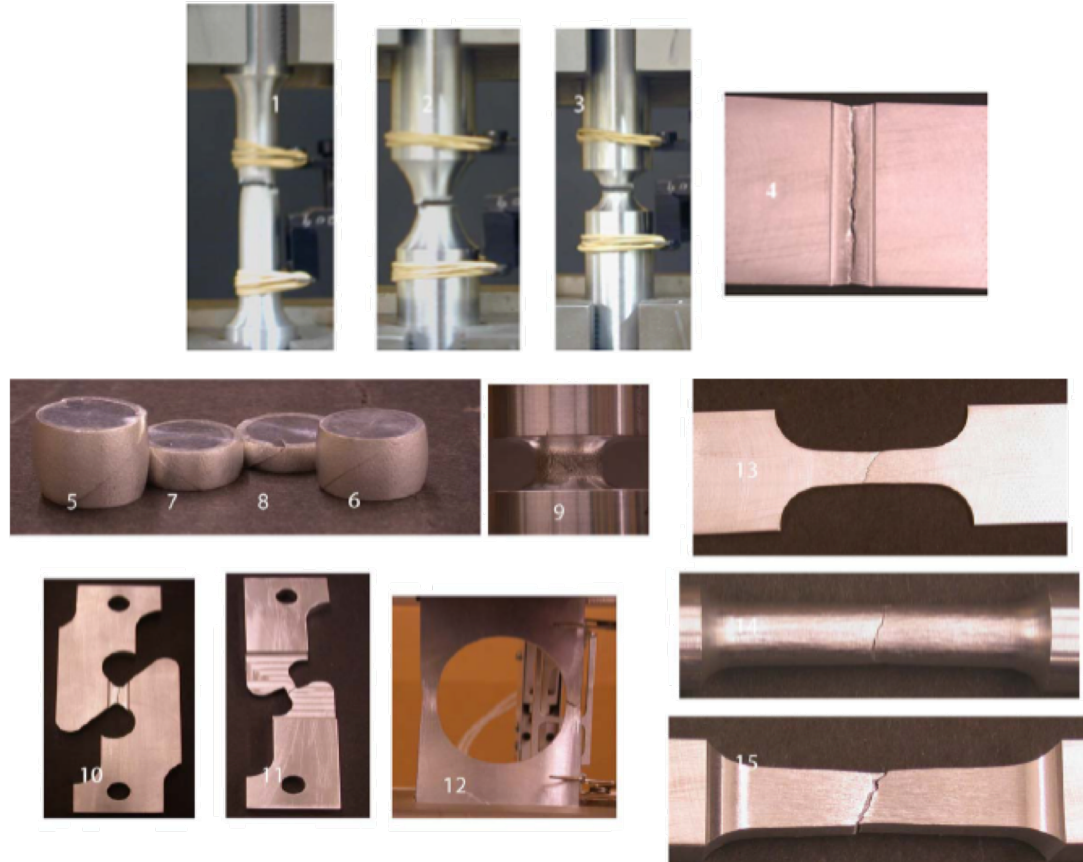
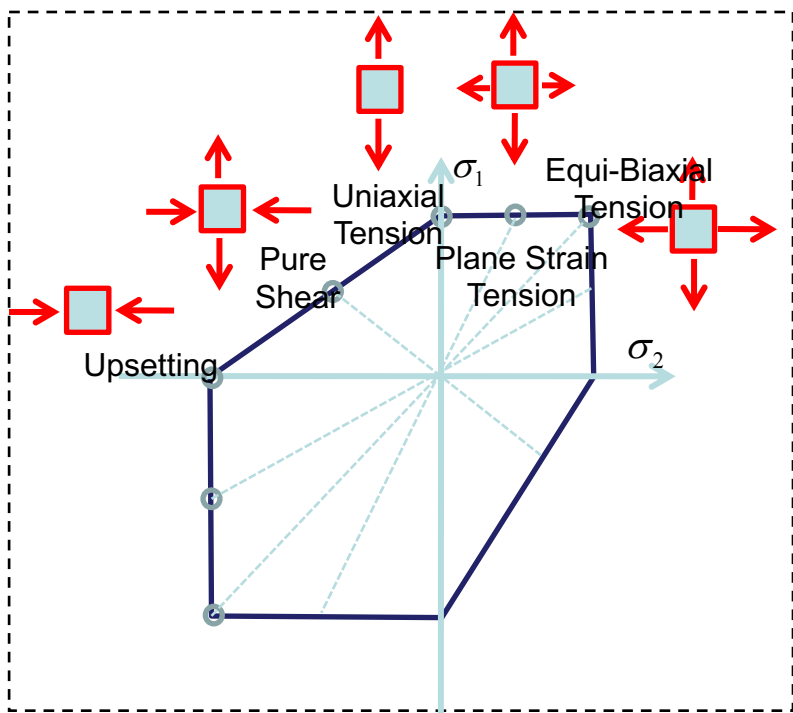
$$\bar{\sigma}_d = \bar{\sigma}_{Hill48} = \sqrt{F(\sigma_{yy} - \sigma_{zz})^2 + G(\sigma_{zz} - \sigma_{xx})^2 + H(\sigma_{xx} - \sigma_{yy})^2 + L\sigma_{yz}^2 + M\sigma_{zx}^2 + N\sigma_{xy}^2}$$

the active plane stress parameters are 8 ($C_1, C_2, C_3, C_4, F, G, H, and N$)

Comparison between Approaches-1 and 2

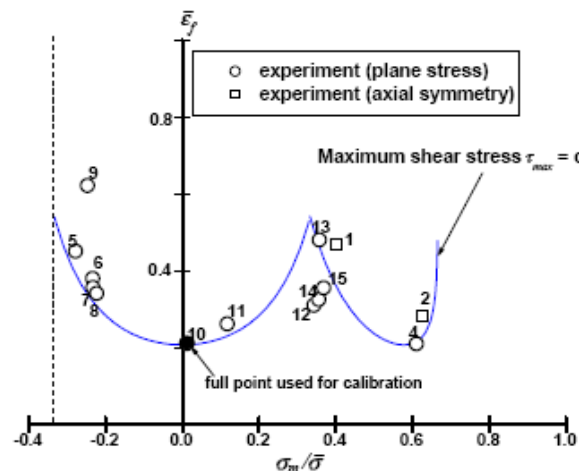


Alternative Approach : Stress-Based Fracture Criterion

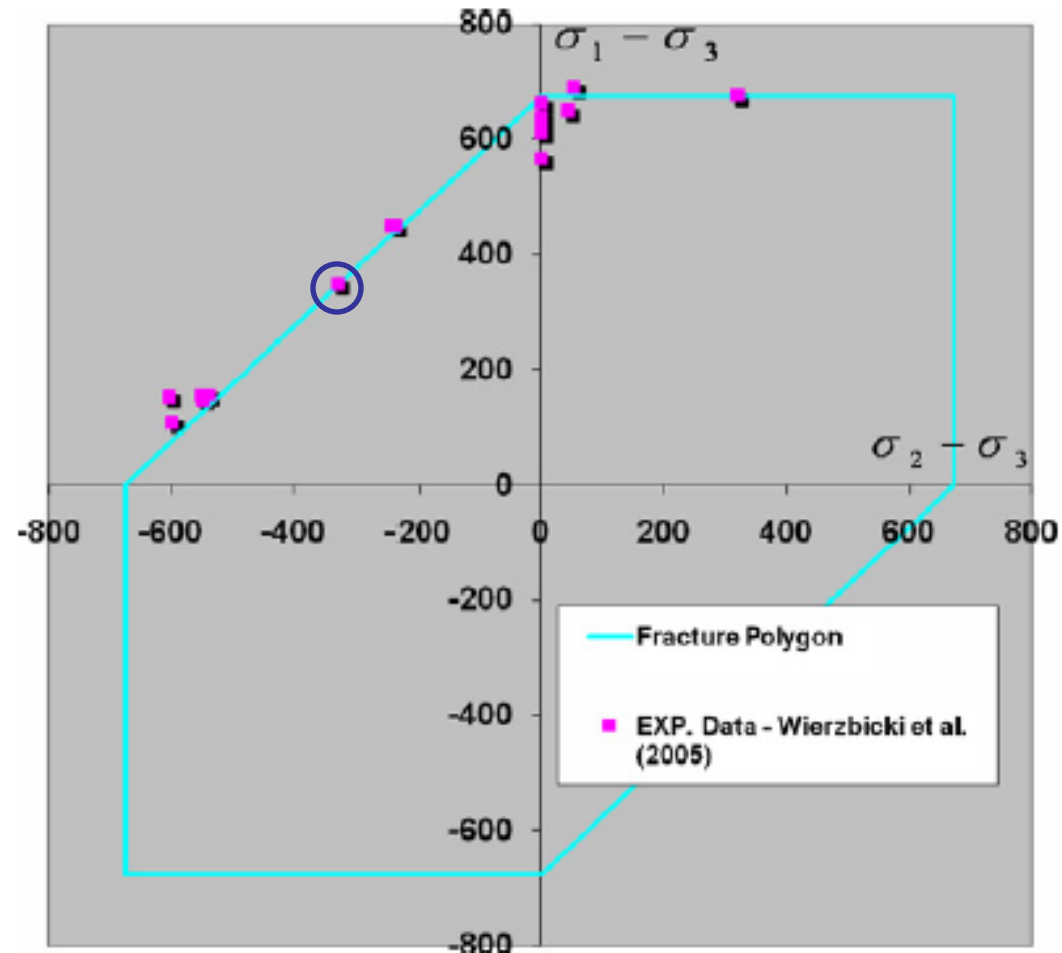


Wierzbick's Experiment (IJMS, 2005)

Representation on Principal Stress Space



Wierzbicki's Presentation

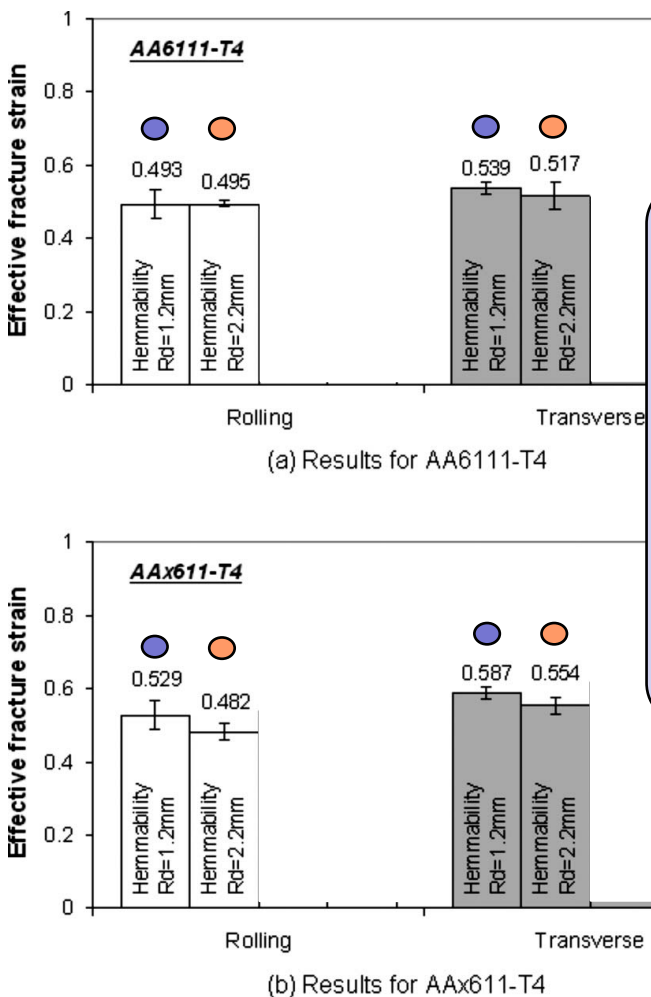


$$f = \frac{\max\left(\frac{|\sigma_1 - \sigma_2|}{\sigma_1}, \frac{|\sigma_2 - \sigma_3|}{\sigma_2}, \frac{|\sigma_3 - \sigma_1|}{\sigma_3}\right)}{\sigma_{MSS}}$$

If $f > 1$: Fracture

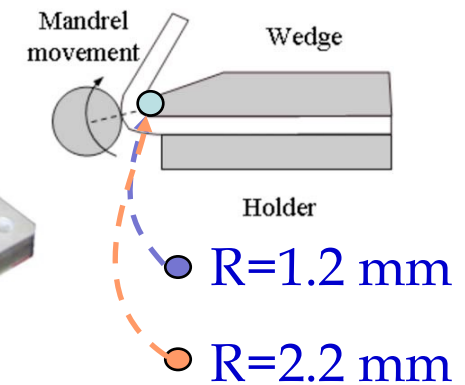
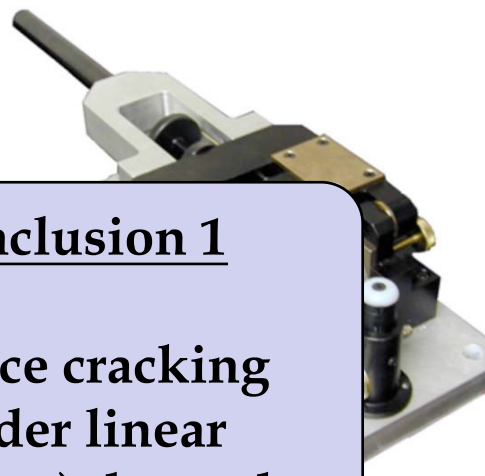
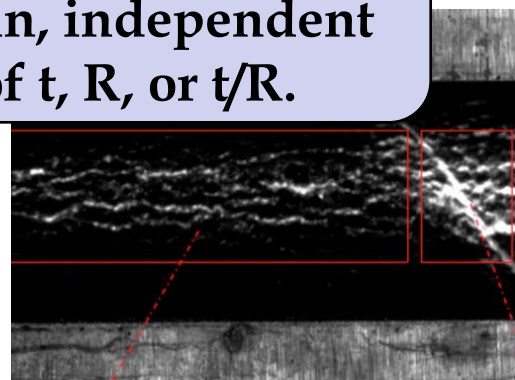
Fracture Model in Stress Space

(Hemming Fracture Study, G. Lin, et al 2006)



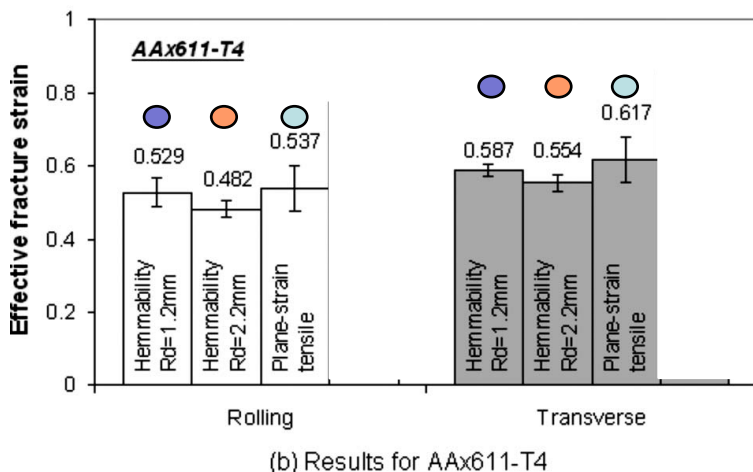
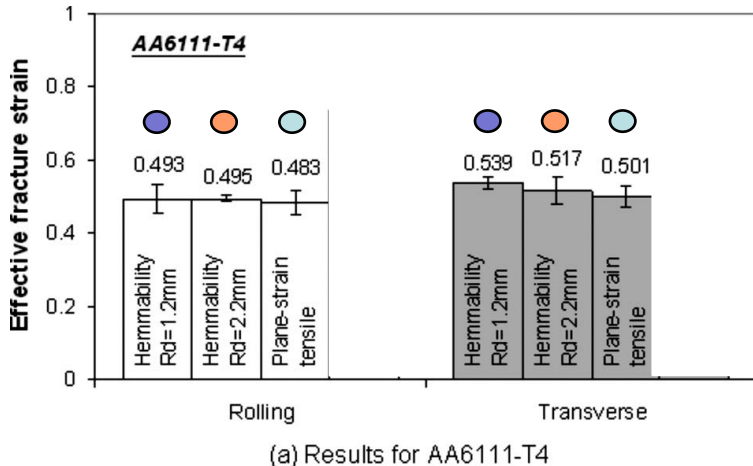
Conclusion 1

Surface cracking
(under linear
straining) depends
only on the surface
strain, independent
of t , R , or t/R .



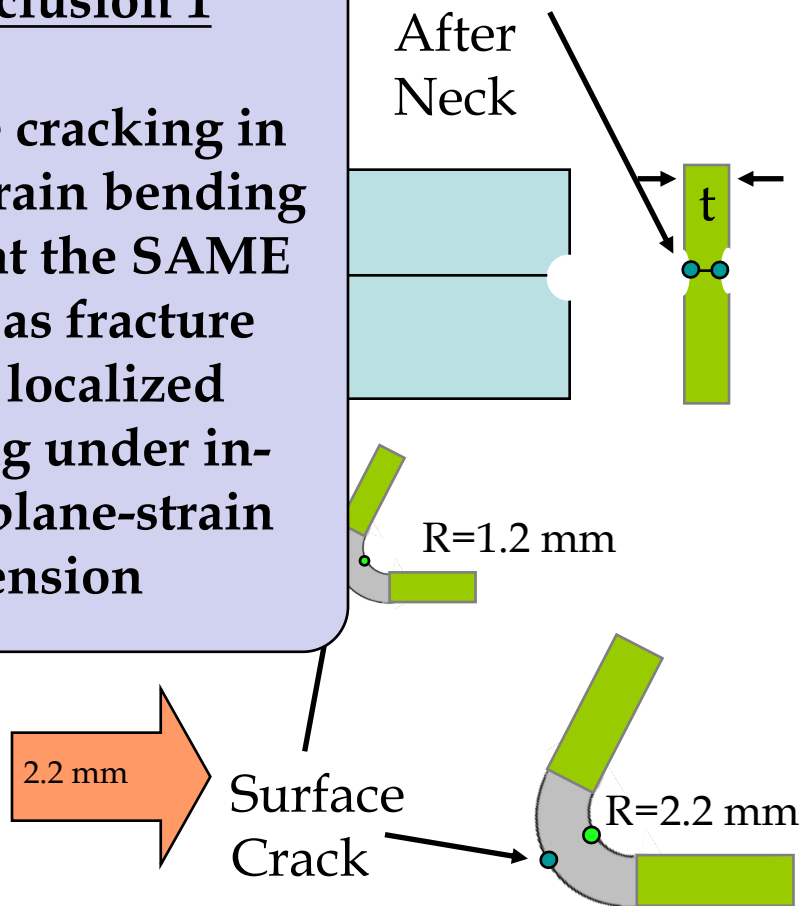
Surface strains are measured at the tome when surface cracks reach a defined detection limit distinct from texture effects

Universal Fracture Criteria

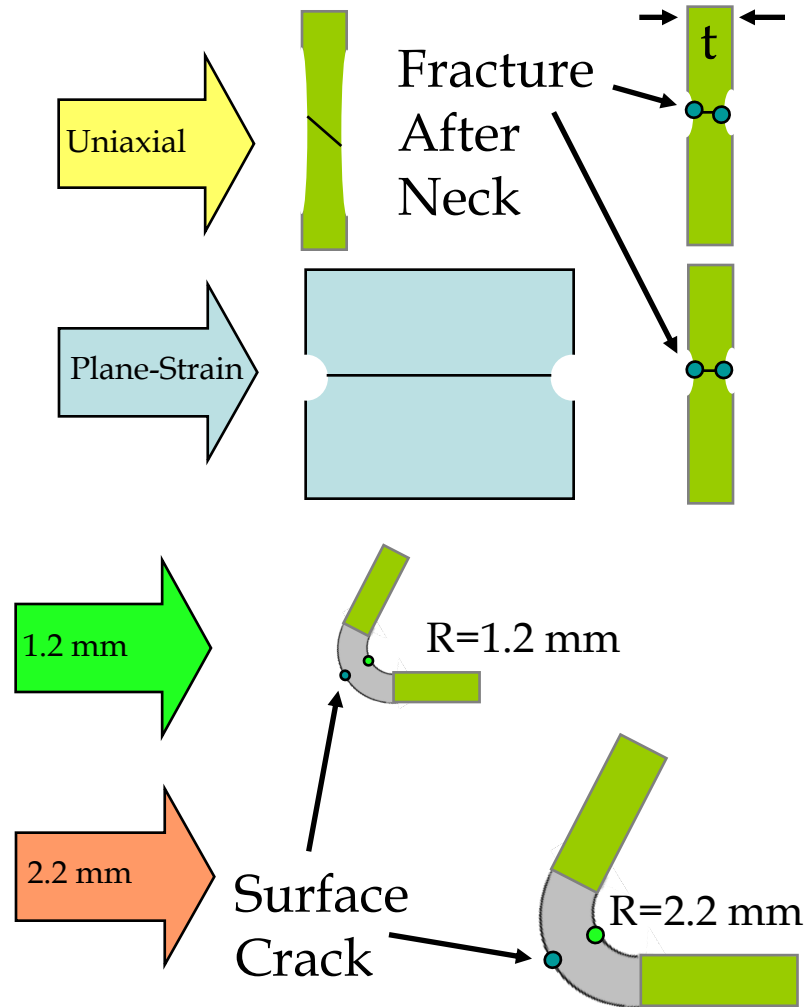
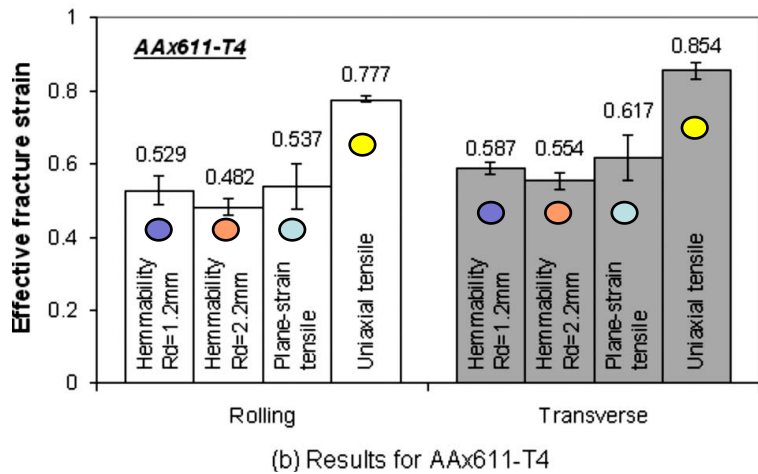
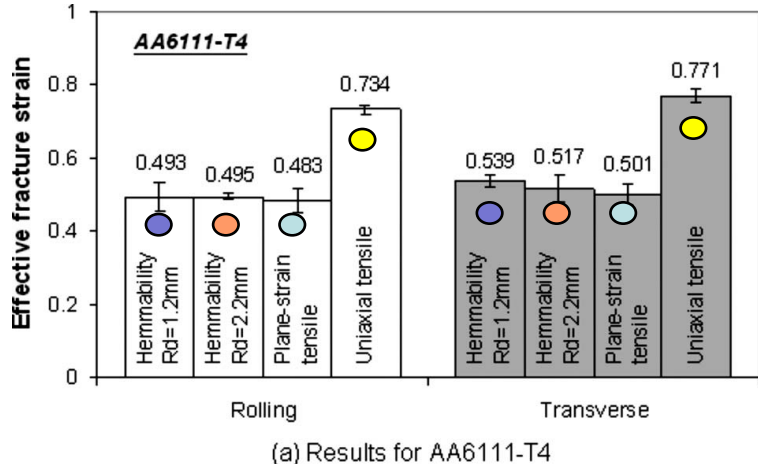


Conclusion 1

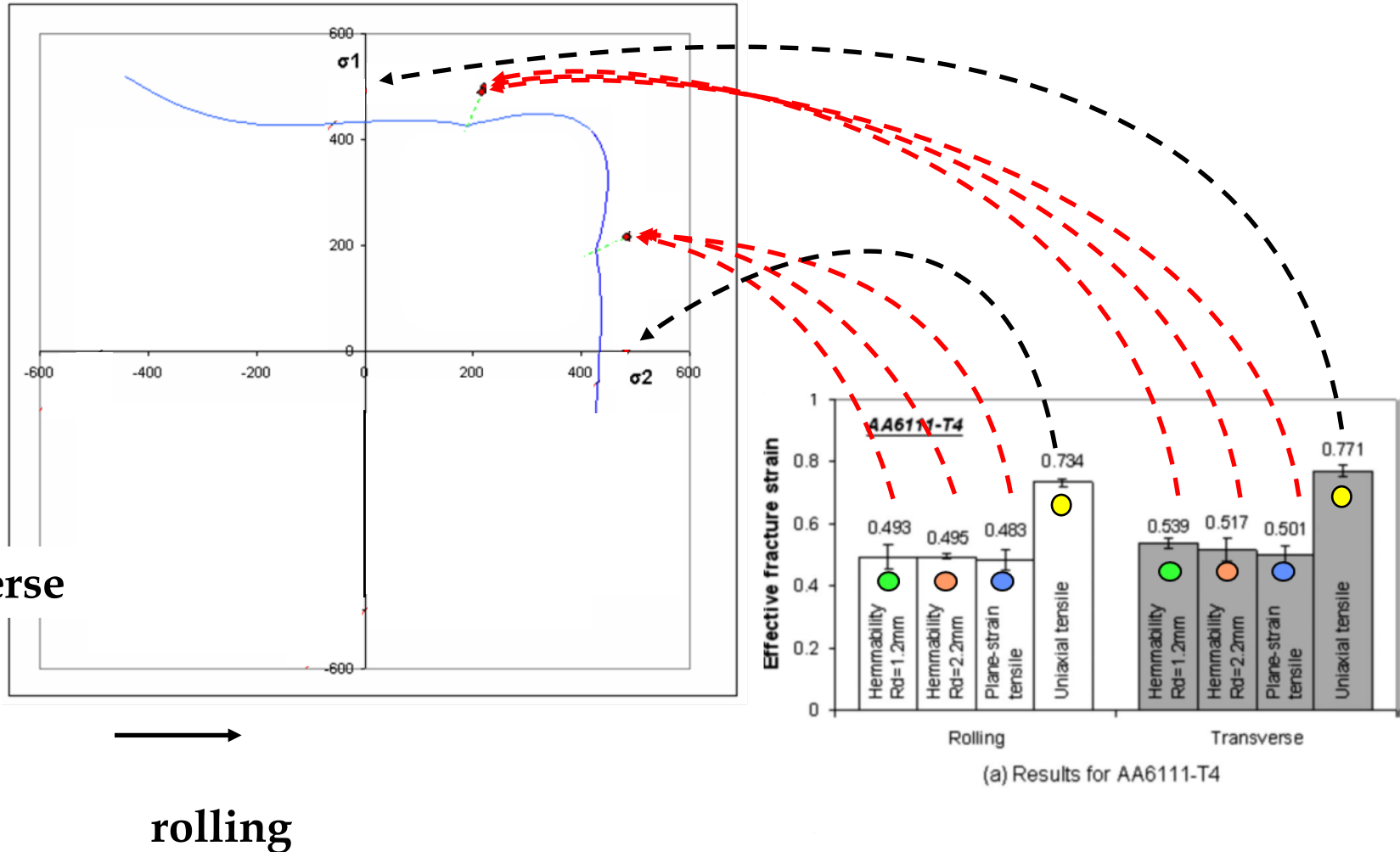
Surface cracking in plane strain bending occurs at the SAME strain as fracture after localized necking under in-plane plane-strain tension



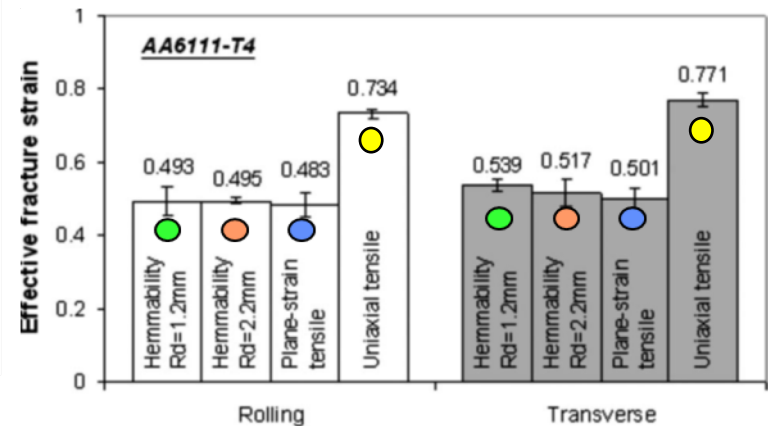
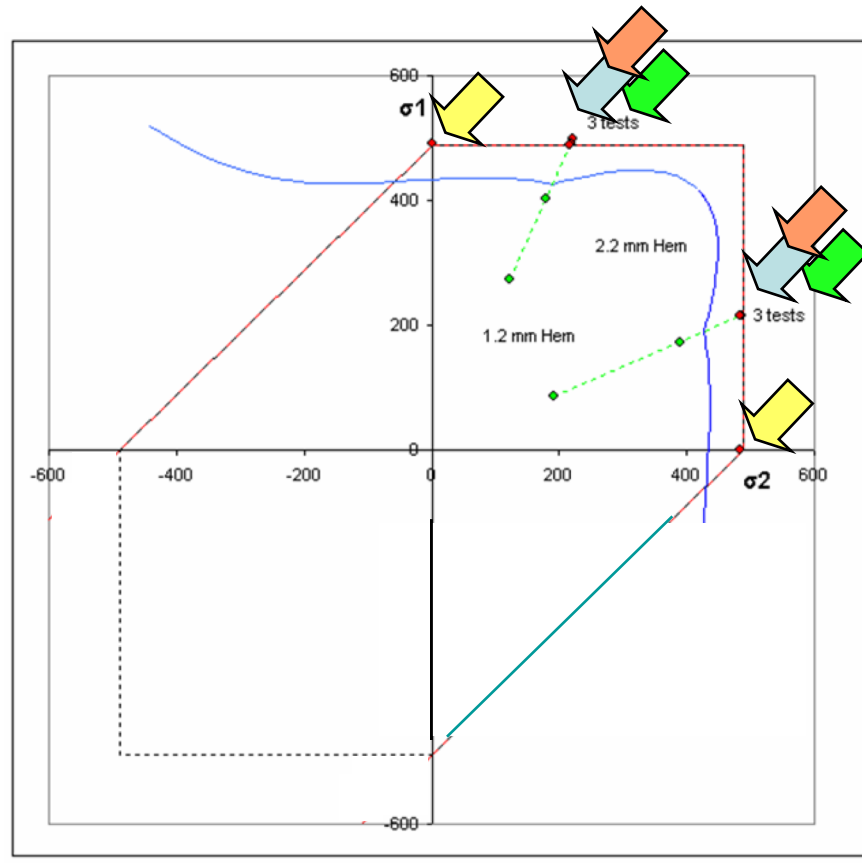
How to Model Fracture ?



Does Stress Space Simplify the Understanding of Fracture?



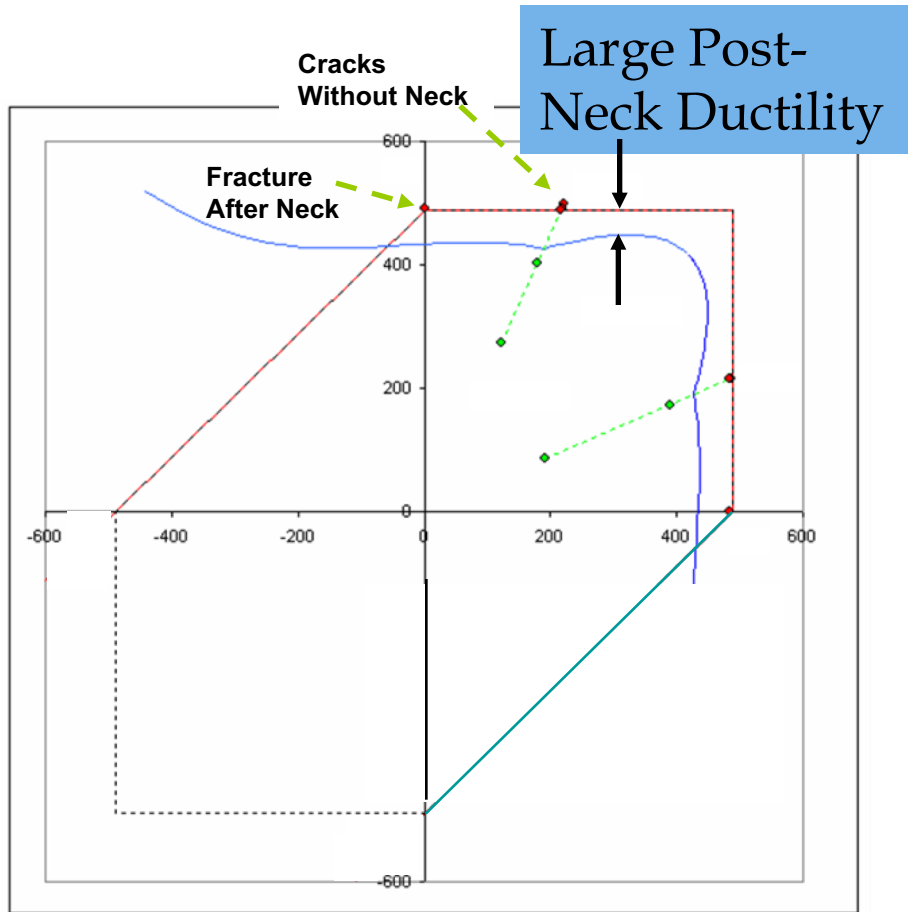
SHEAR Stress may play a critical role in fracture



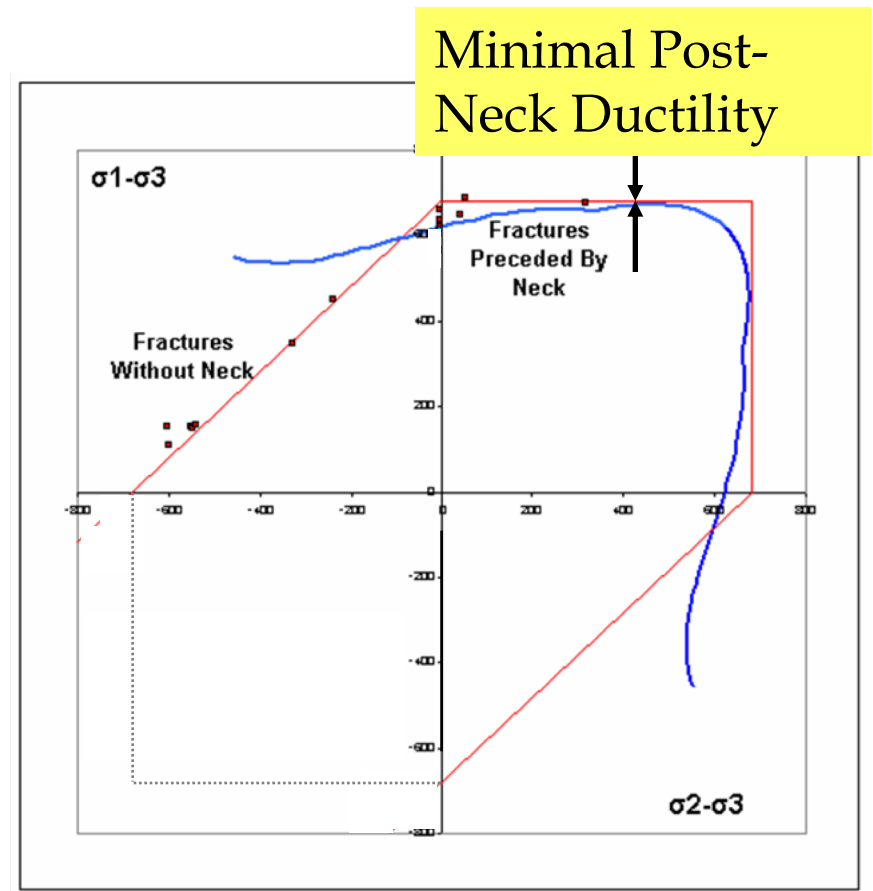
$$\max(\sigma_1, \sigma_2, |\sigma_1 - \sigma_2|) < \sigma_{MS} \quad \text{for} \quad \sigma_2 \geq \sigma_3 = 0$$

Ductile Fracture Vs. Brittle Fracture

Stoughton, T.B., Yoon, J.W., 2011. A new approach for failure criterion for sheet metals. International Journal of Plasticity 27: 440–459.

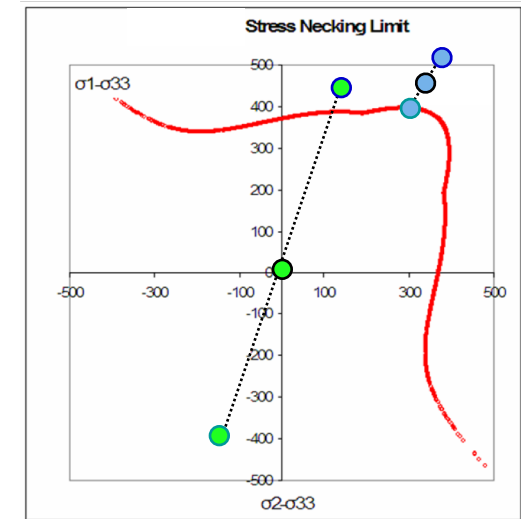
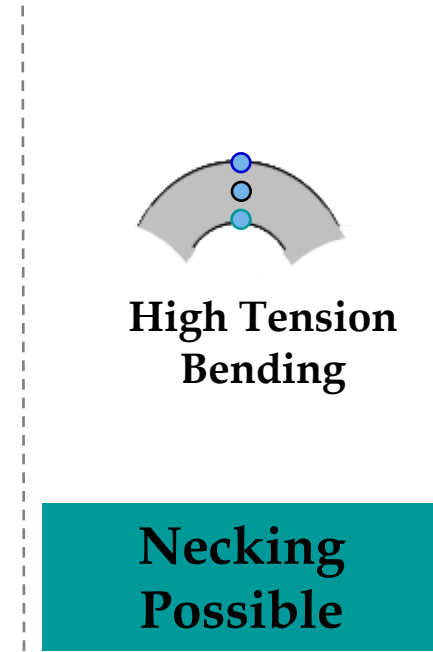
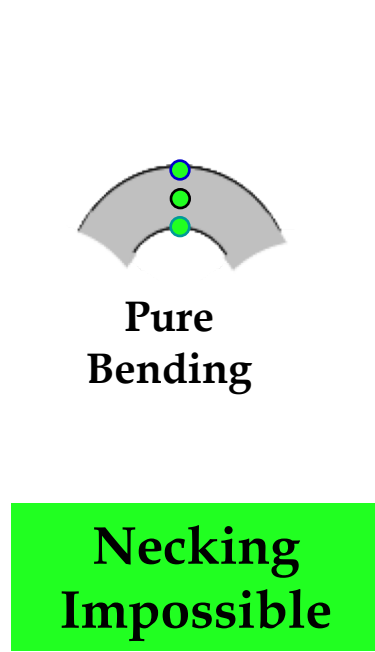


AA 6111-T4 Limits



AA 2024-T351 Limits

Lowest Stress Through Thickness is an Unambiguous Metric for Necking

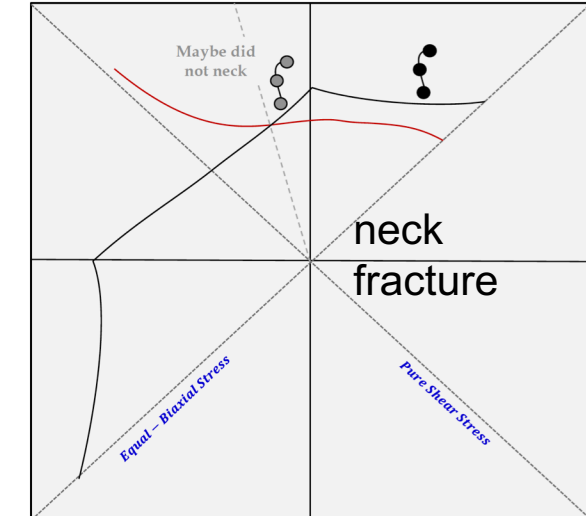
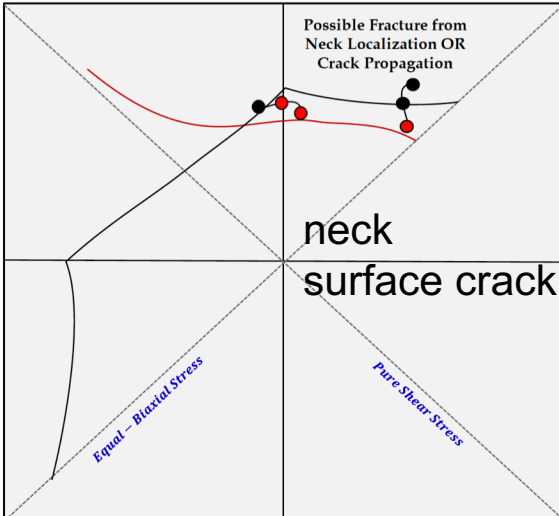
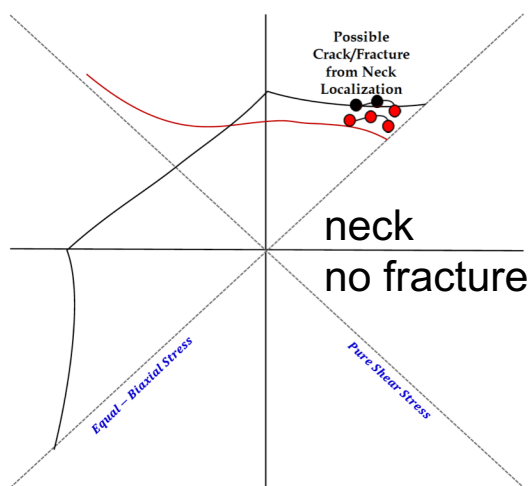
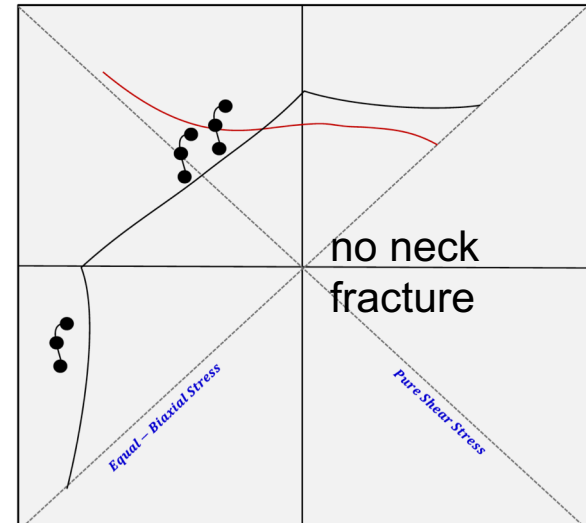
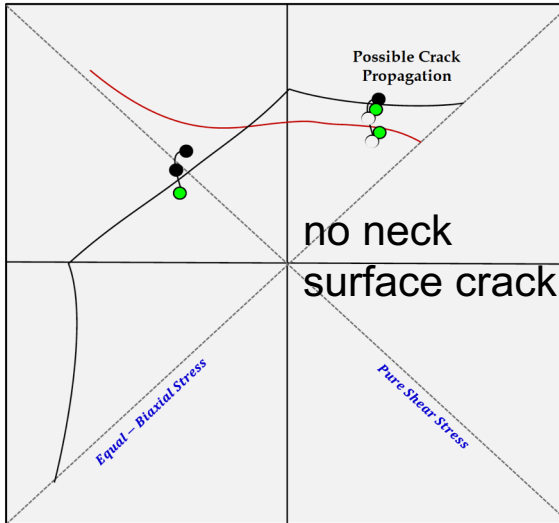
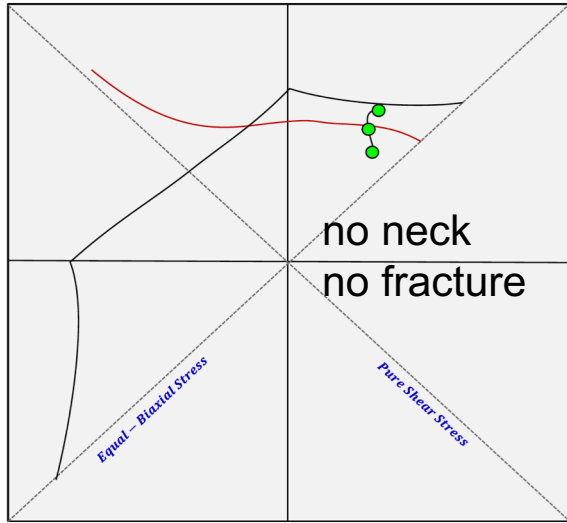


Bending suppresses NECK formation

Necking is forbidden in PURE bending !

Neck and Fracture in Stress Space

(based on the top, middle, bottom surfaces)

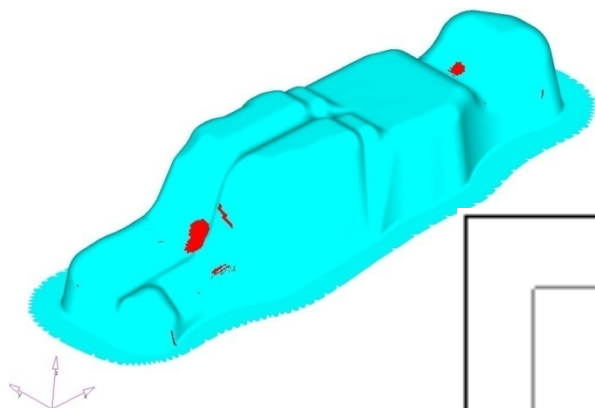


Surface Crack & Fracture Prediction

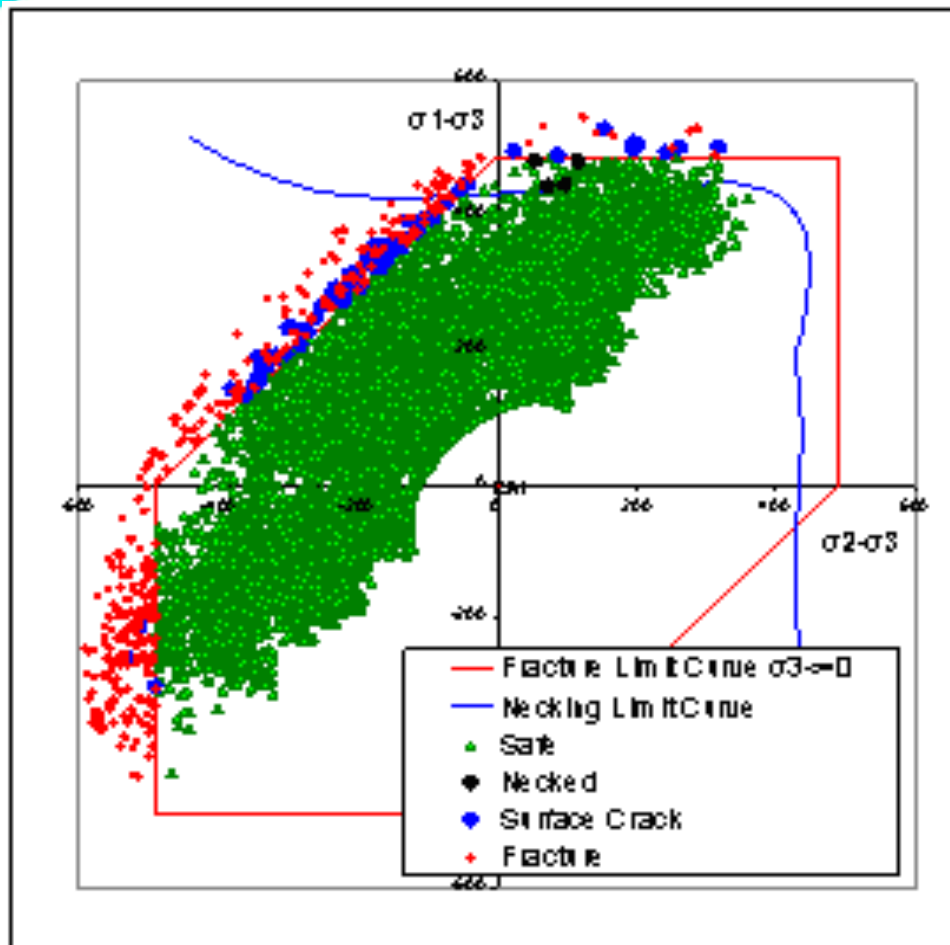
Based on the Stress from FEM

$$f = \frac{\max\left(\frac{|\sigma_1 - \sigma_2|}{\sigma_1}, \frac{|\sigma_2 - \sigma_3|}{\sigma_2}, \frac{|\sigma_3 - \sigma_1|}{\sigma_3}\right)}{\sigma_{MSS}}$$

If $f > 1$: Fracture

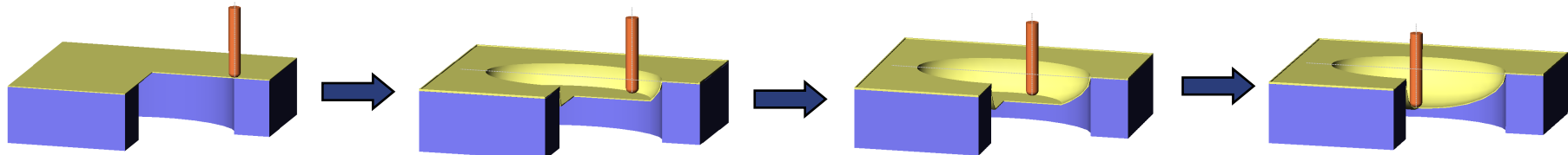


$$\underline{\underline{\sigma}}^{proj} = \underline{\underline{\sigma}} \frac{\bar{\sigma}(\bar{\varepsilon}_p)}{\bar{\sigma}(\underline{\underline{\sigma}})}$$



Modelling of Incremental Sheet Forming

Schematics



Commercial Capability of Boeing for Incremental Sheet Forming

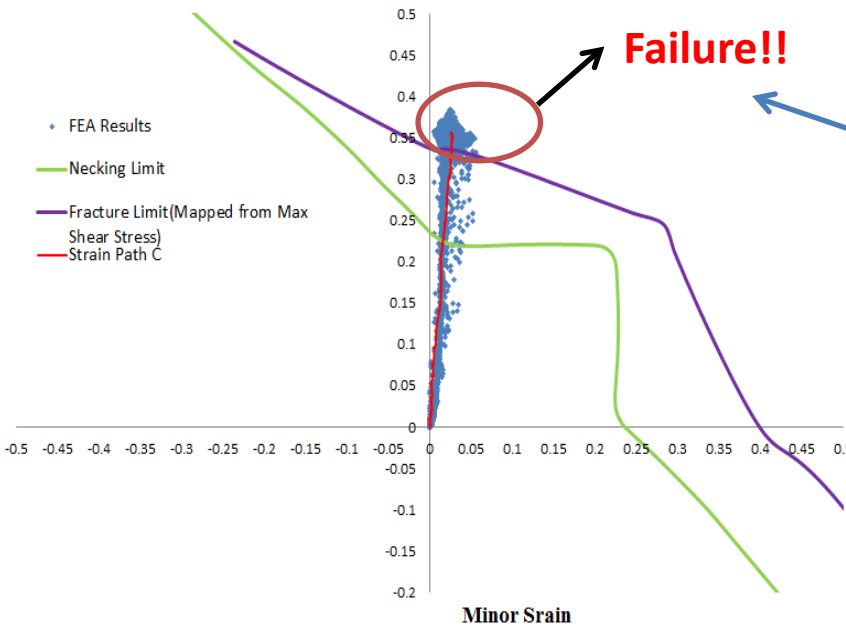


Formability and Failure Prediction (Cone Shape)

Necking and Failure From Strain Plot

Strain FLD for Cone(Material Model Barlat Yld2000-2d)

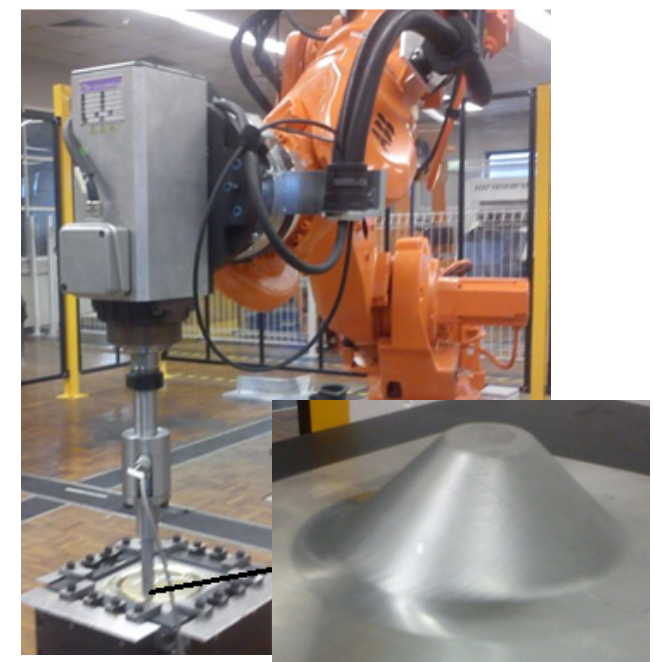
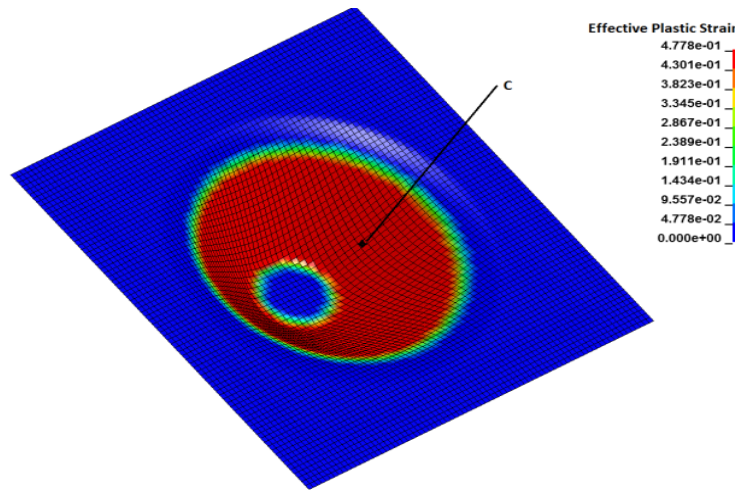
Major Strain



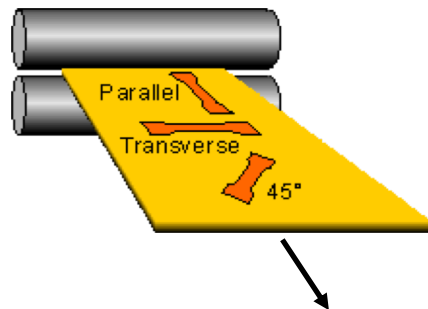
Failure!!

?

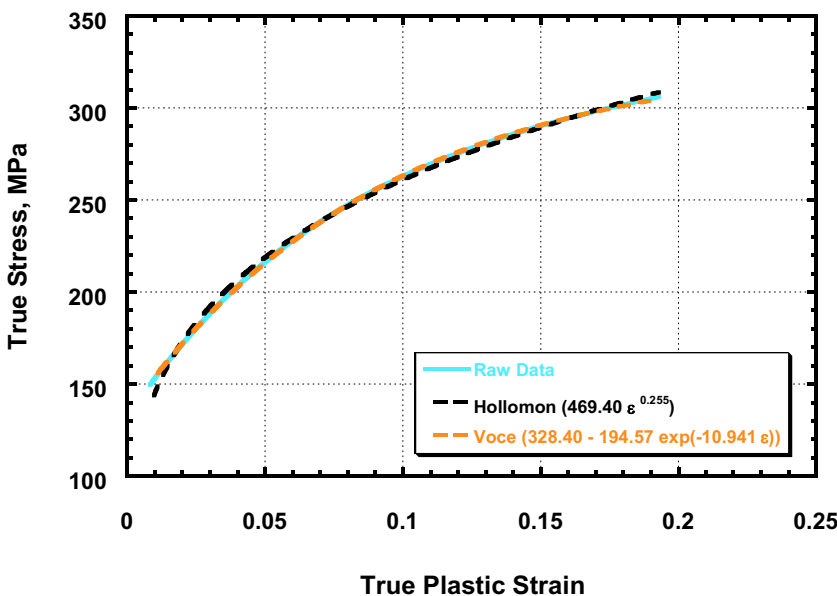
(Success)



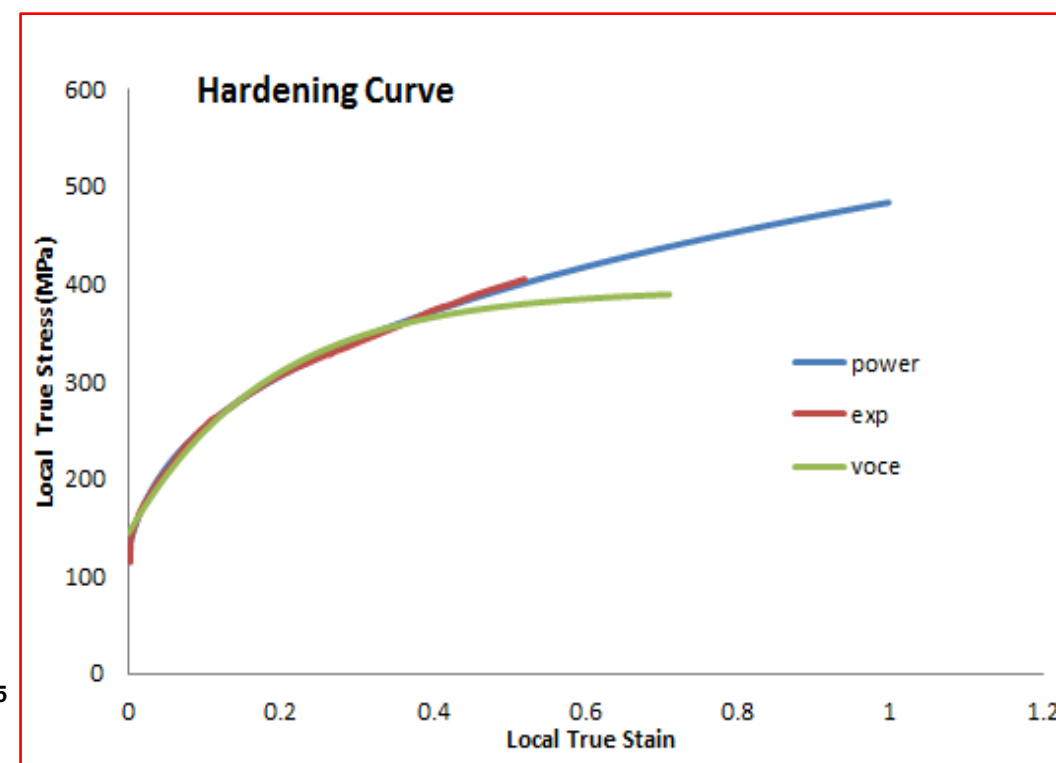
Tensile Test for the Rolling Direction (L) Using DIC Technique



Uniaxial (-L) σ - ϵ Relationship
6022-T4E32 ($t=1\text{-mm}$)
Comparison of Raw and Fitted Data



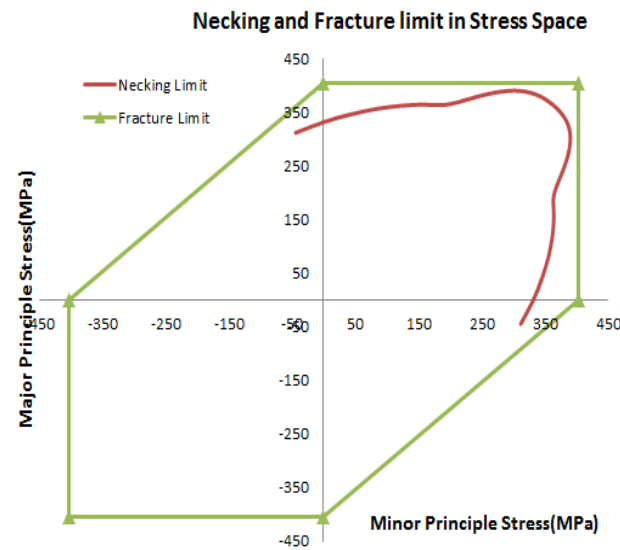
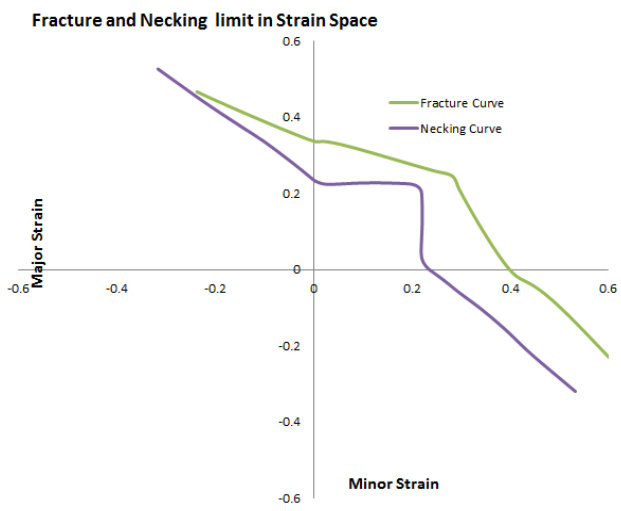
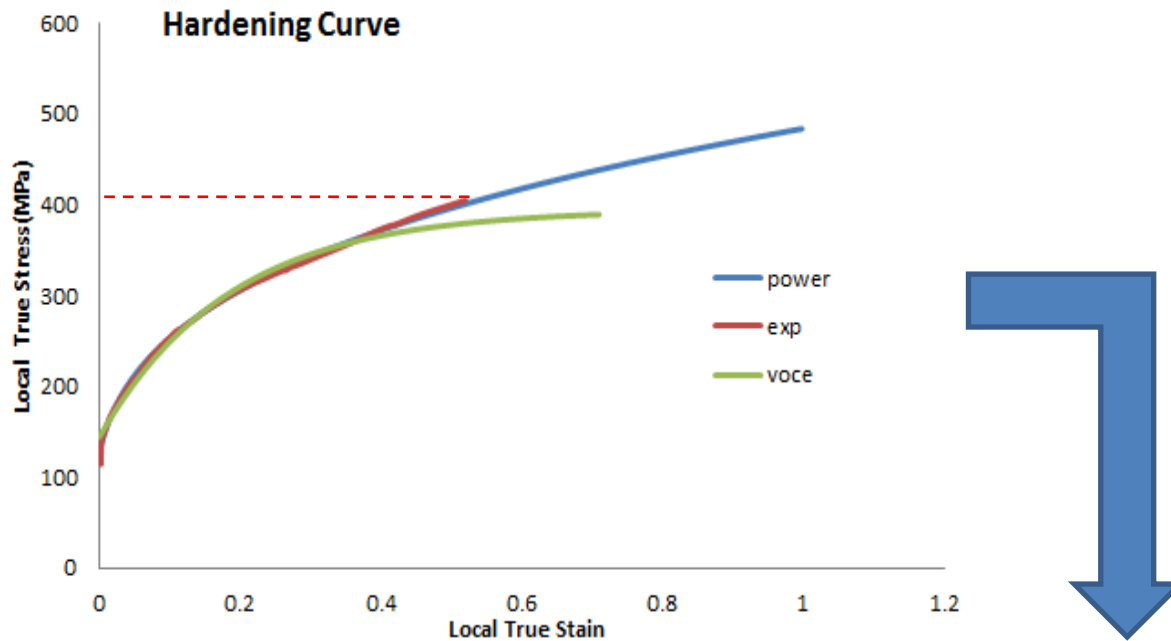
(Conventional)



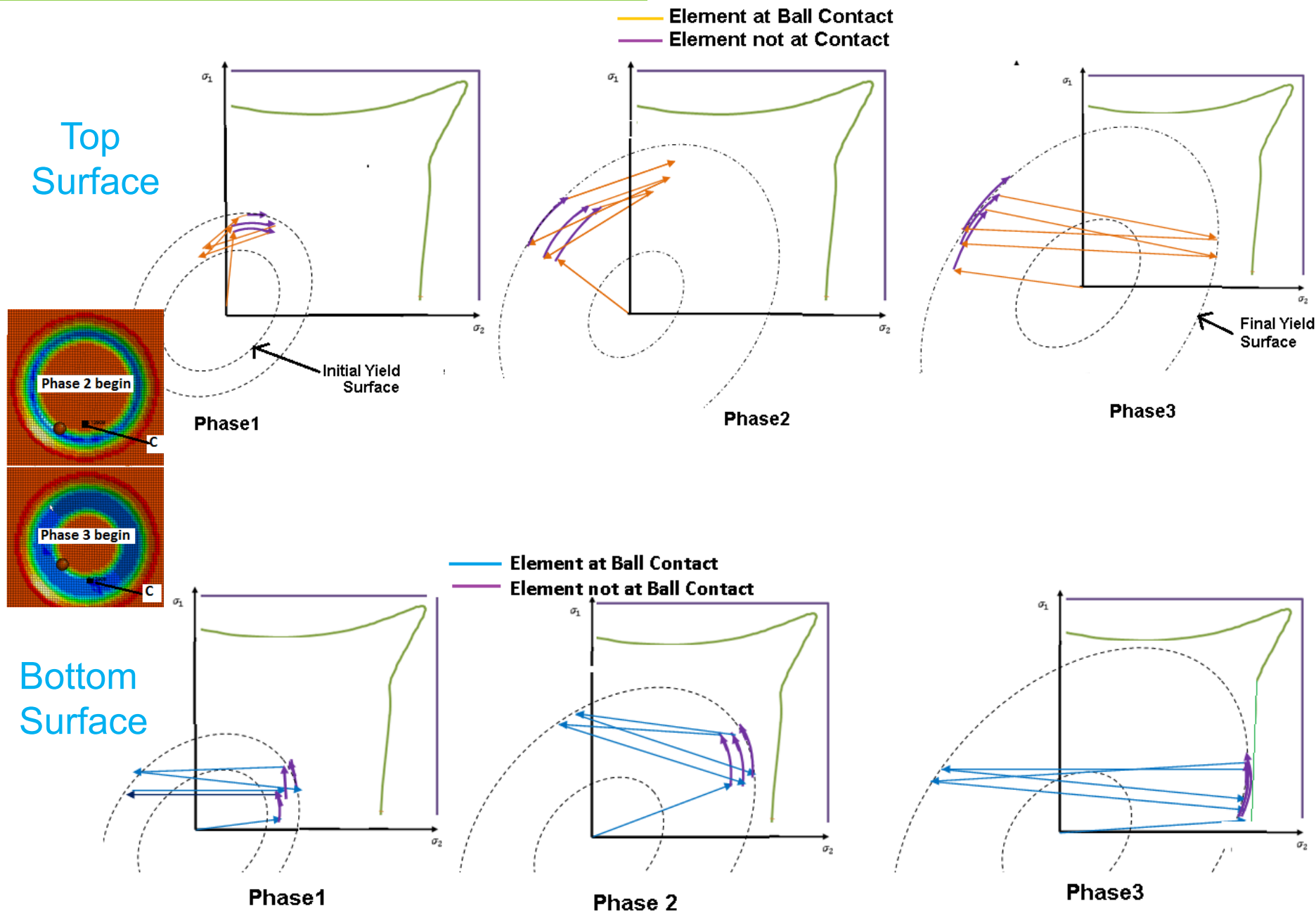
(DIC)

Fracture Criterion Based on MSS (Max. Shear Stress)

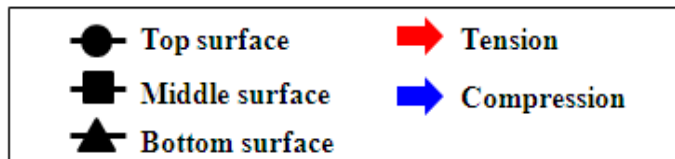
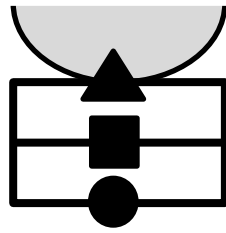
(Stoughton & Yoon, IJP, 2011)



Stress States at three phases

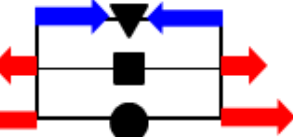


Necking analysis with stress gradient

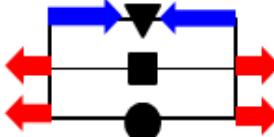


Position B
(before contact)

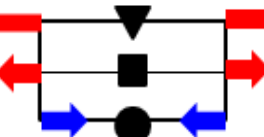
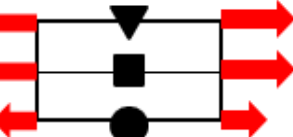
Major Stress



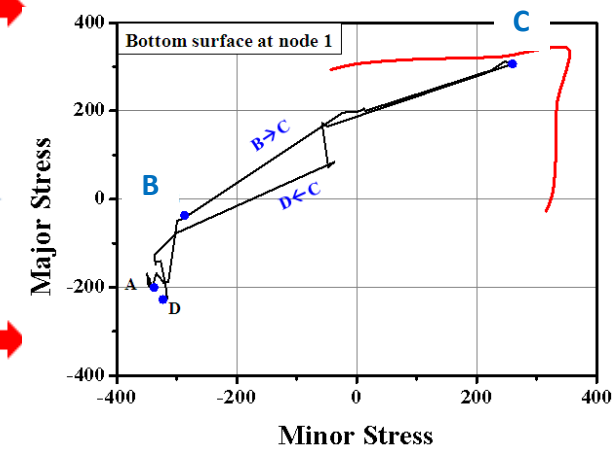
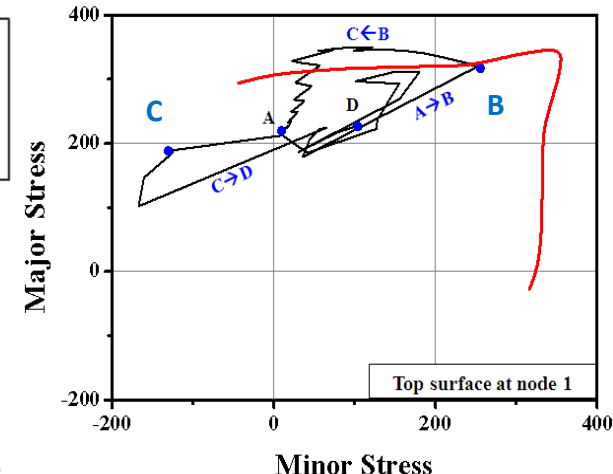
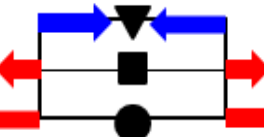
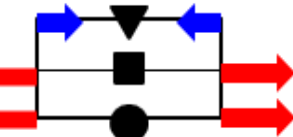
Minor Stress



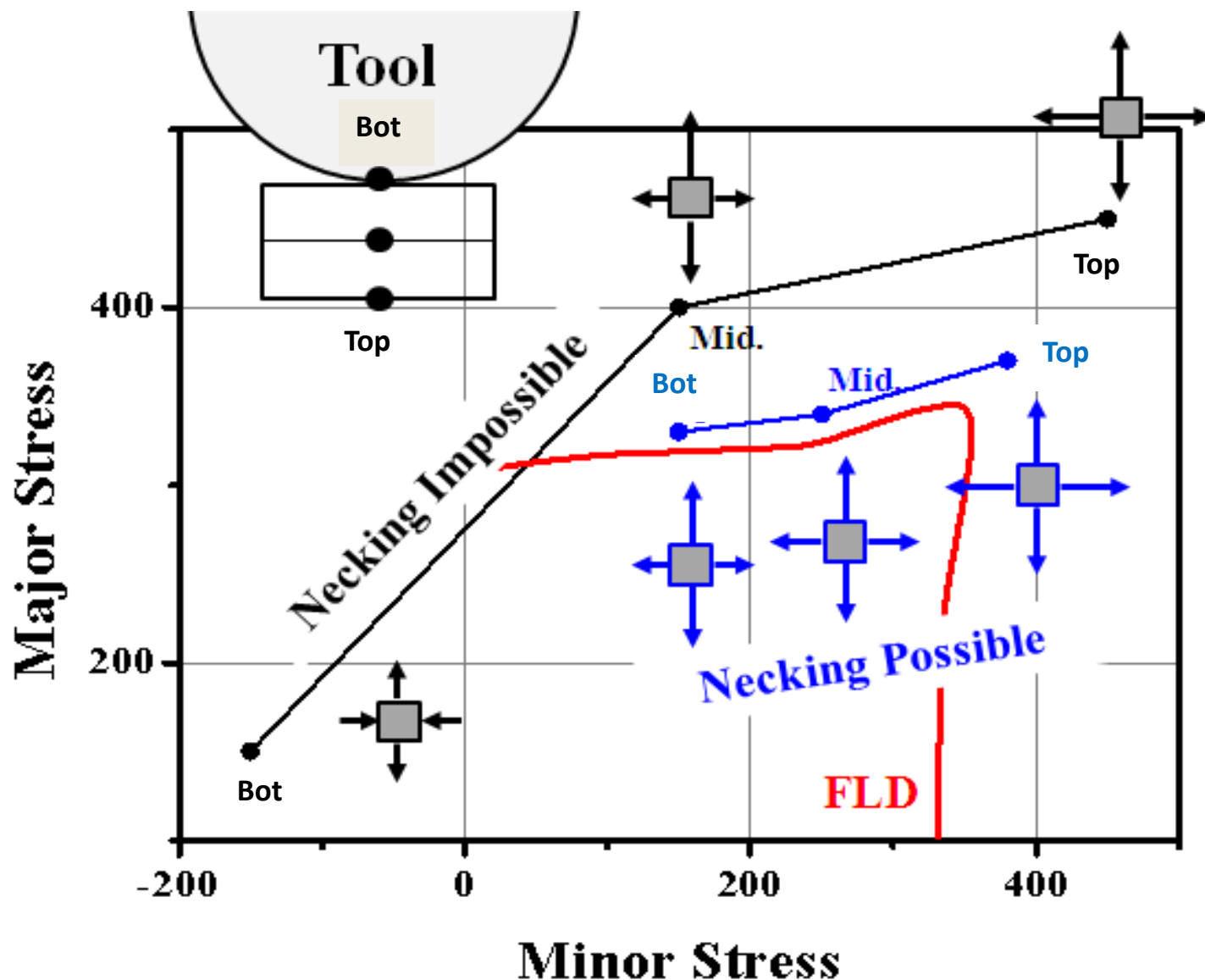
Position C
(At contact)



Position D
(After contact)

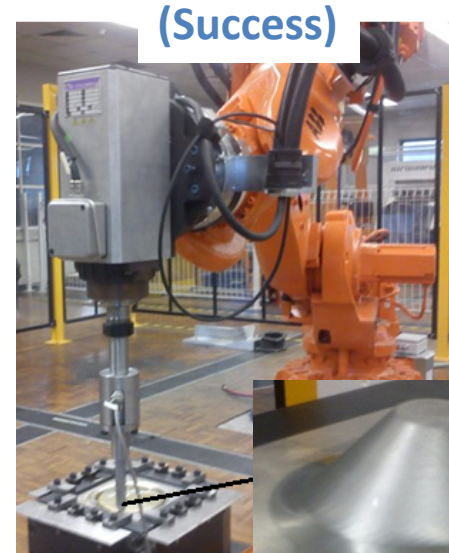
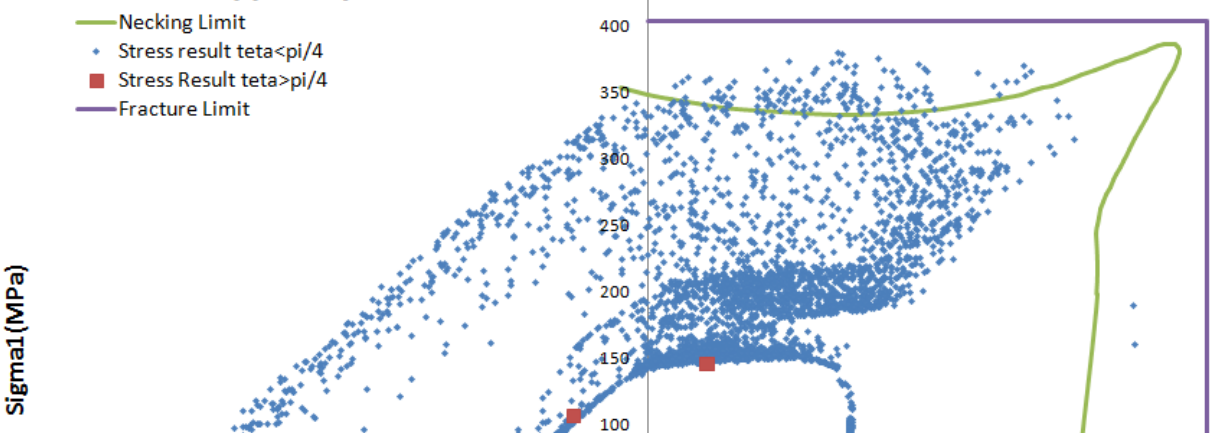


Necking analysis with stress gradient

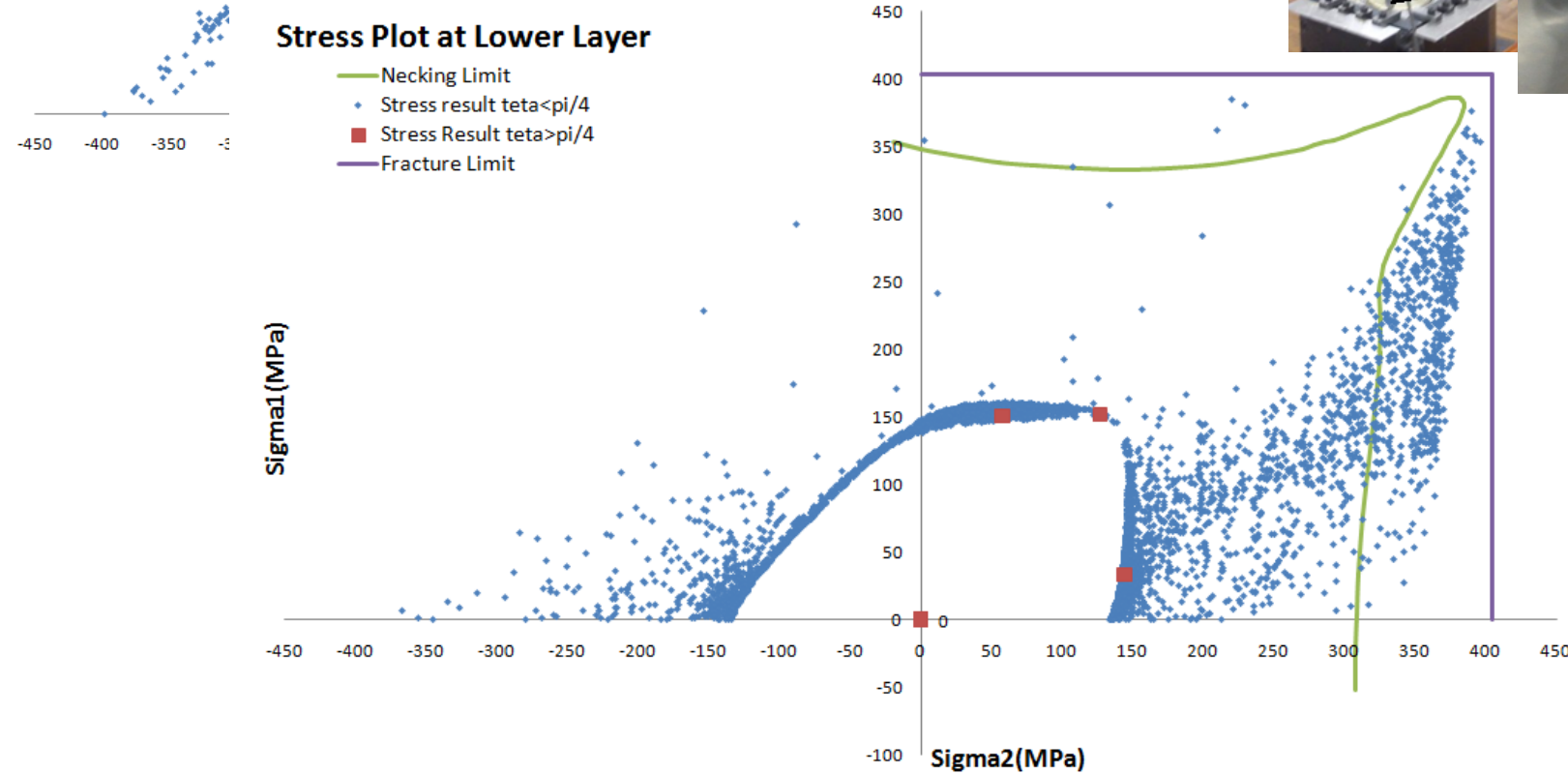


Stress-Based FLC at Top and Bottom Layers (Final Stroke)

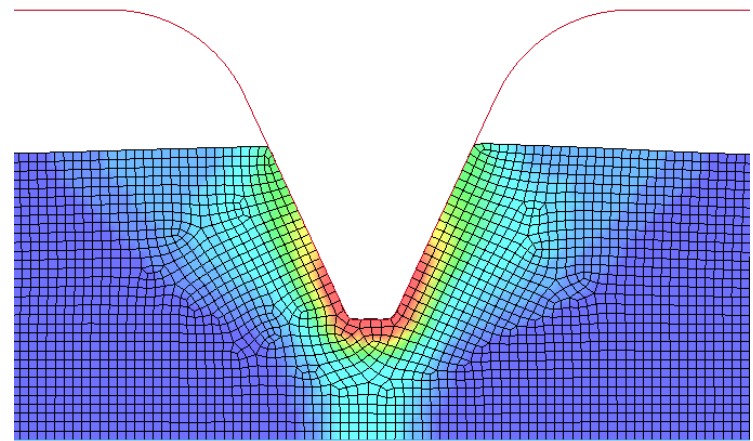
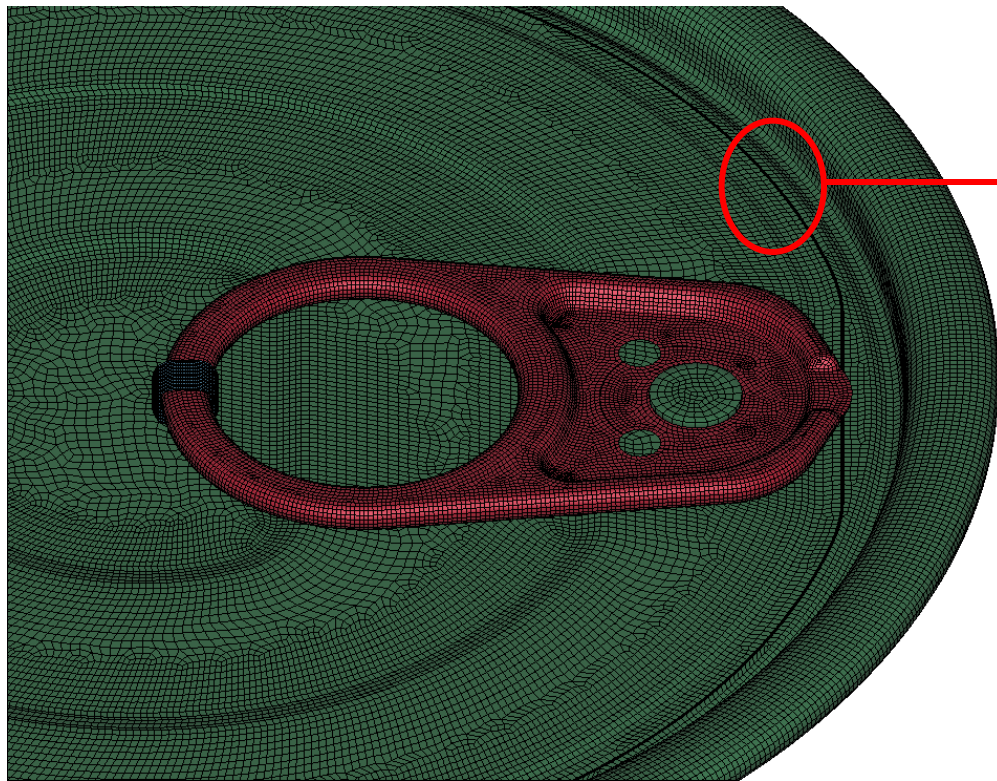
Stress Plot at Upper Layer



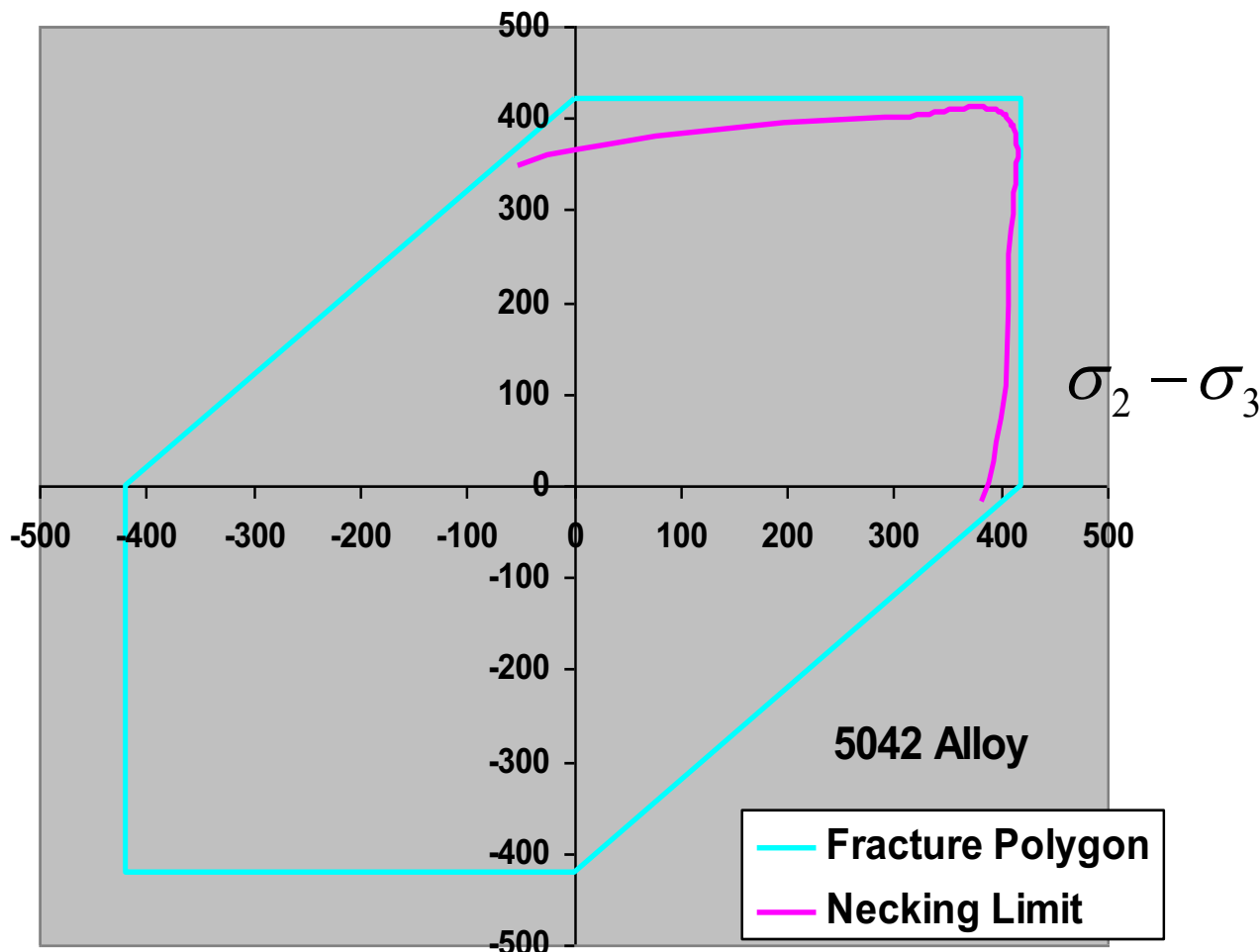
Stress Plot at Lower Layer



Openability

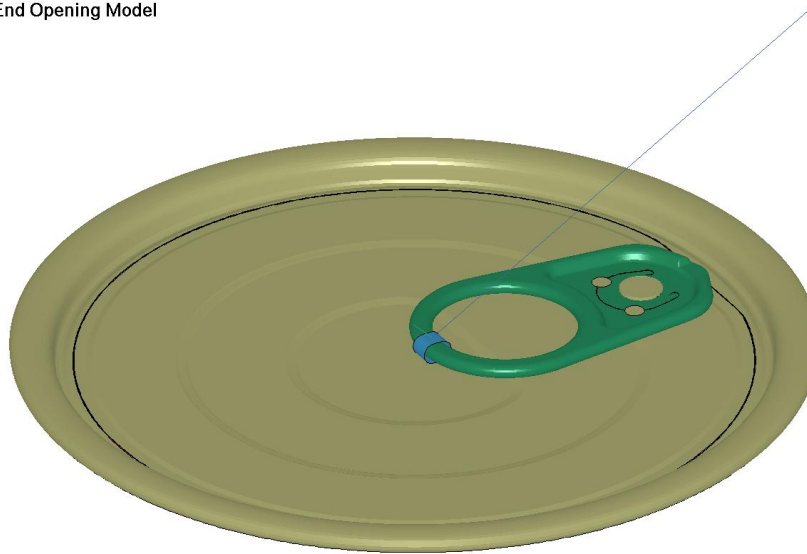


Fracture Polygon for 5042 Alloy



Open Procedure

End Opening Model



(step-1)

End Opening Model



End Opening Model

(step-2)



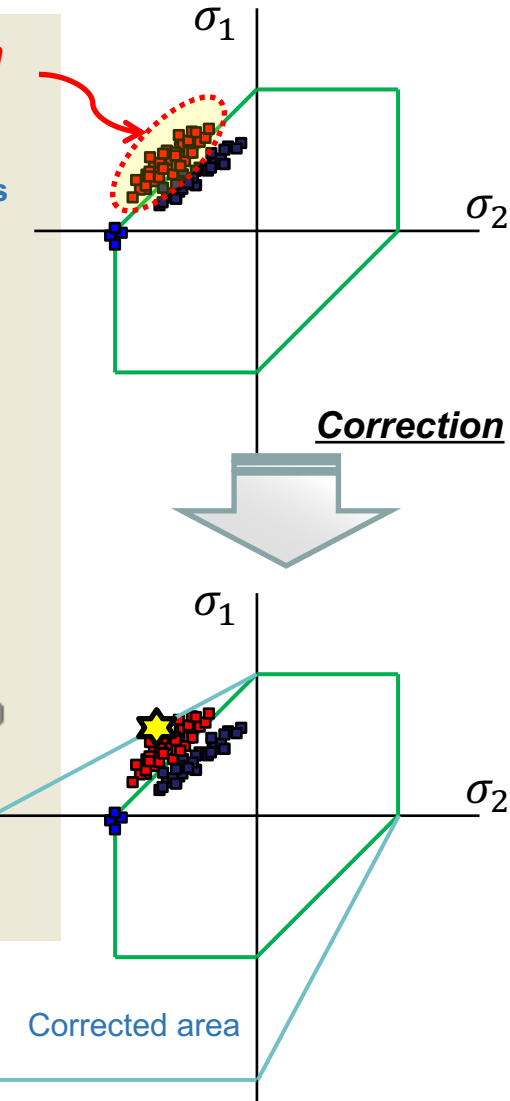
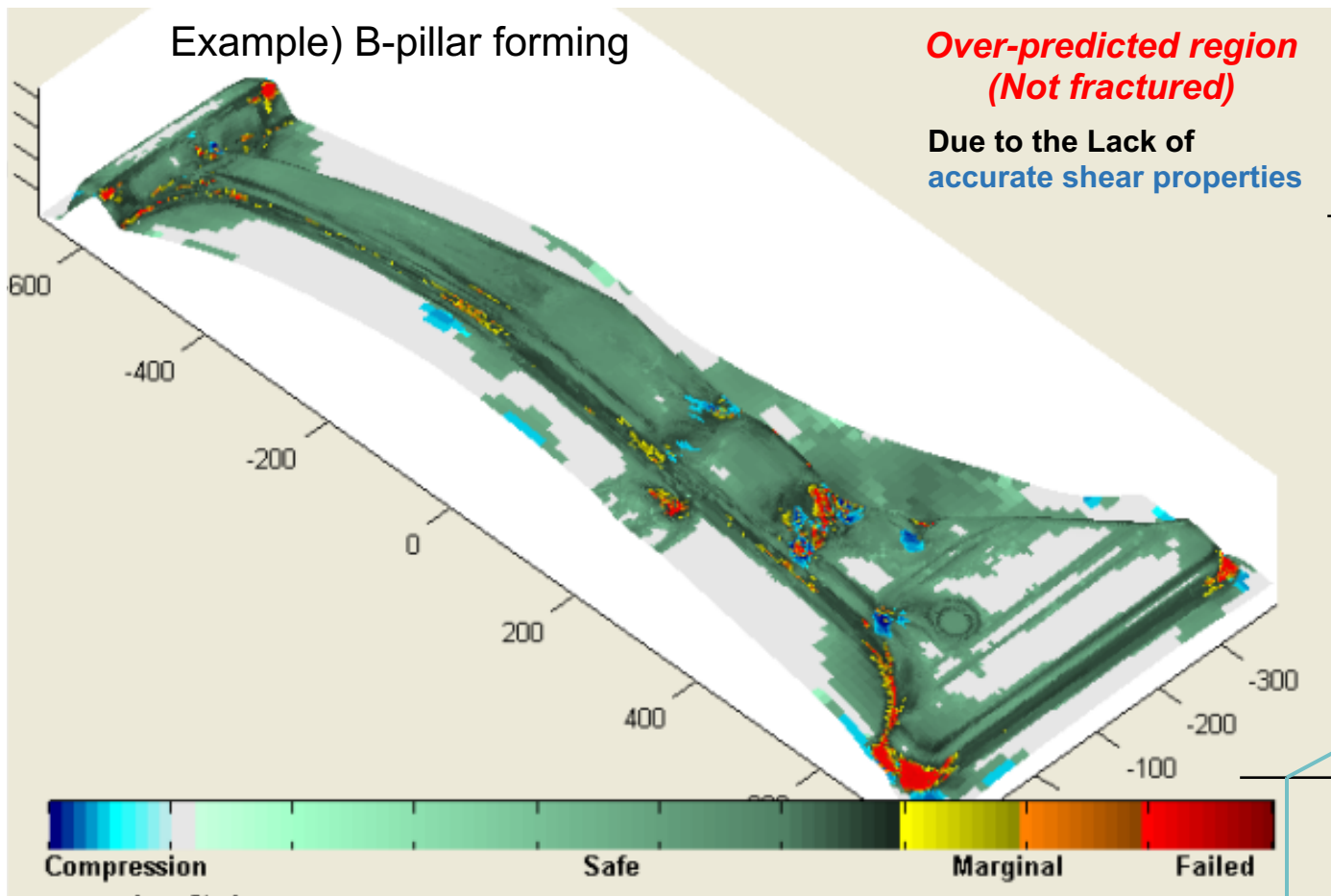
□ Research Motivation for Shear Fracture Calibration

▪ Issue & challenge in sheet forming industry

Incorrect prediction of fracture in pure shear

*MSS: Maximum Shear Stress

Fracture criterion based on MSS*



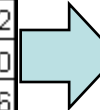
Importance of the accurate shear properties on a stamping process

Wierzbicki's data (Other Stress Metrics)

Test Condition	ID	ϵ_p	η	ξ
Uniaxial Tension	1	0.460	0.400	1.000
Uniaxial Tension	2	0.280	0.630	1.000
Uniaxial Tension	3	0.170	0.930	1.000
Plane Strain Tension	4	0.210	0.610	0.097
Disk Compression	5	0.450	-0.278	-0.910
Disk Compression	6	0.380	-0.234	-0.810
Disk Compression	7	0.356	-0.233	-0.820
Disk Compression	8	0.341	-0.224	-0.800
Compression	9	0.620	-0.248	-0.840
Shear	10	0.210	0.012	0.055
Shear	11	0.260	0.117	0.500
Uniaxial Tension	12	0.310	0.343	1.000
Uniaxial Tension	13	0.480	0.357	0.979
Uniaxial Tension	14	0.330	0.356	0.984
Uniaxial Tension	15	0.360	0.369	1.000



σ_1	σ_2	σ_3
725.8	45.4	45.4
803.8	183.9	183.9
907.3	339.1	339.1
705.8	346.7	25.8
90.8	-20.4	-635.5
138.9	-18.1	-581.2
136.0	-14.9	-574.0
144.3	-13.6	-562.6
136.6	-22.0	-652.6
351.0	0.1	-329.2
454.8	0.8	-240.8
637.6	6.1	6.1
701.4	43.9	-10.3
652.5	36.9	-7.1
672.4	23.2	23.2



$$\sigma_1 \geq \sigma_2 \geq \sigma_3$$

$$\sigma_{mss} = \frac{1}{2}(\sigma_1 - \sigma_3)$$

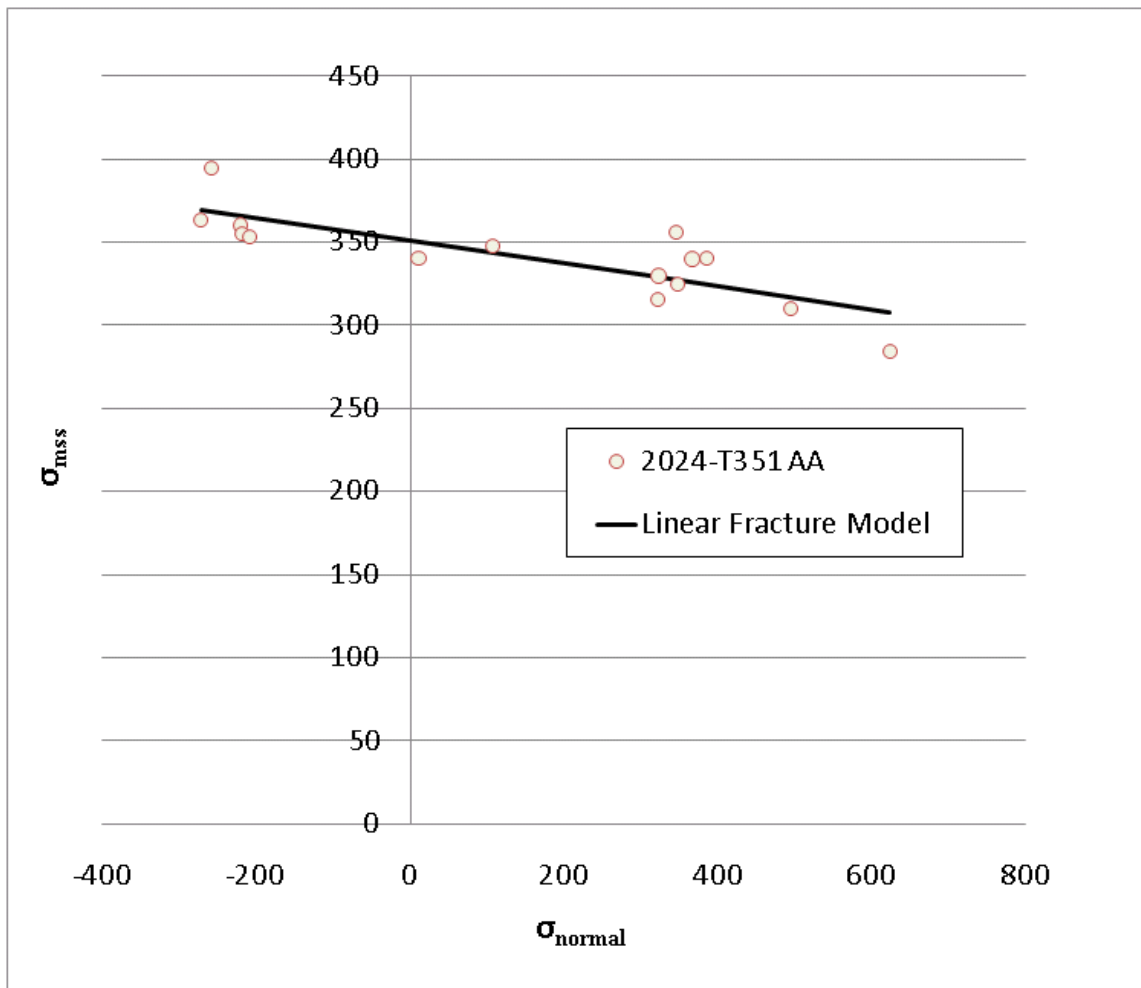


$$\sigma_m = \frac{1}{3}(\sigma_1 + \sigma_2 + \sigma_3)$$



$$\sigma_{normal} = \frac{1}{2}(\sigma_1 + \sigma_3)$$

MSS vs. Normal Stress



$$\frac{\sigma_{mss}}{350.8} + \frac{\sigma_{normal}}{5105.9} = 1$$

$$\delta\sigma_{normal} = 15.7$$

→Mohr-Coulomb Model

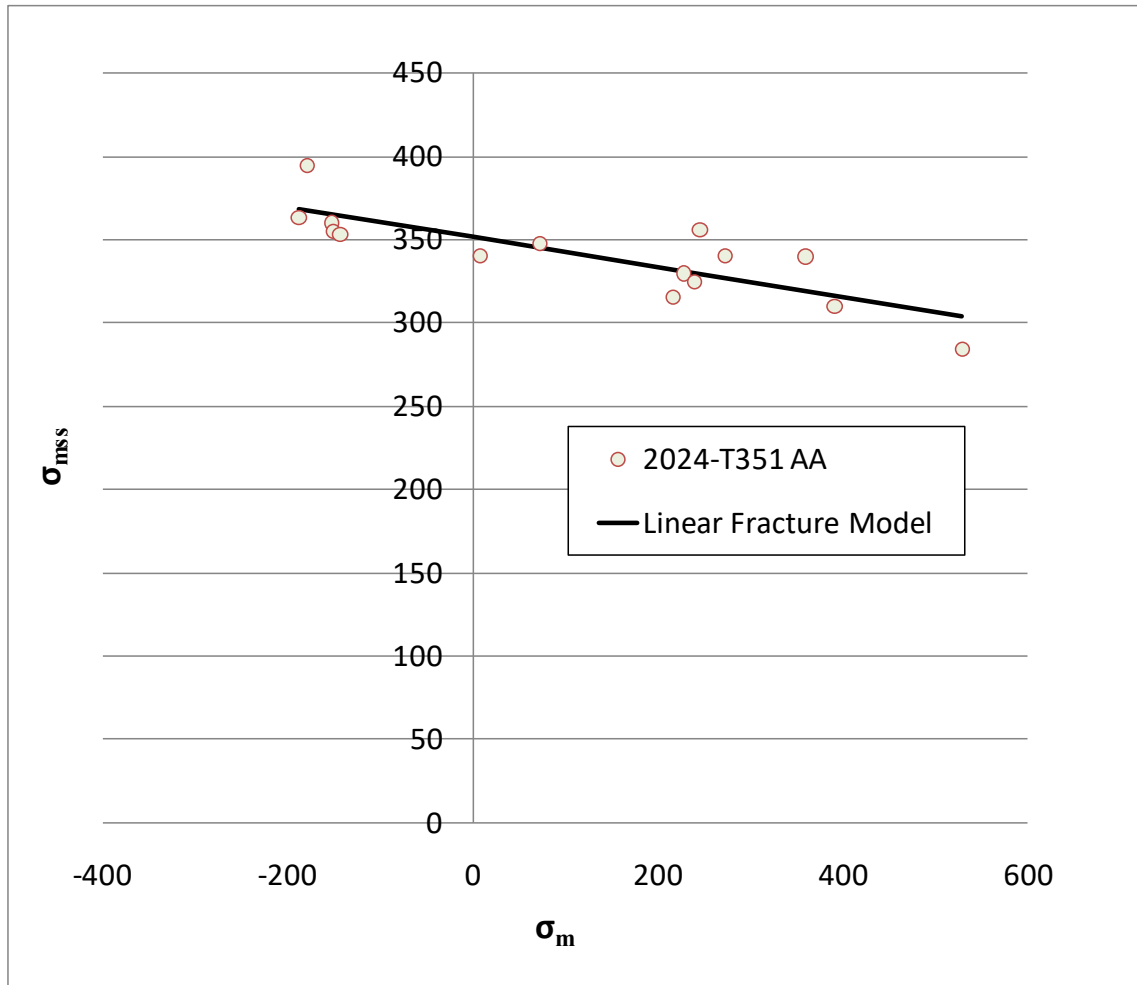
$$\sigma_{mss} + \mu\sigma_{normal} = 350.8$$

$$\mu = 0.0687 = \tan(3.93^\circ)$$

Compare to MSS Model

$$\sigma_{mss} = 341.0 \pm 26.2$$

MSS vs. Mean Stress



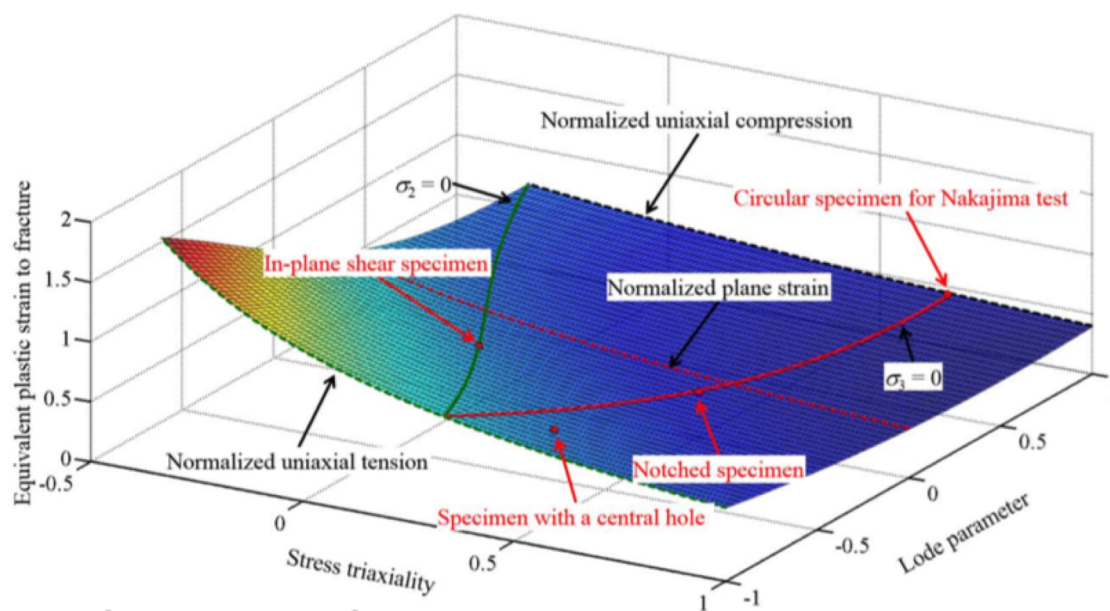
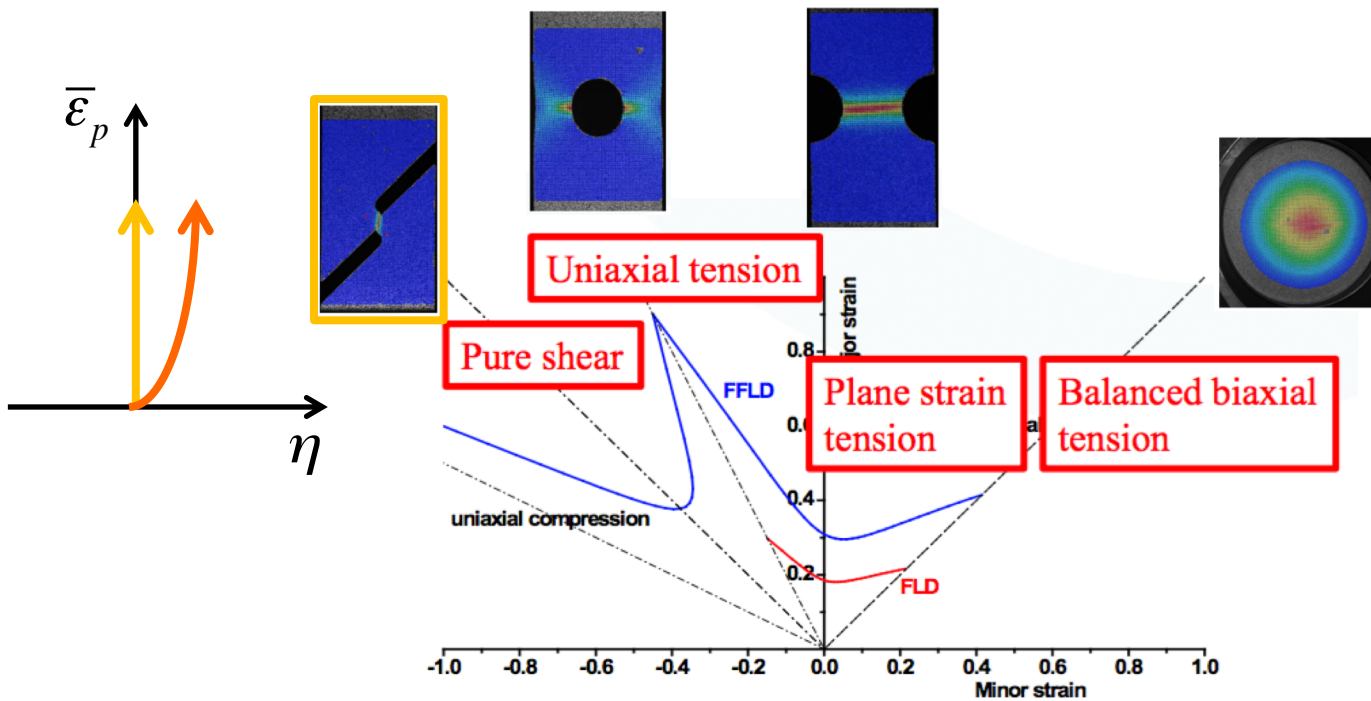
$$\frac{\sigma_{mss}}{351.4} + \frac{\sigma_m}{3897.5} = 1$$

$$\delta\sigma_m = 15.6$$

Compare to MSS Model

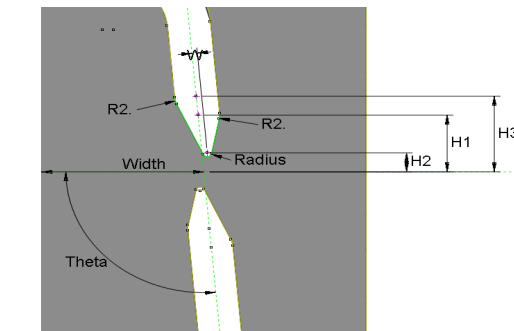
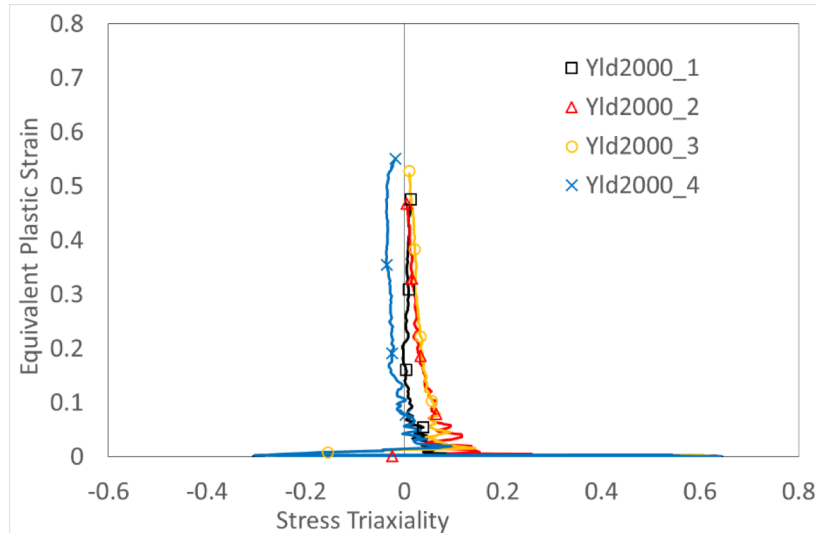
$$\sigma_{mss} = 341.0 \pm 26.2$$

Fracture Experiments and Calibration

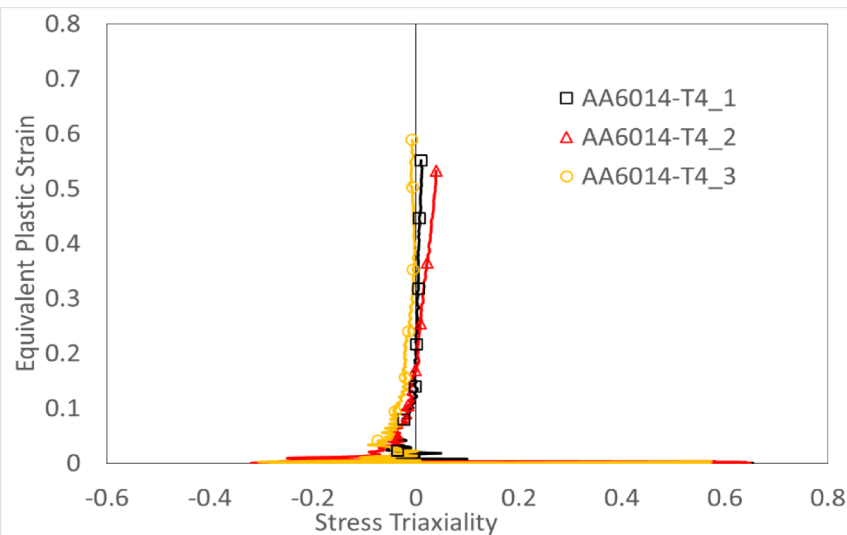


Summary of the results for three different materials (ESAFORM 2016)

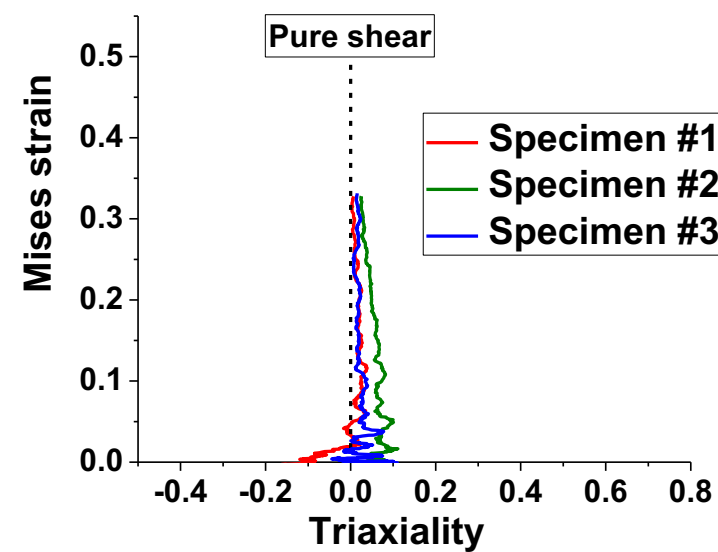
AA 6k21



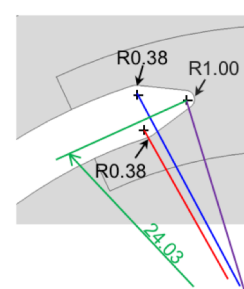
AA 6014



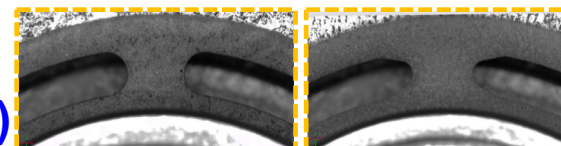
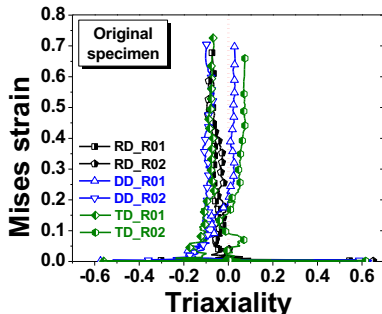
1.5 GPa Steel



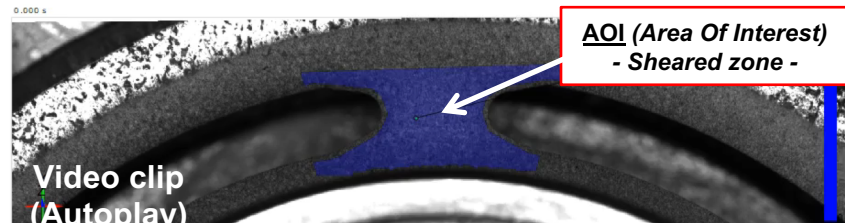
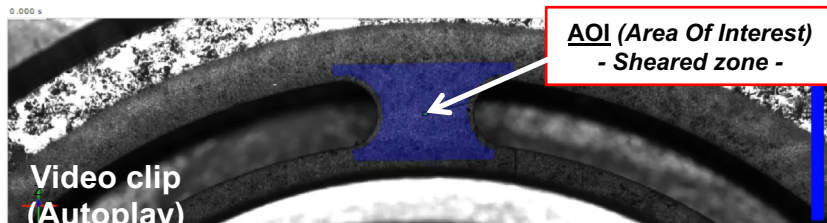
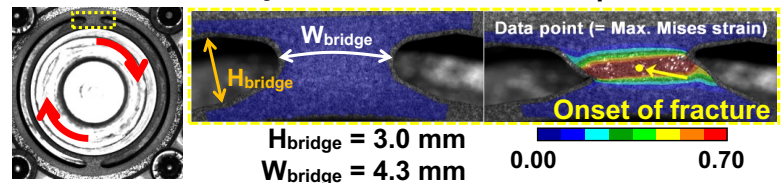
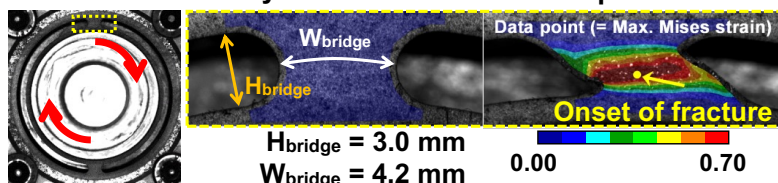
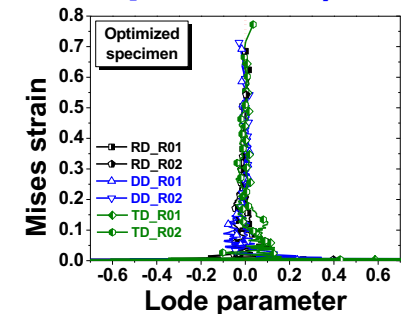
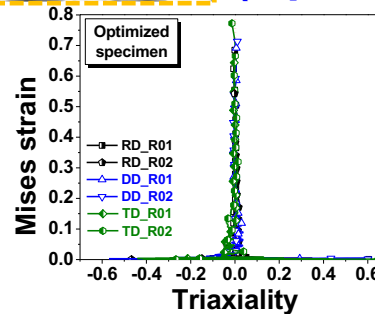
□ Torsion-Based Shear Fracture (CIRP2021 Annals, Kim et al.)



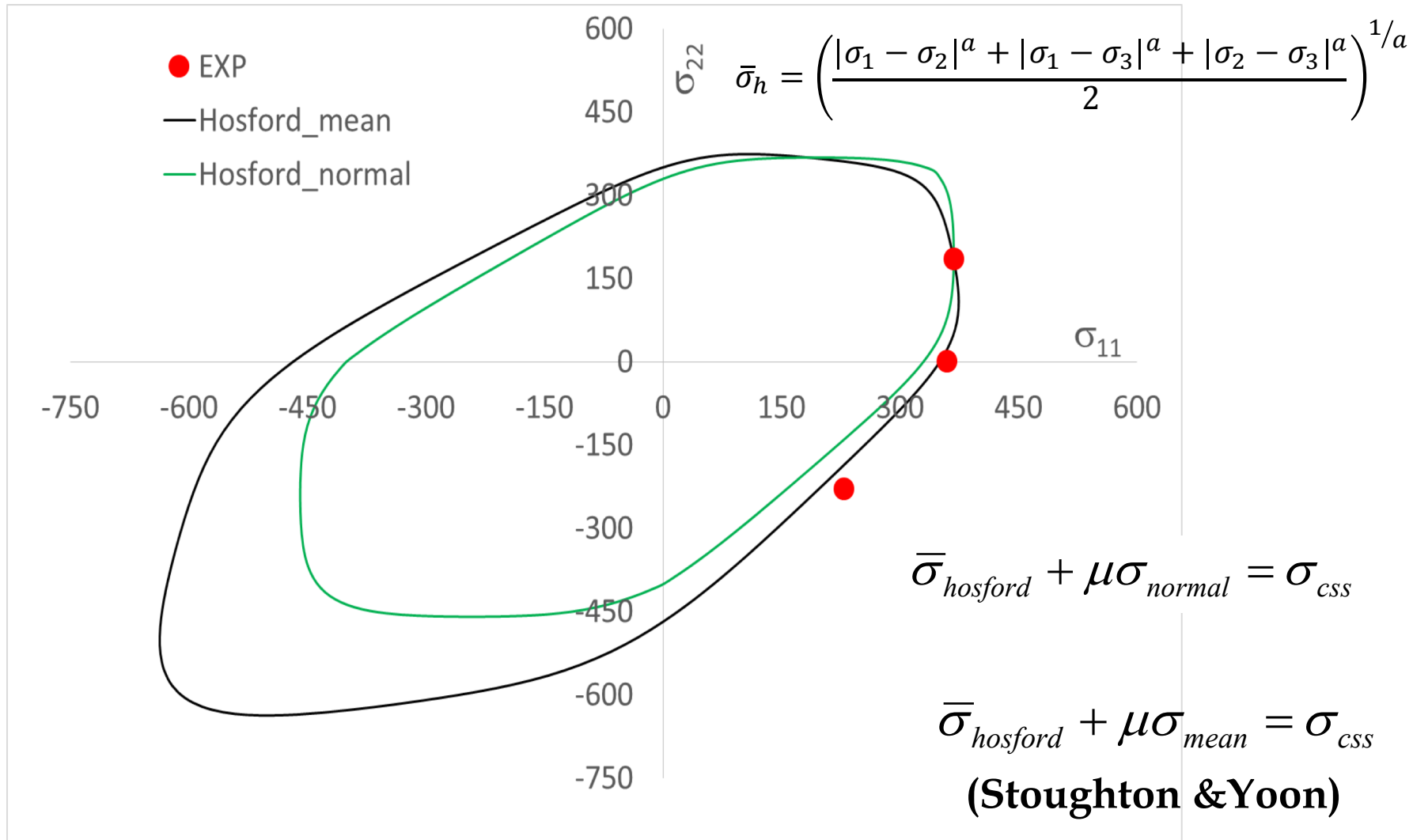
(Original Specimen)



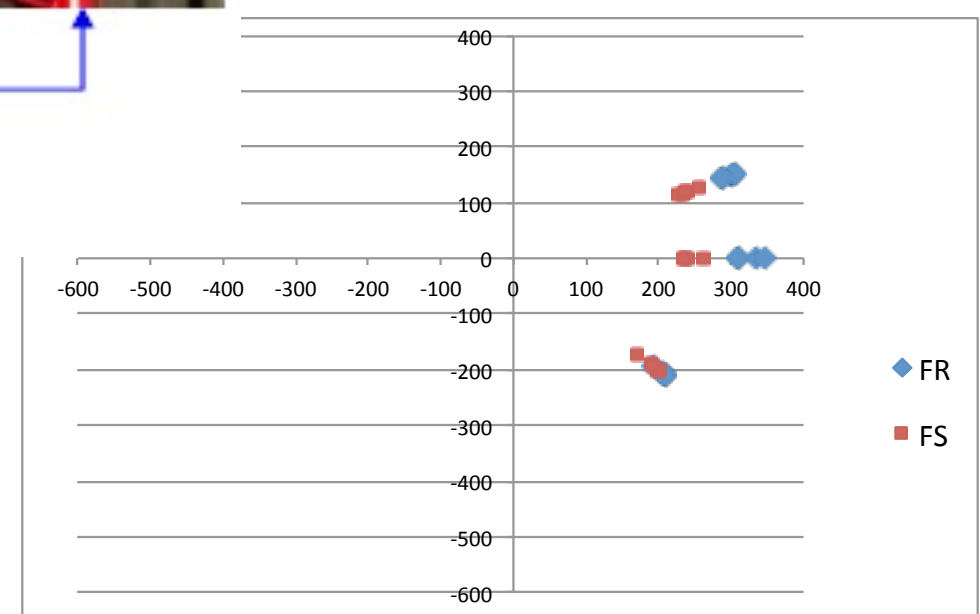
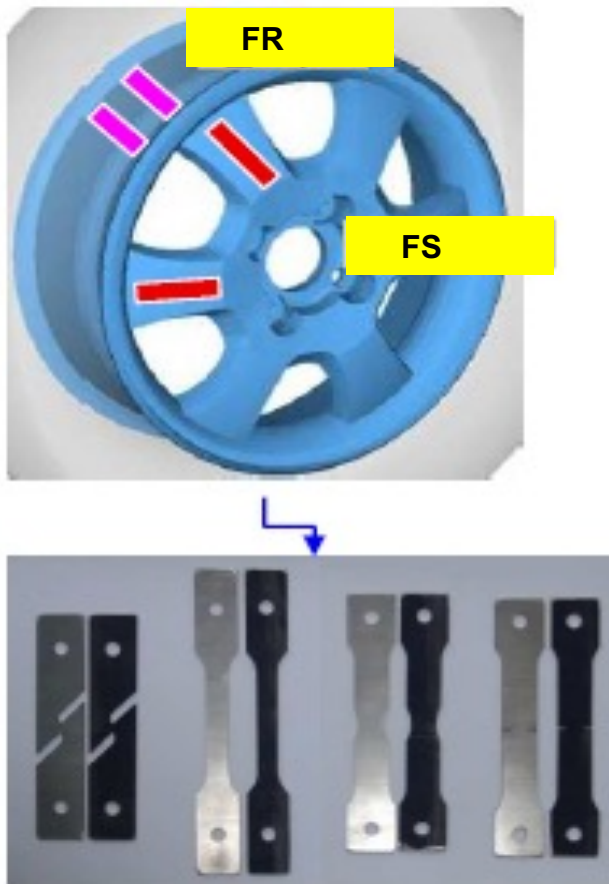
(Optimized Specimen)



MMS-Normal and MSS-Mean nonlinear models with three points calibration (AA 6k21-IH T4)



Aluminum Wheel Fracture Under Crash



Linear Model :

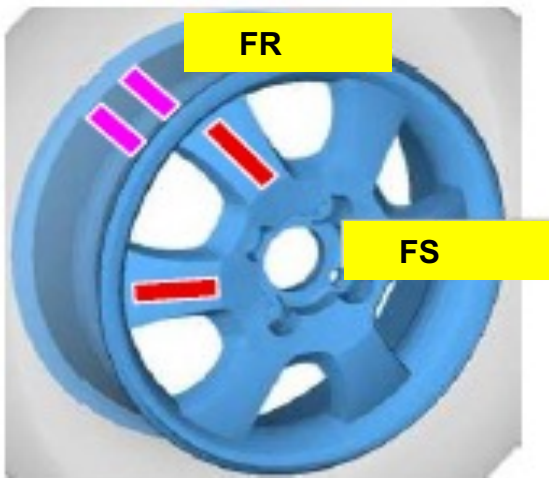
Parameter calibration

(Tensile and Shear)

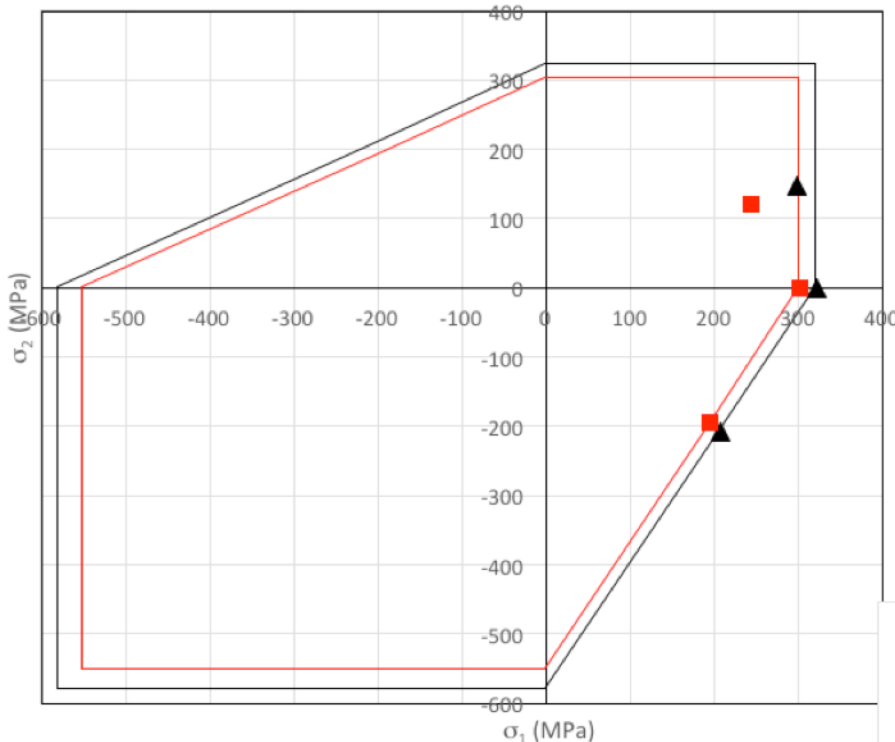
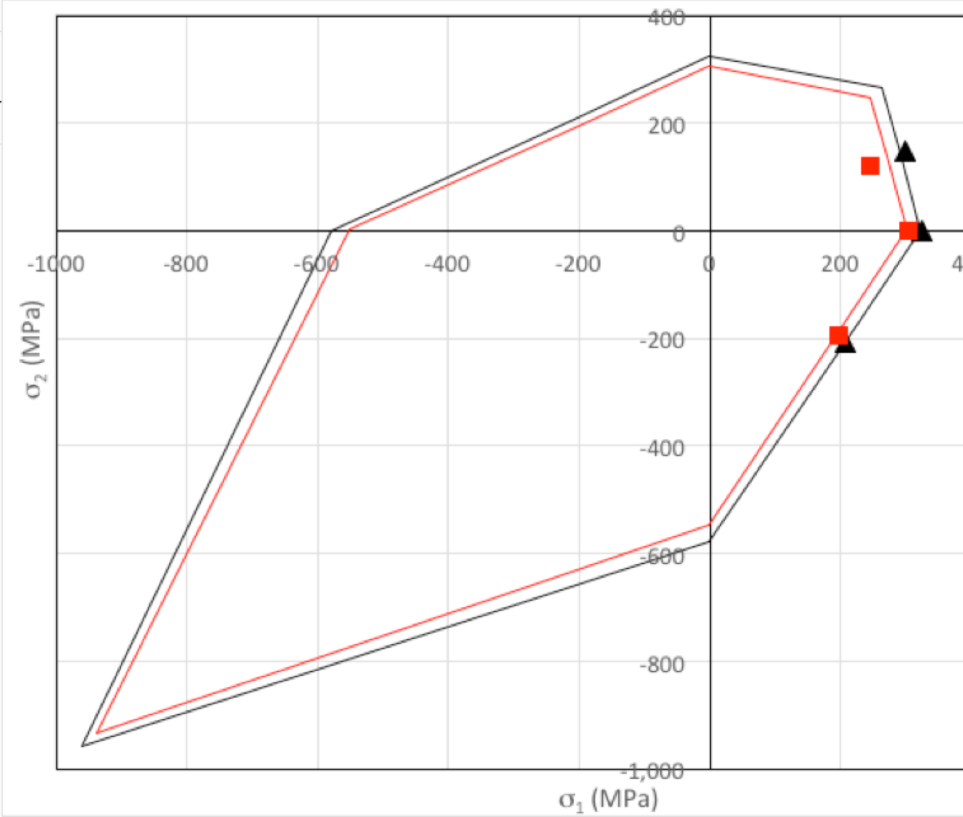
(Stoughton & Yoon, 2014)

$$\sigma_{mss} + \mu \sigma_{mean} = \sigma_{css}$$

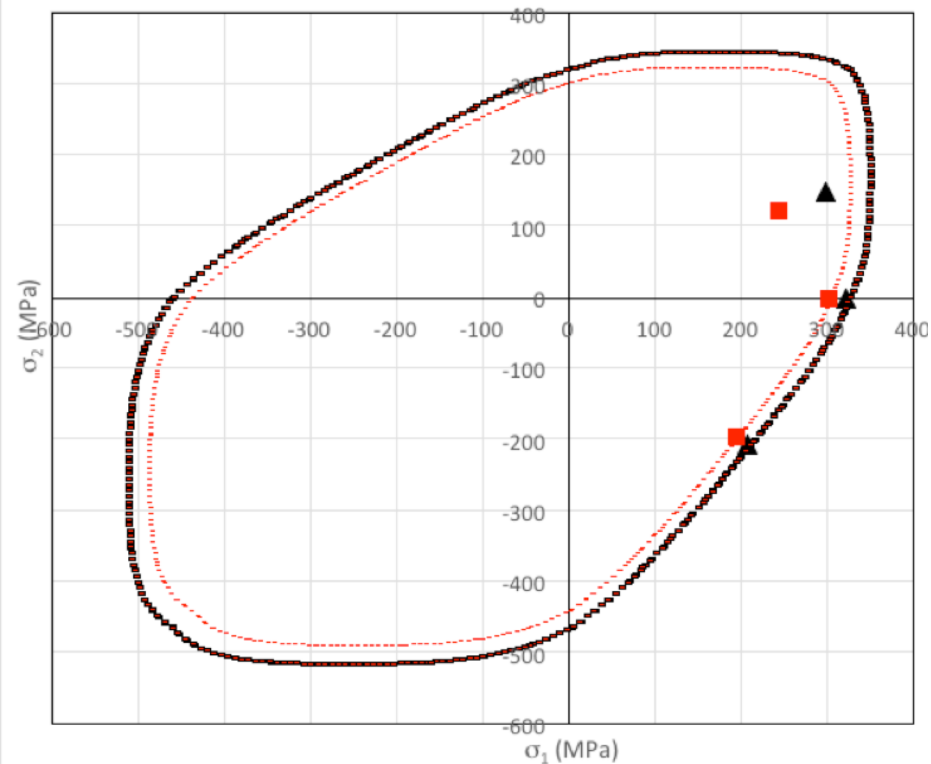
$$\sigma_{mss} + \mu \sigma_{normal} = \sigma_{css}$$



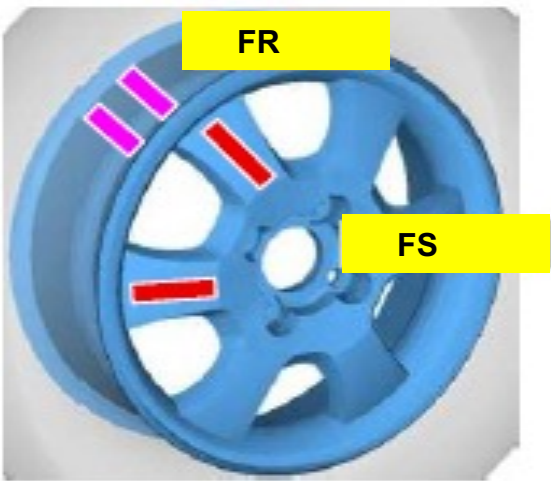
▲ Exp_FR
■ Exp_FS



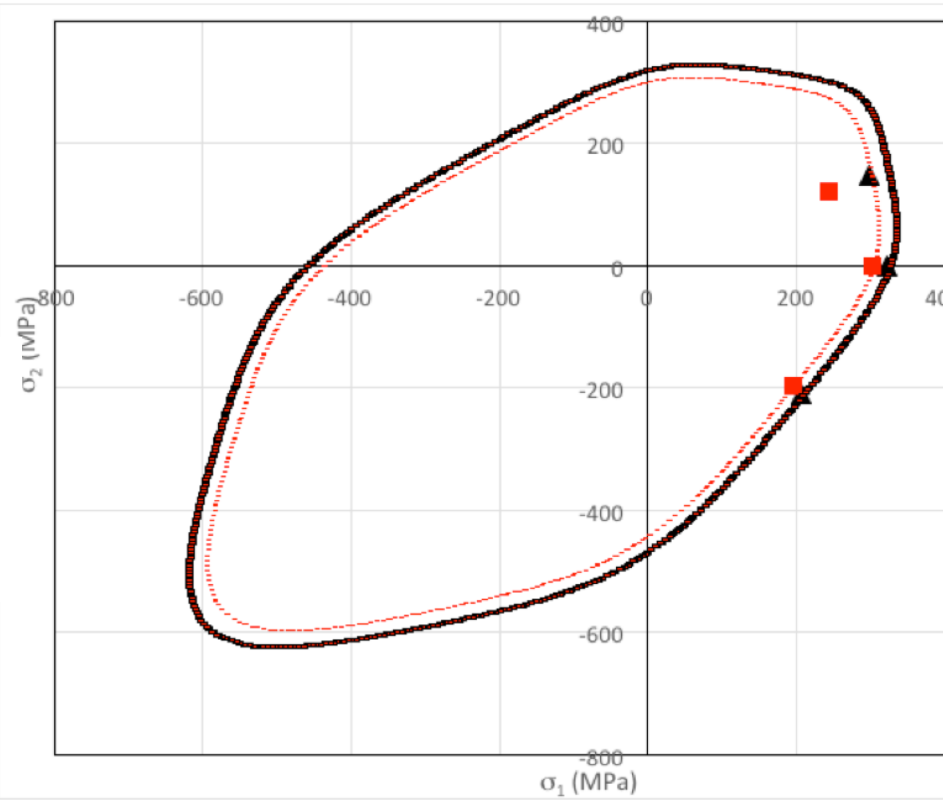
Nonlinear Model : Parameter calibration (Tensile & Shear)



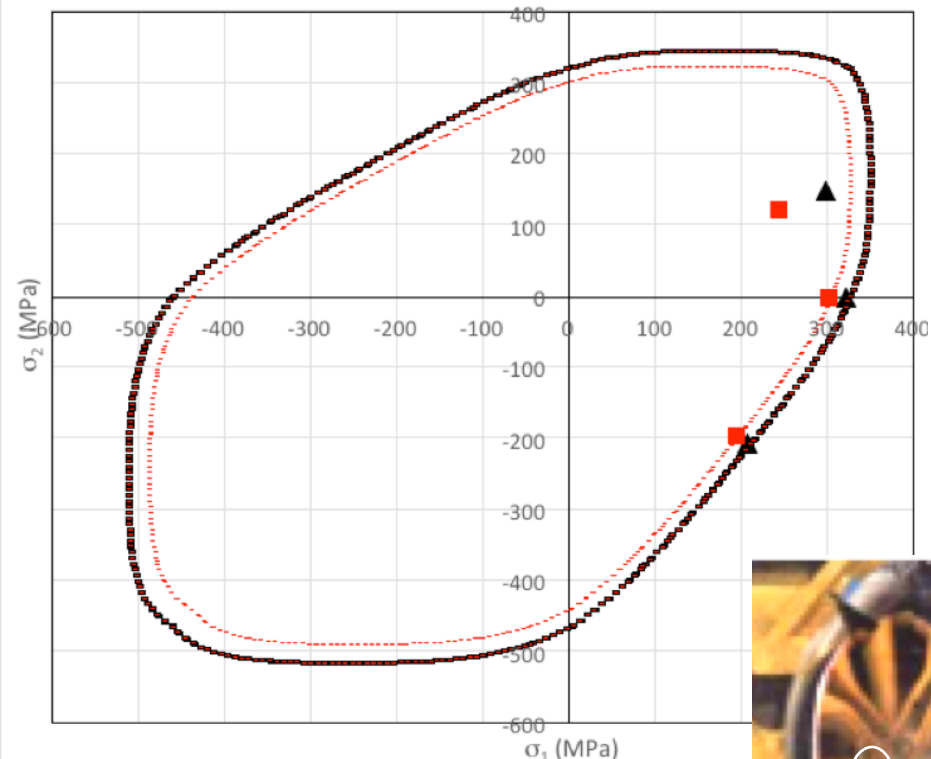
$$\bar{\sigma}_{hosford} + \mu \sigma_{normal} = \sigma_{css}$$



▲ Exp_FR
■ Exp_FS



Parameter calibration (Tensile & Shear)



$$\bar{\sigma}_{hosford} + \mu\sigma_{normal} = \sigma_{css}$$

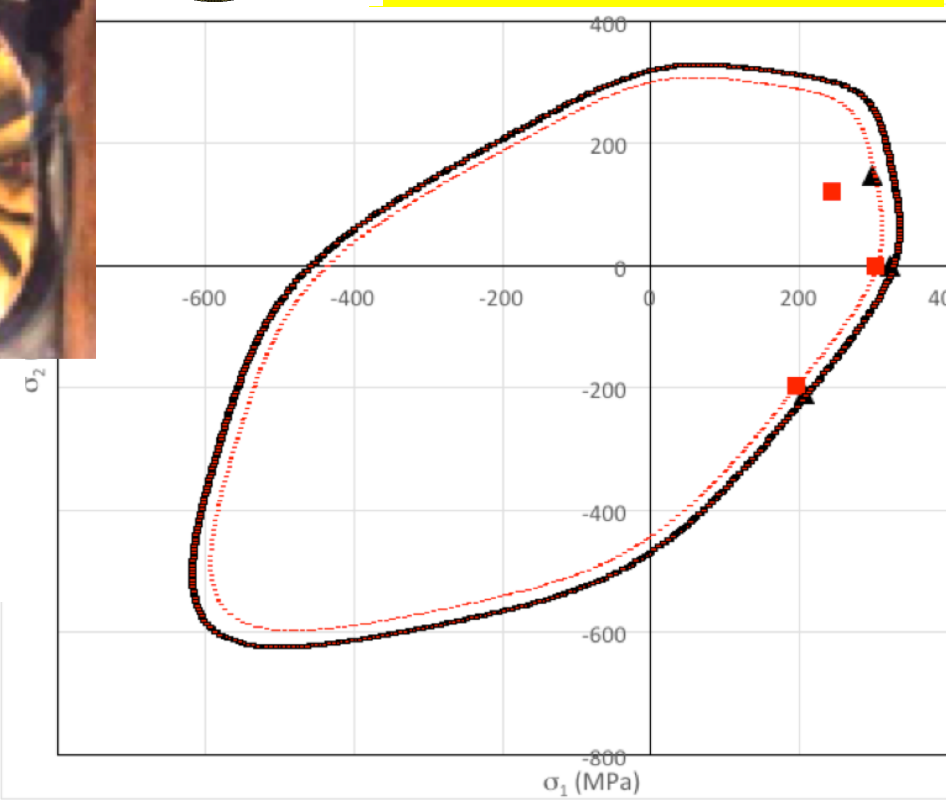


▲ Exp_FR

■ Exp_FS



$$\bar{\sigma}_{hosford} + \mu\sigma_{mean} = \sigma_{css}$$



Potential Solutions in Fracture Modelling

Mohr-Coulomb Model

$$\sigma_{mss} + \mu\sigma_{normal} = \sigma_{css}$$

$$\bar{\sigma}_{Hosford} + \mu\sigma_{normal} = \sigma_{css}$$

$$\sigma_{mss} + \mu\sigma_{mean} = \sigma_{css}$$

$$\bar{\sigma}_{hosford} + \mu\sigma_{mean} = \sigma_{css}$$

Modified Mohr-Coulomb Model



$$\bar{\varepsilon}_p = \bar{\varepsilon}_p(\eta, \xi)$$

$$D = \int_0^t \frac{d\bar{\varepsilon}_p}{\bar{\varepsilon}_p(\eta, \xi)}$$



$$D = \int_0^t \frac{d\bar{\varepsilon}_p}{\bar{\varepsilon}_p(\eta, \xi)}$$

- 1) Ambiguous role of damage on fracture
- 2) Positive and negative **hydrostatic stress** causally accelerate or inhibit separation of cleaved shear planes

Assumed Role of Damage

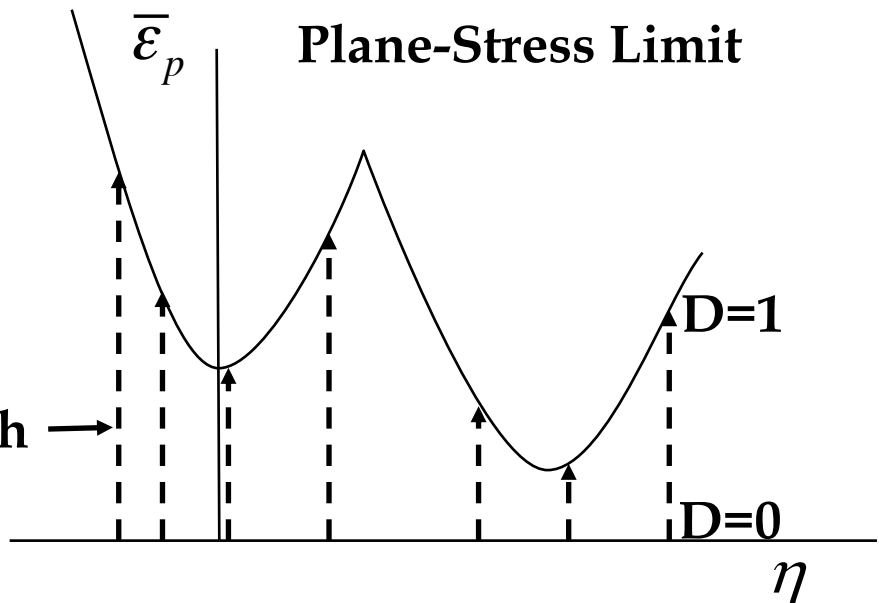
Xue-Wierzbicki Fracture Model (2006)

$$\bar{\varepsilon}_p(\eta, \xi) = c_1 \exp(-c_3 \eta)(1 - \xi^2) + c_2 \exp(-c_4 \eta)\xi^2$$

$$\eta = \frac{\sigma_m}{\bar{\sigma}} \quad \xi = \frac{J_3^{1/3}}{\bar{\sigma}}$$

$$D = \int_0^t \frac{d\bar{\varepsilon}_p}{\bar{\varepsilon}_p(\eta, \xi)}$$

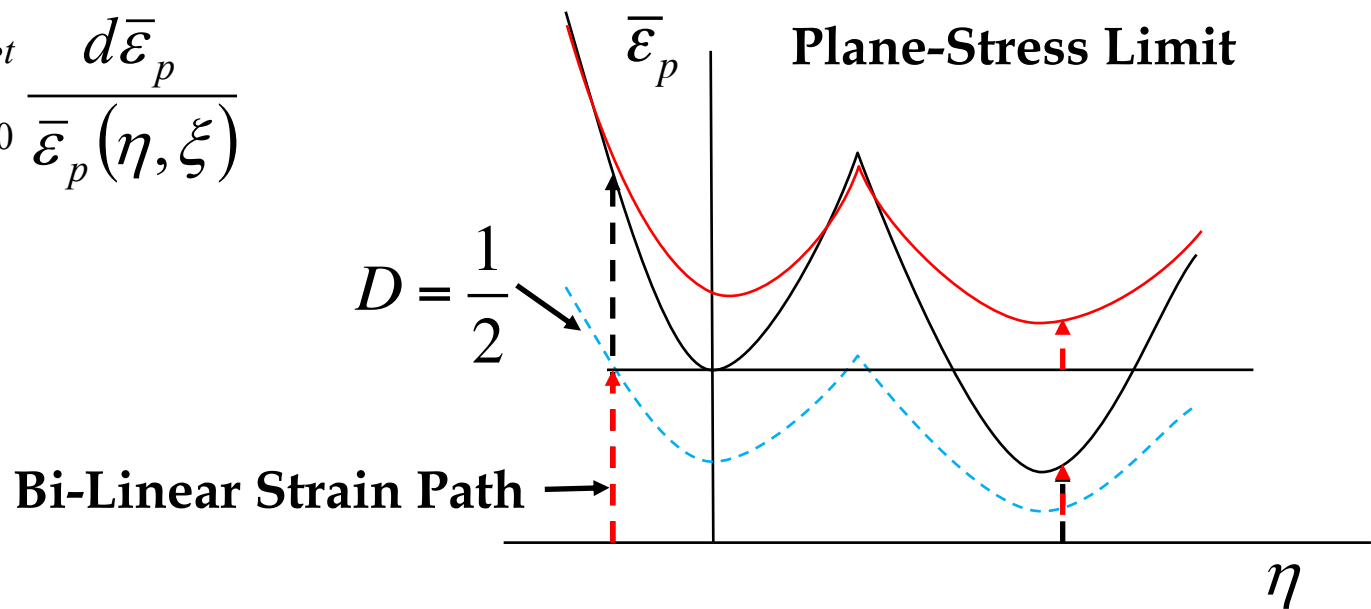
Linear Strain Path →



Assumed Role of Damage

$$\bar{\varepsilon}_p(\eta, \xi) = c_1 \exp(-c_3 \eta)(1 - \xi^2) + c_2 \exp(-c_4 \eta)\xi^2$$

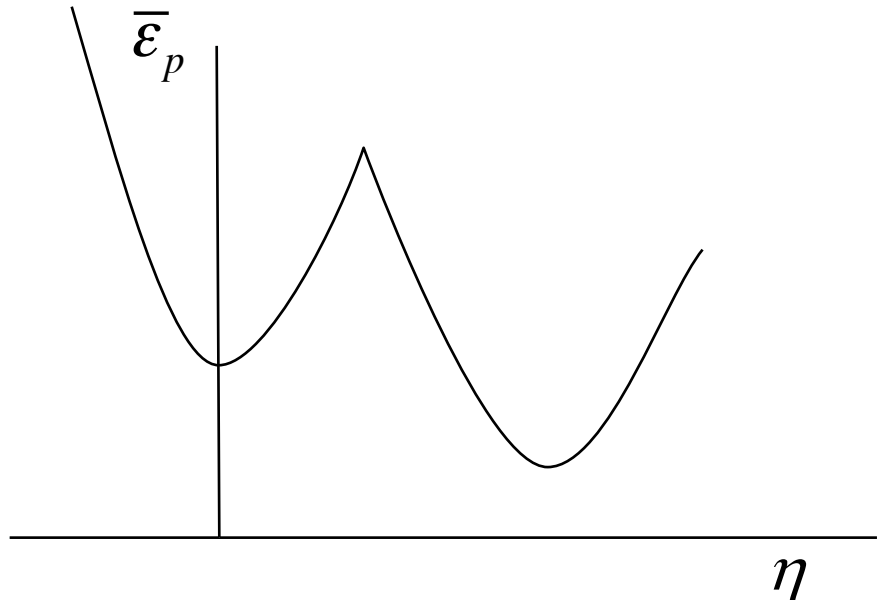
$$D = \int_0^t \frac{d\bar{\varepsilon}_p}{\bar{\varepsilon}_p(\eta, \xi)}$$



Comparison between strain-based and stress-based fracture models

(Damage-based model)

$$D = \int \frac{d\bar{\varepsilon}_p}{\bar{\varepsilon}_p(\eta, \xi)}$$



Fracture Occurs When $D = 1$

(Stress-based model)

$$F = F(\sigma_{ij})$$

Fracture Occurs When $F = 1$

